Modeling Cancer Cell-derived Extracellular Vesicles using Synthetic Nanoparticles

by

ISHMAN KAUR

THESIS PRESENTED TO ÉCOLE DE TECHNOLOGIE SUPÉRIEURE IN PARTIAL FULFILLEMENT FOR A MASTER'S DEGREE WITH THESIS IN ENGINEERING IN HEALTHCARE TECHNOLOGY
M.A.S.c

MONTREAL, JULY 07, 2025

ÉCOLE DE TECHNOLOGIE SUPÉRIEURE
UNIVERSITY OF QUEBEC

BOARD OF EXAMINERS (THESIS M.SC.A.)

THIS THESIS HAS BEEN EVALUATED

BY THE FOLLOWING BOARD OF EXAMINERS

Mr. Vahé Nerguizian, Thesis Supervisor
Department of Electrical Engineering at École de technologie supérieure

Mrs. Julia Valdemarin Burnier, Thesis Co-supervisor
Department of Pathology at McGill University

Mrs. Marie-Hélène Beauséjour, President of the Board of Examiners
Department of System Engineering at École de technologie supérieure

Mr. Maarouf Saad, Member of the jury
Department of Electrical Engineering at École de technologie supérieure

THIS THESIS WAS PRESENTED AND DEFENDED

IN THE PRESENCE OF A BOARD OF EXAMINERS AND

PUBLIC MONTREAL, JULY 02, 2025

AT ÉCOLE DE TECHNOLOGIE SUPÉRIEURE

ACKNOWLEDGMENT

I want to express my deepest gratitude to Dr. Vahé Nerguizian, for always encouraging me and pushing me to do my best. Your guidance and support have made all the difference in this journey. A big thank you to Dr. Julia Valdemarin Burnier, who was always there to help, support, answer my questions, and guide me through the tough parts of my research. A heartfelt thank you to my lab partner, Tad, for being there with me throughout and solving all the problems together. I would also like to sincerely thank the jury members for taking the time to review my thesis and for their thoughtful feedback and evaluation. Your insights and expertise are greatly appreciated.

I am also grateful to my lab mates – Yunxi, Noelie, Laura, Kyle, Thupten, Yousra, Nivedita, Yuning, and Masoud – for their help, teamwork, and for making long days in the lab more fun. Whether it was troubleshooting experiments, sharing advice, or just having a laugh, you all made this journey easier and more enjoyable.

To my family and friends, thank you for always being there for me. Your love, patience, and constant support kept me going, especially during the hardest times. I couldn't have done this without you.

A special thanks to NSERC and CIHR for funding this research and making this project possible.

Finally, to everyone who has been part of this journey in any way – thank you. Your kindness and support mean the world to me.

Modélisation des Vésicules Extracellulaires Dérivées de Cellules Cancéreuses à l'Aide de Nanoparticules Synthétiques

ISHMAN KAUR

RESUME

La métastase représente un défi majeur dans le traitement du cancer, le foie étant un site fréquent de dissémination tumorale. Les vésicules extracellulaires (VEs), de petites vésicules délimitées par une membrane et libérées par les cellules, jouent un rôle clé dans ce processus. Les VEs dérivées des cellules cancéreuses transportent des cargaisons biologiquement actives, telles que des protéines, vers des cellules cibles, contribuant ainsi à la préparation des sites métastatiques pour la colonisation par les cellules tumorales circulantes (un phénomène connu sous le nom de formation de niche pré-métastatique). Cependant, l'étude des VEs est compliquée par leur grande hétérogénéité et la difficulté à les isoler en quantité suffisante.

Pour contourner ces limites, l'objectif de ce mémoire était de créer des VEs synthétiques (SVEs) à partir de liposomes afin de reproduire les propriétés et fonctions des VEs dérivées de cellules cancéreuses, en se concentrant sur l'encapsulation de protéines associées aux VEs. Deux stratégies ont été employées : 1) l'encapsulation dans des liposomes de protéines candidates spécifiques (par exemple, la protéine de choc thermique 70 (HSP70) et CD63) achetées dans le commerce, et 2) l'extraction de protéines totales à partir d'VEs isolées de cellules cancéreuses, suivie de leur encapsulation dans des liposomes. Les SVEs ont été produits par une approche microfluidique, conçue pour imiter la taille et le potentiel zêta des VEs naturelles.

Les SVEs ont été caractérisées en termes de taille et de charge de surface par analyse de suivi de nanoparticules (NTA) et mesures de potentiel zêta. L'efficacité de l'encapsulation des

protéines a été évaluée par des analyses biochimiques, incluant le gel SDS-PAGE sans coloration et le dosage micro-BCA. Le profil protéomique des SVEs a été déterminé par spectrométrie de masse. L'internalisation cellulaire a été étudiée par imagerie cellulaire en temps réel afin de quantifier l'absorption des SVEs par les cellules réceptrices.
Les résultats démontrent que les SVEs peuvent incorporer efficacement des protéines associées aux VEs et présentent des caractéristiques similaires aux VEs naturelles, offrant ainsi un système reproductible pour étudier le rôle des protéines des VEs dans la métastase du cancer. Cette approche combine la nanotechnologie et la biologie du cancer, posant les bases pour le développement futur de systèmes de livraison ciblés inspirés des VEs pour des applications thérapeutiques.

Mots-clés : vésicules extracellulaires, liposomes synthétiques, métastase du cancer, microfluidique, encapsulation de protéines, potentiel zêta, protéomique

Modeling Cancer Cell-derived Extracellular Vesicles using Synthetic Nanoparticles

ISHMAN KAUR

ABSTRACT

Metastasis represents a major challenge in cancer care, with the liver being a common site for cancer to spread. Extracellular vesicles (EVs), small membrane-bound vesicles released by cells, play a crucial role in this process. Cancer derived EVs deliver important cargo, such as proteins, to recipient cells that then prepare metastatic sites for colonization by circulating tumor cells (a process referred to as premetastatic niche formation). However, studying EVs is difficult because they are highly heterogenous and difficult to isolate in large amounts.

To circumvent these challenges, the aim of this thesis was to create synthetic vesicles (SVs) using liposomes to replicate the properties and functions of cancer cell-derived EVs, with a focus on encapsulation of EV proteins. Two methods were used: 1) specific EV candidate proteins (e.g. heat shock protein 70 (HSP70) and CD63) were commercially sourced and encapsulated into liposomes, and 2) whole proteins were extracted directly from EVs isolated from cancer cells and encapsulated into liposomes. SVs were produced using a microfluidic approach, designed to match the size and zeta potential of natural EVs.

The SVs were characterized for their size and surface charge using nanoparticle tracking analysis (NTA) and zeta potential measurements. Protein loading efficiency was evaluated through biochemical assays, including stain-free SDS-PAGE and the micro-BCA protein quantification assay. Proteomic profiling via mass spectrometry identified the encapsulated proteins. Cellular uptake studies were performed using live cell imaging to quantify the internalization of SVs by recipient cells.

The findings demonstrate that engineered SVs can successfully incorporate EV-associated proteins and exhibit properties comparable to natural EVs, offering a scalable system to investigate the role of EV proteins in cancer metastasis. This approach bridges nanotechnology and cancer biology, laying the groundwork for designing targeted, EV-inspired delivery systems for future therapeutic applications.

Keywords: extracellular vesicles, synthetic vesicles, liposomes, cancer metastasis, microfluidics, protein encapsulation, zeta potential, proteomics

TABLE OF CONTENTS

INTRODUCTION 1

CHAPTER 1 LITERATURE REVIEW 7
1.1 Introduction 7
1.2 Extracellular Vesicles 9
1.2.1 Types of EVs 9
1.2.2 Role of EVs in Cancer Biology 12
1.2.3 Applications of EVs in Drug Delivery 14
1.3 Synthetic Nanoparticles (Liposomes) 17
1.3.1 Liposome Properties and Applications 18
1.3.2 Liposomes as Drug Delivery Vehicles 19
1.3.3 Liposome production using micromixers 20
1.4 Protein Encapsulation in Nanoparticles 24
1.4.1 Techniques for Protein Loading 27
1.4.2 Challenges 27
1.5 Conclusion 28

CHAPTER 2 MATERIALS AND METHODS 31
2.1 Introduction 31
2.2 Cell culture and EV isolation 33
2.2.1 EV isolation protocols 34
2.2.2 EV protein extraction 36
2.2.3 Proteomics 38
2.2.4 EV Characterization 39
2.3 Liposome Preparation 42
2.3.1 PDM Micromixer 42
2.3.2 Flex S System 43
2.3.3 Lipid Composition and Molar Ratios 45
2.3.4 Liposome synthesis method using PDM micromixer (TFR, FRR) 47
2.3.5 Characterization of liposomes 50
2.4 Encapsulation of Proteins into liposomes 51
2.4.1 Protein composition calculation 52
2.4.2 Protein loading method and synthesis of liposomes 53
2.4.3 Characterization and protein detection 57
2.5 Uptake 59
2.5.1 Cell culture 59
2.5.2 Liposome Labeling 60
2.5.3 Quantification and Standardization 61
2.5.4 Liposome treatment on cells 61

2.5.5 Liposome detection (Incucyte) 61
2.6 Conclusion 62

CHAPTER 3 RESULTS 63
3.1 Introduction 63
3.2 Characterization of Extracellular Vesicles (EVs) from SW620 64
3.2.1 Size and zeta potential (ZetaView) 65
3.2.2 Morphological Assessment by Transmission Electron Microscopy (TEM) 67
3.3 Liposome Synthesis Using the PDM System 68
3.3.1 Size Distribution and Stability of Empty Liposomes 68
3.3.2 Protein Loading Trials with Albumin 70
3.4 Liposome Synthesis Using the Flex S System 74
3.4.1 Albumin Encapsulation and Comparison with PDM 74
3.4.2 Targeted Protein Encapsulation: CD63 and HSP70 78
3.4.3 Enhanced Encapsulation of HSP70 Across Varying Lipid Ratios 87
3.4.4 Summary of Protein Encapsulation Outcomes (CD63 and HSP70) 91
3.4.5 Encapsulation of EV-Derived Proteins into SVs 91
3.5 Proteomic Analysis of EVs and SVs 94
3.6 Cellular Uptake Studies 98
3.7 Conclusion 100

DISCUSSION AND CONCLUSION 101

RECOMMENDATIONS 103

APPENDIX 1……..... 105

LIST OF BIBLIOGRAPHICAL REFERENCES 107

LIST OF TABLES

Page

Table 2.1 Molecular weights and calculated masses required to prepare 15 mL of a 20 mM lipid solution of DMPC and cholesterol (CHOL).....46

Table 2.2 Total flow rate (TFR) and flow rate ratio (FRR) conditions used for liposome synthesis using the PDM micromixer.....49

Table 2.3 Aqueous phase composition for protein encapsulation at different volumes.....53

Table 2.4 Flow conditions for liposome synthesis using the PDM micromixer.....55

Table 3.1 Micro BCA quantification of protein-loaded liposomes. No band was observed in the corresponding gel for CD63, indicating possible overestimation by BCA or non-encapsulated protein remaining after purification.....84

Table 3.2 Encapsulation efficiency (EE%) of HSP70-loaded SVs prepared with varying DMPC:CHOL molar ratios 89

LIST OF FIGURES

Page

Figure 0.1 Small extracellular vesicles (sEVs) from CRC cells facilitate liver pre-metastatic niche formation....1

Figure 0.2 Structural features of extracellular vesicles and synthetic liposomes as phospholipid-based delivery platforms....2

Figure 1.1 Overview of the Literature Review Structure 8

Figure 1.2 Schematic representation of the diverse sources and molecular cargo of extracellular vesicles (EVs). 10

Figure 1.3 Relative size range of extracellular vesicles....11

Figure 1.4 Cargo content, and uptake pathways of small extracellular vesicles (sEVs), including proteins like HSP, ALIX, HRS, and TSG101 From Gao et al., (2023)....13

Figure 1.5 Extracellular vesicles (EVs) as promising tools for cancer therapy From Kumar et al., (2023) 15

Figure 1.6 Schematic representation of liposomes Adapted from Biorender....18

Figure 1.7 Microfluidic synthesis of liposomes Adapted from Zouggari Ben El Khyat, C. (2022), Master's thesis, ÉTS 21

Figure 1.8 Schematic of the 3D-printed polydimethylsiloxane (PDM) micromixer design Image taken from the thesis of Rubén Rodrigo López Salazar (2023)....22

Figure 1.9 Flex S NanoGenerator system used for liposome and nanoparticle synthesis Image reproduced from the official website of Precigenome 23

Figure 1.10 Surface proteins enhancing EV and liposome function From Van der Koog et al., (2021) 25

Figure 1.11 Microfluidic-based protein encapsulation and purification workflow using the PDM micromixer Figure created with Biorender 26

Figure 2.1 Overview of Chapter 2: Materials and Methods 32

Figure 2.2 Schematic representation of extracellular vesicle (EV) isolation from SW620 conditioned medium Created using Biorender 34

Figure 2.3 Workflow for protein extraction from extracellular vesicles (EVs) Created using Biorender 37

Figure 2.4 Overview of analytical techniques used to characterize the physicochemical properties of extracellular vesicles (EVs) and synthetic vesicles (SVs) Adapted from Biorender.....39

Figure 2.5 ZetaView PMX 120 nanoparticle tracking analyzer (Particle Metrix) used for measuring size distribution and zeta potential of extracellular vesicles (EVs) and synthetic vesicles (SVs).....40

Figure 2.6 Schematic representation of Transmission Electron Microscopy (TEM) Created using Biorender 41

Figure 2.7 Polydimethylsiloxane (PDMS)-based microfluidic chip used for the synthesis of synthetic liposomes via passive mixing Originally developed by López et al. (2021) 43

Figure 2.8 Flex S NanoGenerator system (Precision NanoSystems Inc.) used for the microfluidic synthesis of synthetic vesicles (SVs) 44

Figure 2.9 Experimental setup for microfluidic synthesis of synthetic vesicles (SVs) using the PDM micromixer 48

Figure 2.10 Beckman Coulter Optima™ MAX-XP ultracentrifuge used for the isolation and purification of extracellular vesicles SVs 50

Figure 2.11 Workflow for IncuCyte-based cellular uptake assay Created using Biorender 60

Figure 3.1 Summary of Results Chapter Structure 64

Figure 3.2 Size distribution of EVs measured by ZetaView 66

Figure 3.3 Zeta Potential of Isolated EVs from SW620 cells.....67

Figure 3.4 Morphological analysis of EVs from SW620 cells. (A–B) TEM at 11,000× shows spherical, membrane-bound vesicles. (C) At 30,000×, lipid bilayers are clearly visible. Scale bars: A–B = 600 nm; C = 200 nm 68

Figure 3.5 Size distribution of empty liposomes synthesized via PDM at varying TFRs (FRR 2:1). ZetaView analysis shows larger vesicles at higher TFRs, peaking at 600 mL/h 70

Figure 3.6 Zeta potential of empty liposomes synthesized using the PDM micromixer at varying total flow rates (TFR)....71

Figure 3.7 Size distribution of albumin-loaded liposomes synthesized using the PDM micromixer at different total flow rates (TFR). All formulations were prepared at an FRR of 2:1. Sizes were measured using ZetaView....72

Figure 3.8 Zeta potential of albumin-loaded liposomes synthesized using the PDM micromixer at different total flow rates (TFR). Zeta potential was measured using ZetaView....73

Figure 3.9 Stain-free SDS-PAGE analysis of albumin-loaded liposomes synthesized using the PDM micromixer. A faint band is observed near ~66 kDa in the SV lane, consistent with the molecular weight of BSA (orange arrow) 74

Figure 3.10 Size comparison of albumin-loaded liposomes synthesized using Flex S and PDM micromixers 76

Figure 3.11 Zeta potential of albumin-loaded liposomes produced using Flex S and PDM systems 77

Figure 3.12 Stain-free SDS-PAGE analysis of albumin-loaded liposomes synthesized using the Flex S NanoGenerator system. Lanes represent alternating liposome samples and their respective supernatant controls after ultracentrifugation....78

Figure 3.13 Stain-free SDS-PAGE analysis of albumin-loaded liposomes synthesized using the PDM micromixer. Lanes represent alternating liposome samples and their respective supernatant controls after ultracentrifugation....79

Figure 3.14 Size distribution of empty and protein-loaded liposomes measured by ZetaView.....81

Figure 3.15 Zeta potential of empty and protein-loaded liposomes measured by ZetaView.....82

Figure 3.16 Stain-free SDS-PAGE analysis of protein-loaded liposomes and raw proteins 83

Figure 3.17 Stain-free SDS-PAGE analysis of protein-loaded liposomes prepared at different DMPC:CHOL ratios. HSP70-loaded liposomes showed increased band intensity at 2:1 lipid ratio, indicating enhanced encapsulation. Raw proteins were included as references to confirm expected molecular weights.....85

Figure 3.18 Effect of lipid ratio on size distribution of protein-loaded liposomes measured by ZetaView. Liposome size increased with higher DMPC content, particularly in HSP70-loaded samples (124.6 nm at 1:1 vs. 151.8 nm at 2:1).....86

Figure 3.19 Zeta potential of protein-loaded liposomes at different DMPC:CHOL ratios measured by ZetaView 87

Figure 3.20 Stain-free SDS-PAGE analysis of HSP70-loaded liposomes at 1:1, 2:1, and 3:1 lipid ratios. HSP70 bands intensified with increasing DMPC content, with the strongest signal observed at 3:1.....88

Figure 3.21 Size distribution of HSP70-loaded liposomes at different lipid ratios measured by ZetaView 89

Figure 3.22 Zeta potential of HSP70-loaded liposomes at varying DMPC:CHOL ratios 90

Figure 3.23 Size distribution of EV SVs measured using ZetaView, showing a uniform nano sized population 92

Figure 3.24 Zeta potential analysis of EV SVs indicating stable surface charge 92

Figure 3.25 Protein profile of EV protein-loaded synthetic vesicles (EV SVs) visualized by stain-free SDS-PAGE**.** Distinct bands spanning a broad molecular weight range confirm successful encapsulation of diverse EV-derived proteins.....93

Figure 3.26 Venn diagram comparing protein identities between EVSV and natural EVs 94

Figure 3.27 Comparative spectral counts of EV marker proteins in EVSV and natural EVSV samples 95

Figure 3.28 Volcano plot of differentially expressed proteins between EVs and EV SVs. Red and blue points represent proteins significantly enriched or depleted in EV SVs compared to native EVs ($p < 0.01$, $|\log_2 FC| > 2$) 96

Figure 3.29 Correlation of total spectral counts between EVs and EV SVs 97

Figure 3.30 A. Uptake of EV protein-loaded liposomes by SW620 cells visualized by IncuCyte at 48 h post-treatment 98

Figure 3.30 B. Uptake of HSP 70 protein-loaded liposomes by HCT 116 cells visualized by IncuCyte at 48 h post-treatment 99

Figure A.1.1 Screenshot of raw proteomics data for EV and EV SV samples analyzed using Scaffold Viewer. Spectral counts across replicates (Control_1, Control_2, EVSV_1, EVSV_2) are shown 105

LIST OF ABREVIATIONS

3D	Three-Dimensional
CD63	Cluster of Differentiation 63
CHOL	Cholesterol
CRC	Colorectal Cancer
DMEM/F-12	Dulbecco's Modified Eagle Medium/Nutrient Mixture F-12
DMPC	1,2-Dimyristoyl-sn-glycero-3-phosphocholine
DMPG	1,2-Dimyristoyl-sn-glycero-3-phosphoglycerol
DMSO	Dimethyl sulfoxide
DLS	Dynamic Light Scattering
DoE	Design of Experiments
DNA	Deoxyribonucleic acid
EV	Extracellular Vesicle
Flex S	Flex S NanoGenerator System
FRR	Flow Rate Ratio
GFP	Green Fluorescent Protein
HSP70	Heat Shock Protein 70

LNP	Lipid Nanoparticle
mRNA	Messenger Ribonucleic Acid
miRNA	Micro RNA
MISEV	Minimal information for studies of extracellular vesicles
MS	Mass Spectrometry
MVB	Multivescular Body
NTA	Nanoparticle Tracking Analysis
PBS	Phosphate-Buffered Saline
PD-L1	Programmed death-ligand 1
PDM	Polydimethylsiloxane Micromixer
PEG	Polyethylene Glycol
PS	Phosphatidylserine
RNA	Ribonucleic Acid
RSM	Response Surface Methodology
SDS-PAGE	Sodium Dodecyl Sulfate–Polyacrylamide Gel Electrophoresis
SOD 1	Superoxide Dismutase 1
SV	Synthetic Vesicle
T cells	Thymus-derived lymphocytes

TEM	Transmission Electron Microscopy
TFR	Total Flow Rate
ZP	Zeta Potential

INTRODUCTION

Cancer is one of the biggest health challenges worldwide (reviewed in Sung et al., 2021), with the majority of cancer-related deaths occurring due to metastasis (reviewed in Sjoblom et al., 2024). In Colorectal Cancer (CRC), which is the most common cancer worldwide, (reviewed in Ahmadi et al., 2024) the liver is one of the most common sites for metastasis. The prognosis of metastatic CRC is poor, with an estimated 5-year survival of about 13–16% (American Cancer Society, 2025).

As illustrated in Figure 0.1, small extracellular vesicles (sEVs) from CRC cells contribute to liver pre-metastatic niche formation by promoting inflammation, immunosuppression, angiogenesis, and extracellular matrix remodeling (Wu et al., 2024).

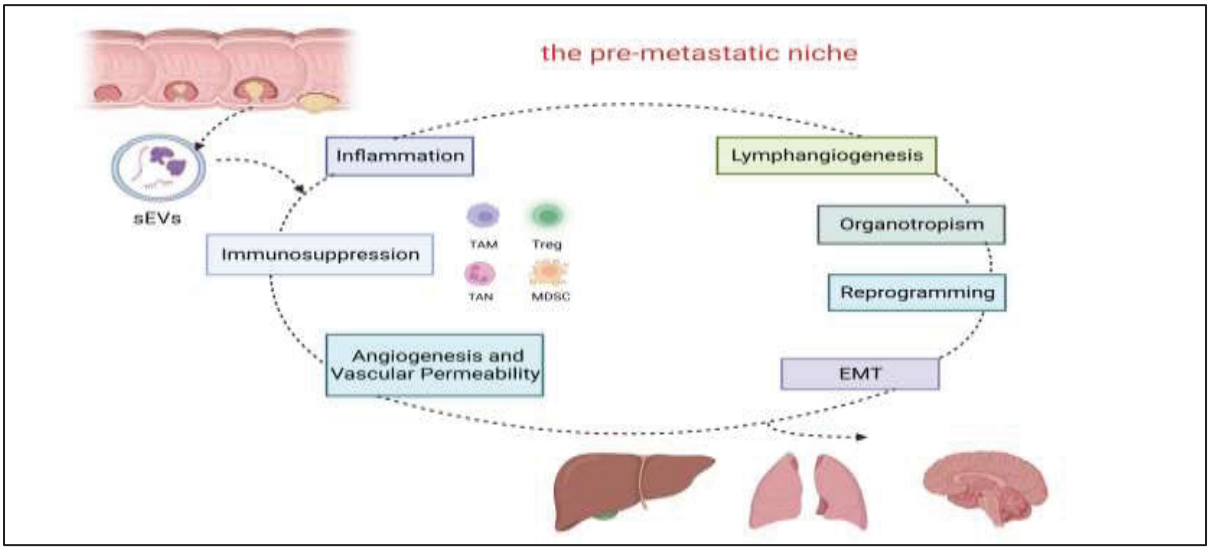

Figure 0.1 Small extracellular vesicles (sEVs) from CRC cells facilitate liver pre-metastatic niche formation

Figure from Wu et al., 2024, Cell Cycle, 23(2)

A major discovery in recent years is the role of EVs. These nano-sized particles, naturally released by cells, act like messengers, carrying proteins and genetic material from one cell to another. Research has shown that EVs help cancer cells invade new tissues and create a supportive environment for tumors to grow (Raposo & Stoorvogel, 2013; Théry et al., 2018). Because of their natural ability to transfer biomolecules, EVs have also gained attention for drug delivery, but there remains a big problem—they are hard to isolate and/or produce in large amounts, and are highly heterogenous (Bunggulawa et al., 2018). Because of these challenges, researchers are now exploring synthetic options like liposomes, which are lab-made nanoparticles that can help overcome the problems seen with natural EVs. Figure 0.2 highlights the structural similarities and differences between extracellular vesicles and synthetic liposomes, both of which are phospholipid-based delivery platforms.

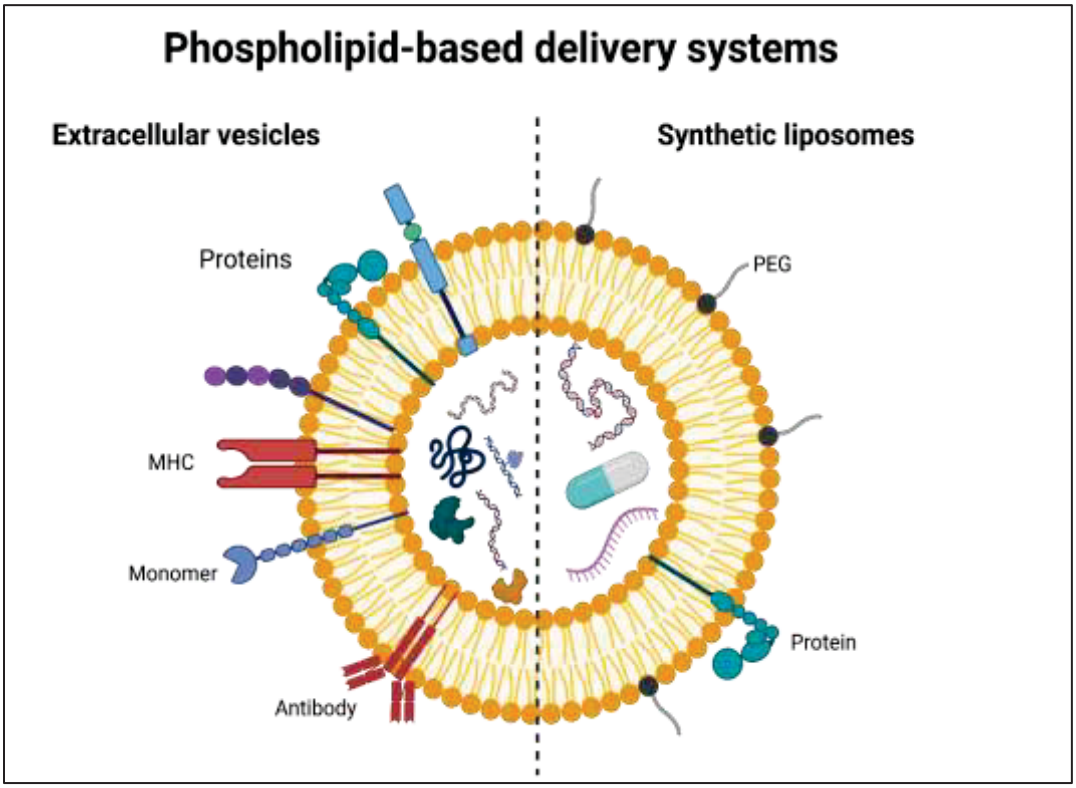

Figure 0.2 Structural features of extracellular vesicles and synthetic liposomes as phospholipid-based delivery platforms

Liposomes have long been used in medicine due to their stability, biocompatibility and ability to carry different cargo such as hydrophilic drugs in their aqueous core and lipophilic drugs within their lipid bilayer, enabling the delivery of a wide range of therapeutic agents including anticancer drugs, proteins, and genetic material (reviewed in Torchilin, 2005). However, the big question remains if liposomes can mimic the biological functions of EVs, especially in cancer progression and metastasis.

Objectives

This study aims to bridge the gap between naturally derived EVs and synthetic nanoparticles by developing engineered EV-like liposomes that incorporate key EV proteins. The goal is to determine whether these synthetic vesicles (SVs) can replicate the biological effects of cancer cell-derived EVs using liver metastatic CRC cells. To investigate this, EVs are isolated from CRC cells, their protein cargo is extracted and analyzed, and microfluidic technology is used to synthesize protein-loaded liposomes. The SVs are tested for their size, structure, protein content, and their uptake by CRC cells.

Chapter 1 is the literature review which focuses on EVs, their role in cancer and metastasis. This background helps explain why EVs are important in understanding the mechanisms underlying metastasis. The next part focuses on liposomes—what they are, how they are made, and why they have been chosen to model EV-like behavior in this study. Chapter 2 is the method section describing how EVs were isolated, how their proteins were extracted, and how SVs were produced and tested in the lab. The results in Chapter 3 explore whether these SVs, especially when loaded with EV proteins, can behave like natural EVs in terms of size, stability, and uptake by cells. This is important because, unlike EVs, liposomes can be made more easily and in larger amounts, which makes them useful tools for studying how cancer spreads. By comparing the properties of EVs and liposomes, this research helps build a model for studying cancer metastasis in a more controlled and scalable way.

Contributions

During my master's research, I have actively worked to share my work beyond the lab and engage with the broader academic community. I participated in the ÉTS Science Poster Competition (February 2025), where I presented my project and won second place. I was also selected for the Three-Minute Thesis (3MT) competition in both 2024 and 2025, placing second in the regional pre-selection rounds both years. These events helped me strengthen my science communication skills and present complex research in a simple and engaging way. In addition, I was part of the team that won second place in the Micro and Nano Bioengineering Chip Design Challenge organized during the 14th Annual Hands-On Workshop hosted by McGill University in May 2024.

I also presented my research at academic events such as LACIME Research Day and the ReSMIQ student conference, where I had the chance to receive feedback from other students and professors in related fields. These interactions helped me better understand the potential impact of my work and explore future directions.

In April 2025, our work was selected for an oral presentation at the International Society for Extracellular Vesicles (ISEV) annual meeting in Vienna. This was a significant opportunity to present results to a global audience and connect with experts in the EV field. I also contributed as a co-author on a collaborative paper titled "Leveraging Nature's Nanocarriers: Translating Insights from Extracellular Vesicles to Biomimetic Synthetic Vesicles for Biomedical Applications" (Chen et al., 2025), where I assisted with writing the original draft.

This research was made possible through the collaborative efforts of many members of the lab. I would especially like to acknowledge Tad, my partner in experiments, with whom I carried out much of the hands-on work. I also thank Laura for her help with cell culture, and Yunxi

for her early guidance and support when I joined the project, and Thupten for preparing me and supporting my initial training in EV experiments. I am grateful to Noélie for always contributing insightful ideas during discussions, and to Kyle for consistently addressing lab issues and creating a supportive, welcoming environment.

Outside of conferences and publications, I contributed to peer learning and lab support. I mentored students on liposome preparation techniques and assisted with cell culture training. As part of the ÉTS Contact program, I volunteered to support international students, helping them adjust to academic life in Canada and navigate their early months in Montreal.

CHAPTER 1

LITERATURE REVIEW

1.1 Introduction

Researchers have increasingly turned to synthetic nanoparticles, such as liposomes, as alternatives to natural EVs. Liposomes are artificially made vesicles composed of lipid bilayers that closely resemble the architecture of cellular membranes. Owing to their biocompatibility, scalability, and capacity to encapsulate a broad range of molecules, liposomes have become widely utilized in medical applications. For example, liposomal formulations like Doxil® have received clinical approval for the delivery of chemotherapeutic agents, offering reduced systemic toxicity compared to conventional formulations (Torchilin, 2005). Despite these advantages, traditional liposomes lack the intrinsic targeting capabilities and complex biological functions of EVs.

This literature review examines how combining the unique advantages of EVs and liposomes could help overcome their individual limitations. The first section characterizes the major EV subtypes—exosomes, microvesicles, and apoptotic bodies—and their functional roles in cancer progression. The second section explores liposome engineering, including their physicochemical properties, applications in drug delivery, and recent advances in the development of hybrid systems that aim to merge EV and liposome functionality. The final section reviews strategies for protein encapsulation—specifically involving HSP70 and CD63—within liposomes, to demonstrate how SVs may recapitulate key EV features within a scalable, controlled platform.

Note: Throughout this thesis, the term *synthetic vesicles (SVs)* refers to engineered liposomes designed to mimic the physicochemical and functional characteristics of extracellular vesicles (EVs).

By bridging the gap between naturally derived EVs and synthetic systems such as SVs, this chapter establishes the conceptual framework for understanding how SVs may serve as reliable tools in cancer research and the development of targeted therapeutic approaches. Figure 1.1 provides an overview of the literature review structure and outlines the key topics covered in this chapter.

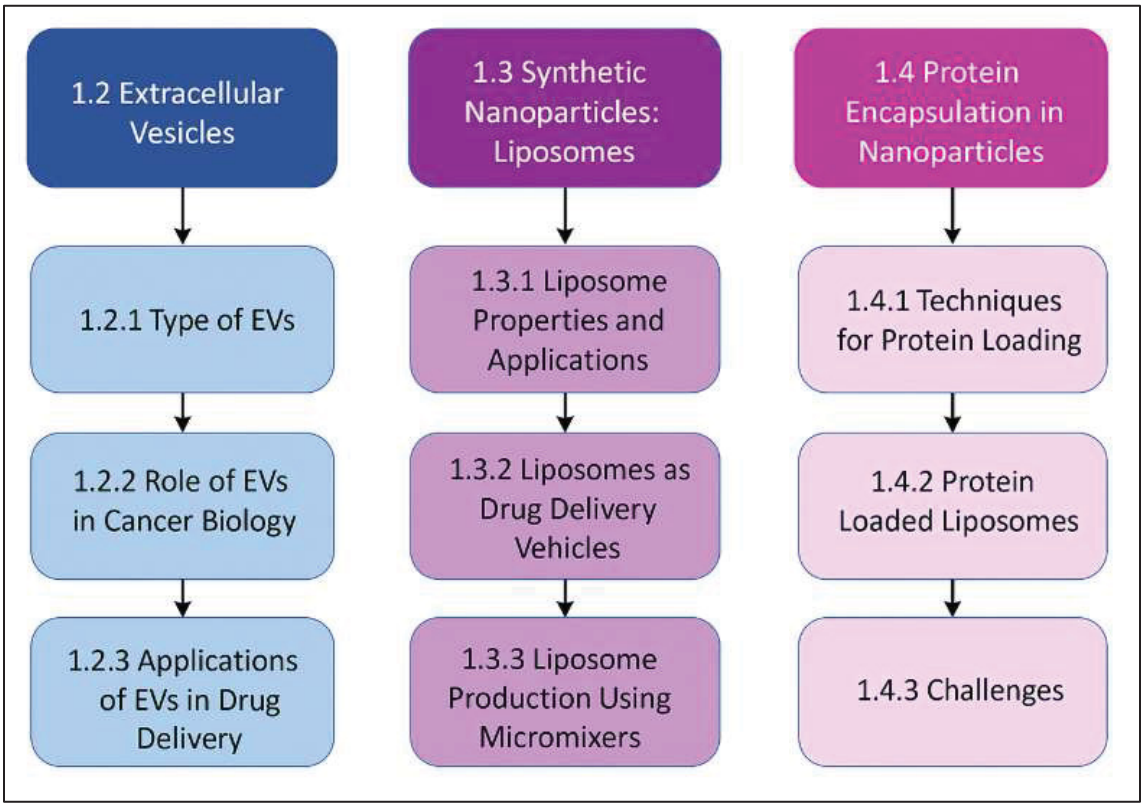

Figure 1.1 Overview of the Literature Review Structure

1.2 Extracellular Vesicles

EVs are nano-sized, membrane-bound particles actively released by cells into the extracellular environment. These vesicles have emerged as key mediators of intercellular communication, transporting a variety of bioactive molecules, including proteins, lipids, Ribonucleic acid (RNA), and Deoxyribonucleic acid (DNA). EVs contribute to numerous physiological processes, such as immune regulation and tissue regeneration, but are also critically involved in pathological conditions, notably in cancer progression and metastasis (Raposo and Stoorvogel, 2013; Petersen et al., 2020).

1.2.1 Types of EVs

According to the MISEV2018 guidelines (Théry et al., 2018), EVs should be classified based on measurable characteristics such as size, density, or surface markers, rather than assumed biogenesis pathways unless experimentally validated. However, for descriptive purposes, EVs are commonly grouped into three subtypes: exosomes, microvesicles, and apoptotic bodies. Figure 1.2 illustrates the diverse cellular origins and molecular cargo of EVs, highlighting their functional complexity.

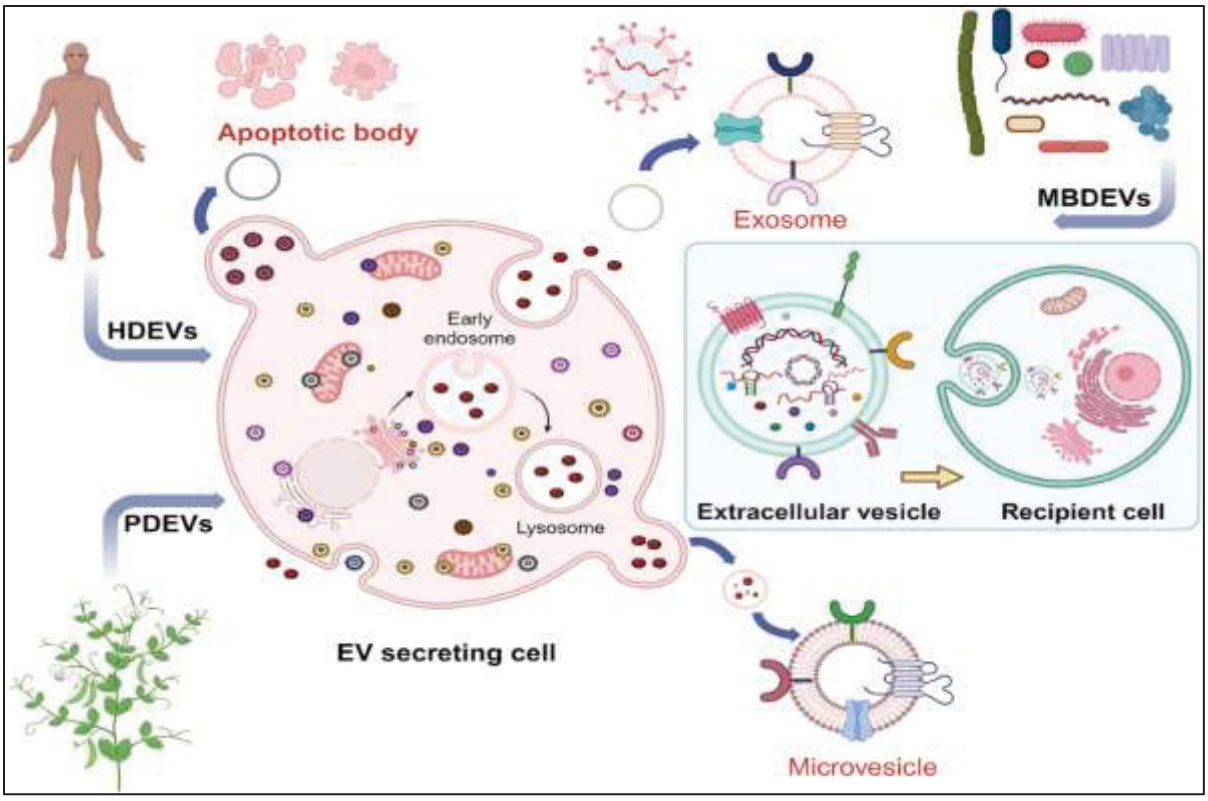

Figure 1.2 Schematic representation of the diverse sources and molecular cargo of extracellular vesicles (EVs)

Adapted from Kumar et al., (2024) under CC BY 4.0

Exosomes are the smallest EVs, typically ranging from 30 to 150 nm in size. They originate from the endosomal pathway, where multivesicular bodies (MVBs) fuse with the plasma membrane to release exosomes into the extracellular space. Exosomes carry diverse cargo, including proteins like CD63 and RNA molecules such as miRNAs, which reflect the state of their parent cells (Théry et al., 2002; Kowal et al., 2016). Exosomes are particularly significant in cancer biology due to their ability to transfer oncogenic material that promotes tumor growth and metastasis (Dong et al., 2002; Hoshino et al., 2015).

Microvesicles, ranging from 100 to 1,000 nm in size, are formed directly from the outward budding of the plasma membrane. Unlike exosomes, microvesicle formation is regulated by

cytoskeletal proteins such as actin and myosin. Microvesicles often carry phosphatidylserine (PS) on their surface, which facilitates their interaction with recipient cells (Balaj et al., 2011; Dhondt et al., 2020). These vesicles are involved in processes like coagulation and immune modulation but also play a role in cancer metastasis by transferring tumor-promoting molecules.

Apoptotic bodies are the largest EVs, measuring up to 5 μm in diameter. They are released by cells undergoing programmed cell death (apoptosis) and contain cellular debris such as fragmented DNA and organelles. While apoptotic bodies primarily function in clearing dying cells from tissues, they can also influence immune responses and contribute to cancer progression under certain conditions (Kahlert et al., 2014). Figure 1.3 compares exosomes, microvesicles, and apoptotic bodies.

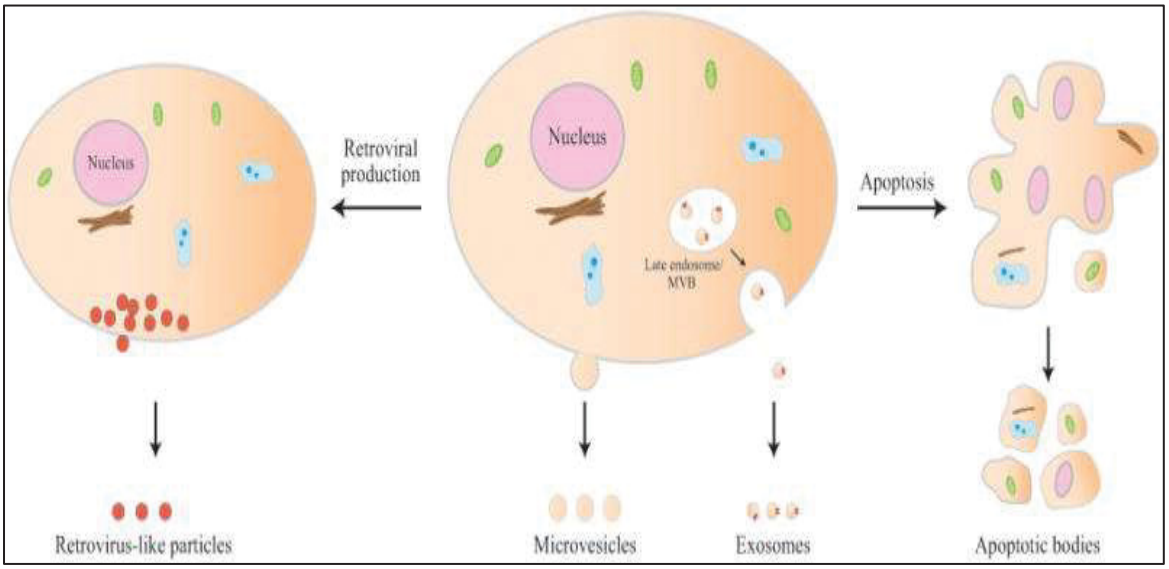

Figure 1.3 Relative size range of extracellular vesicles

Reproduced from Akers J.C. et al., (2013)

In this project, the focus is specifically on mimicking exosome-sized vesicles, as these represent the most extensively studied EV subtype in cancer biology. Exosomes fall within the nanoscale size range (30–150 nm), which corresponds to the size of SVs generated through microfluidic production methods. Given their established role in intercellular communication and pre-metastatic niche formation, exosomes are considered the most relevant target for the development of biomimetic drug delivery systems in this study (reviewed in Jie et al., 2021; Li et al., 2019; Théry et al., 2018).

1.2.2 Role of EVs in Cancer Biology

EVs are now widely recognized as critical mediators of communication in cancer biology. They are actively released by various types of cancer cells and play essential roles in facilitating interactions between tumor cells and their surrounding microenvironment. These vesicles transport a diverse range of biomolecules, including proteins, lipids, DNA, and RNA, which can modulate the behavior of recipient cells (Yáñez-Mó et al., 2015).

In CRC, as well as in other solid tumors, EVs have been implicated in key pathological processes such as tumor growth, angiogenesis, immune suppression, and metastasis (Peinado et al., 2012; Costa-Silva et al., 2015). One of the most extensively studied functions of EVs in this context is their role in the formation of pre-metastatic niches. Evidence indicates that EVs released by primary tumors can travel to distant organs, such as the liver, and condition these tissues to become more permissive to metastatic colonization. For example, the membrane receptor protein integrins expressed on the surface of tumor-derived EVs have been shown to guide their organ-specific distribution and facilitate interactions with local stromal and immune cells, ultimately promoting a pro-metastatic microenvironment (Hoshino et al., 2015).

Heat shock proteins such as HSP70 and tetraspanin membrane proteins like CD63 are among the commonly identified components of cancer-derived EVs. These proteins not only serve as molecular markers for EV identification but also contribute to functional roles in cellular stress

responses and signal transduction (Clayton et al., 2005; Vega et al., 2008). HSP70, in particular, is associated with cancer cell survival and has been shown to activate immune cells, including macrophages and dendritic cells, when displayed on the surface of EVs (Gastpar et al., 2005). Figure 1.4 summarizes common EV cargo, such as HSPs and ESCRT-related proteins, along with their proposed uptake pathways.

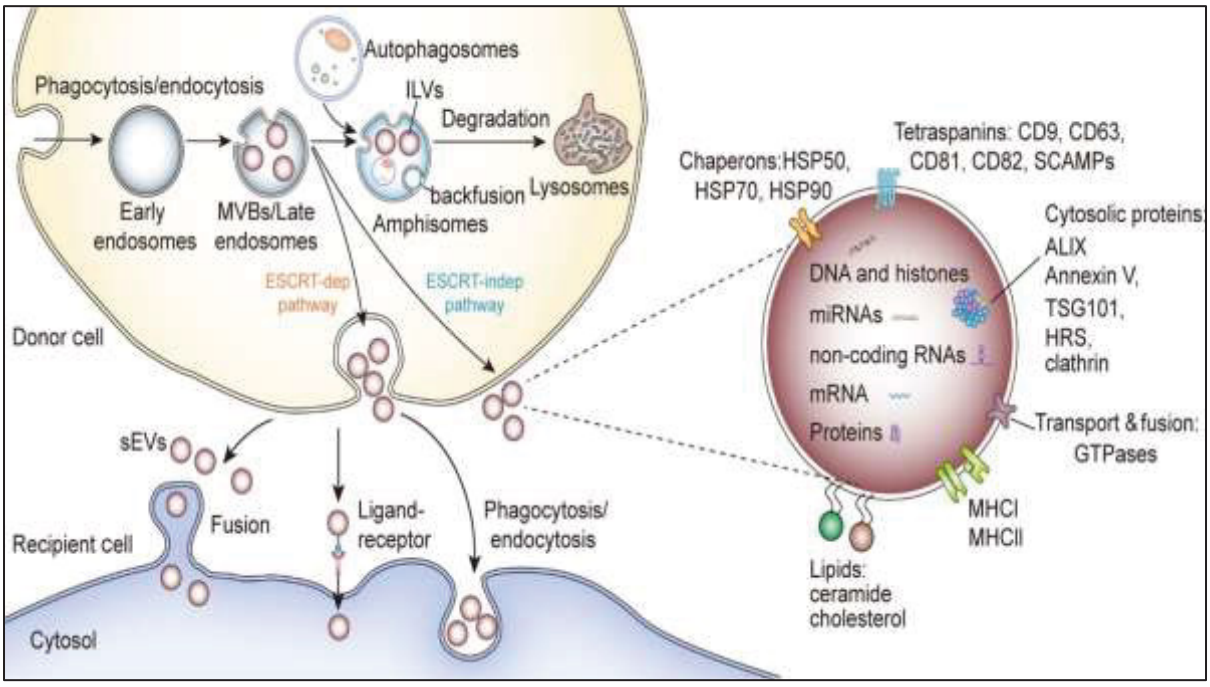

Figure 1.4 Cargo content, and uptake pathways of small extracellular vesicles (sEVs), including proteins like HSP, ALIX, HRS, and TSG101
From Gao et al., (2023)

In addition to promoting metastasis, EVs also help tumors escape immune detection. Some cancer-derived EVs carry immune checkpoint proteins like programmed death-ligand 1 (PD-L1), which suppress the activity of Thymus-derived lymphocytes cells (T cells)

and prevent them from attacking cancer cells (Chen et al., 2018). Others contain microRNAs or long non-coding RNAs that influence immune-related pathways and shape responses in the tumor microenvironment (Skog et al., 2008).

Because of these properties, EVs are being widely studied—not just to better understand cancer progression but also for their potential in drug delivery. Their natural biocompatibility and ability to cross biological barriers make them attractive for transporting therapeutic molecules, especially to harder-to-reach areas like the brain or metastatic organs (Alvarez-Erviti et al., 2011). That said, challenges still exist, such as the difficulty of isolating large quantities of EVs and the variability in their composition.

Even with these hurdles, EVs remain a major focus in cancer research, and there is growing interest in mimicking their behavior using engineered nanoparticle systems.

1.2.3 Applications of EVs in Drug Delivery

Extracellular vesicles (EVs) have emerged as a promising tool in drug delivery research (Figure 1.5) due to their natural origin and ability to transport a wide range of molecules. Since EVs are derived from cells, they are inherently biocompatible and are less likely to trigger immune responses compared to synthetic nanoparticles (Elsharkasy et al., 2020; Meng et al., 2020). Their lipid bilayer helps protect the encapsulated cargo, allowing for the efficient delivery of proteins, RNAs, and small-molecule drugs directly to recipient cells.

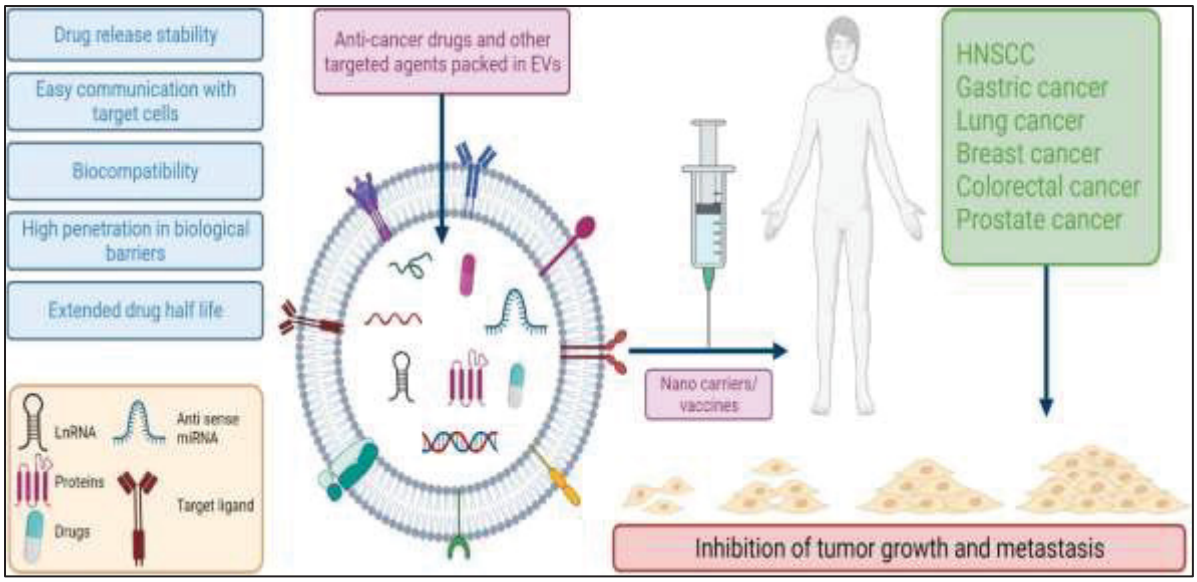

Figure 1.5 Extracellular vesicles (EVs) as promising tools for cancer therapy
From Kumar et al., (2023)

One of the most promising features of EVs is their ability to cross biological barriers. For example, exosomes have been shown to traverse the blood–brain barrier, making them a valuable tool for delivering treatments to the brain (Alvarez-Erviti et al., 2011). Similarly, EVs derived from stem cells have demonstrated the capacity to reach inflamed or injured tissues, making them attractive candidates for therapies targeting autoimmune diseases and other inflammatory conditions (Rani et al., 2023).

EVs can be loaded with therapeutic cargo using either endogenous or exogenous strategies. In the endogenous approach, donor cells are genetically modified or stimulated to naturally produce EVs containing the desired molecules (reviewed in Vader et al., 2016). While this method maintains vesicle integrity, it often results in low and inconsistent loading efficiency, as cargo incorporation depends on factors such as cell type, cargo properties, and poorly understood intracellular sorting mechanisms (Lener et al., 2015; El Andaloussi et al., 2013). For instance, the loading of RNA or proteins can be highly variable due to unpredictable trafficking within the cell and potential degradation by proteases prior to EV release (Syn et

al., 2017; Rankin-Turner et al., 2023). These limitations complicate reproducibility and pose challenges for clinical translation (Mendt et al., 2018; Kamaly et al., 2016).

Exogenous loading, on the other hand, involves introducing therapeutic cargo into pre-isolated EVs through physical or chemical means, such as electroporation, sonication, or membrane permeabilization. Although this method can achieve higher loading efficiency, it is often associated with membrane damage, vesicle aggregation, and the presence of residual chemicals, which may affect EV function and safety (Kooijmans et al., 2015; Shtam et al., 2013). Moreover, passive loading methods are mainly suitable for small hydrophobic compounds, while hydrophilic or larger molecules—such as nucleic acids—typically require protocol optimization to improve incorporation (Yang et al., 2015; Rani et al., 2015). Both strategies face scalability issues due to the lack of standardized protocols and variations in EV isolation techniques (Syn et al., 2017; Bruno et al., 2013).

Given these limitations, researchers have begun exploring hybrid systems that combine EVs with synthetic nanoparticles to enhance their therapeutic utility (reviewed in Beh et al., 2022). These engineered systems aim to improve vesicle stability, drug loading efficiency, and targeting capabilities. For instance, several studies have integrated EV membranes with liposomes to produce SVs capable of carrying higher drug payloads while preserving natural targeting features (Tian et al., 2022; Zhang et al., 2021). Other approaches have involved surface modifications—such as antibody or peptide conjugation—to direct EVs to specific cell types, including cancer cells (Xu et al., 2023).

To date, EVs have shown considerable promise across various medical fields. In cancer therapy, they have been loaded with siRNA or chemotherapeutic drugs for targeted tumor delivery with reduced systemic toxicity (Mondal et al., 2023). In neurological disorders, EVs have been used to transport anti-inflammatory molecules to the brain (Alvarez-Erviti et al., 2011). They have also attracted attention in regenerative medicine due to their role in tissue repair and immune modulation (Rani et al., 2023).

Despite their potential, several challenges remain. Large-scale EV production remains costly and labor-intensive, with significant batch-to-batch variability (Théry et al., 2018). In addition, achieving consistently high cargo loading and effective targeting continues to require optimization.

Looking ahead, combining the natural advantages of EVs with the precision and scalability of synthetic systems—such as microfluidic-synthesized liposomes—offers a promising direction. These hybrid approaches could enable the development of more reliable and clinically translatable drug delivery platforms in the future.

1.3 Synthetic Nanoparticles (Liposomes)

Liposomes are artificial, spherical vesicles composed of lipid bilayers that mimic the architecture of natural cell membranes. Since their discovery in the 1960s (Bangham et al., 1965), liposomes have become one of the most extensively studied and widely applied drug delivery systems. Their biocompatibility, capacity to encapsulate both hydrophilic and lipophilic molecules, and scalability make them an appealing option for therapeutic use (Torchilin, 2005). In contrast to extracellular vesicles (EVs), which present challenges such as low yield and high production costs, liposomes provide a more controlled and reproducible platform for the delivery of drugs, proteins, and genetic material (Barenholz, 2012). Figure 1.6 illustrates the basic structure of liposomes, highlighting their lipid bilayer and drug-carrying compartments.

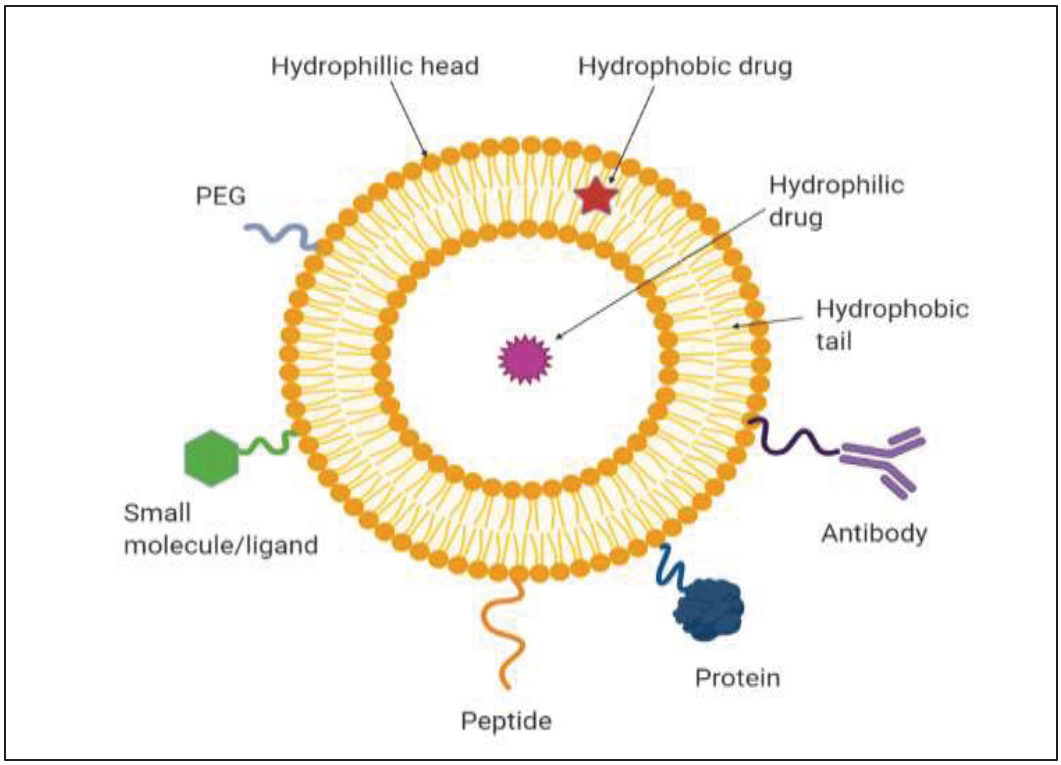

Figure 1.6 Schematic representation of liposomes
Adapted from Biorender

1.3.1 Liposome Properties and Applications

Liposomes are composed of phospholipids, such as phosphatidylcholine, which assemble into bilayer structures resembling natural cell membranes. This bilayer architecture enables liposomes to encapsulate hydrophilic drugs in their aqueous core and hydrophobic compounds within the lipid membrane. Cholesterol (CHOL) is commonly incorporated to enhance membrane rigidity and stability, while surface modifications such as polyethylene glycol (PEG) are used to prolong circulation time by reducing immune recognition and clearance (Allen and Cullis, 2013). The structural versatility of liposomes has enabled their use in a wide range of medical applications:

- **Cancer Therapy**: Liposomal formulations, such as Doxil® (doxorubicin-loaded liposomes), reduce side effects like cardiotoxicity while maintaining anticancer activity by passively accumulating in tumor tissues through the enhanced permeability and retention (EPR) effect (Barenholz, 2012).
- **Gene Therapy**: Liposomes can be used to deliver siRNA or mRNA to silence pathogenic genes or induce therapeutic protein expression. For instance, lipid nanoparticle formulations were employed in COVID-19 vaccines to enable efficient intracellular delivery of mRNA (Hou et al., 2021).
- **Protein Delivery**: Liposomes can protect therapeutic proteins from enzymatic degradation and improve their stability during transport. Recent studies have demonstrated the use of liposome-based carriers for encapsulating enzymes or antibodies to support targeted therapy (Gong et al., 2023).

Despite these advantages, traditional liposomes lack the innate targeting capabilities of EVs. While they can accumulate in tumors via the EPR effect, they often do not achieve the organ-specific targeting observed with EVs (Xu et al., 2023).

1.3.2 Liposomes as Drug Delivery Vehicles

Liposomes are widely recognized for their ability to enhance drug solubility, protect encapsulated cargo from degradation, and reduce off-target effects. These properties make them especially valuable in cancer therapy:

- **Chemotherapy**: Liposomal doxorubicin (Doxil®) improves drug accumulation at tumor sites while minimizing systemic toxicity. This formulation has received FDA approval for the treatment of ovarian cancer and Kaposi's sarcoma (Barenholz, 2012).

- **Multidrug Delivery**: Liposomes can be used to co-deliver multiple therapeutic agents, offering synergistic treatment outcomes. For instance, combining chemotherapeutic agents with RNA molecules in a single liposomal formulation has been shown to enhance efficacy while reducing drug resistance (Mondal et al., 2023).

Despite these advances, optimizing liposome composition and surface characteristics to improve targeting efficiency and pharmacokinetic behavior remains a challenge. Recent developments in microfluidic technologies have addressed some of these issues by allowing for precise control over liposome size, surface charge, and cargo loading efficiency (Fluigent, 2024).

1.3.3 Liposome production using micromixers

Liposomes are widely used in drug delivery because they can encapsulate both hydrophilic (water-loving) and lipophilic (fat-loving) drugs. This versatility helps protect therapeutic molecules from degradation and enhances their bioavailability. However, producing liposomes with consistent size and drug loading has historically been a challenge. Conventional techniques like thin-film hydration and ethanol injection often generate heterogeneous populations and require additional steps—such as sonication or extrusion—that increase processing time and material loss (Jahn et al., 2007; van Swaay and deMello, 2016).

Microfluidic systems have emerged as a more precise and scalable solution for liposome synthesis. These systems use microscale channels to control mixing between lipid (typically in ethanol) and aqueous phases, allowing spontaneous self-assembly of liposomes at the interface. This controlled environment enables the production of liposomes with uniform size and morphology, without the need for further processing (van Swaay and deMello, 2016; Jahn et al., 2007). Figure 1.7 provides a schematic overview of the microfluidic setup used for liposome synthesis, highlighting the controlled mixing and self-assembly process.

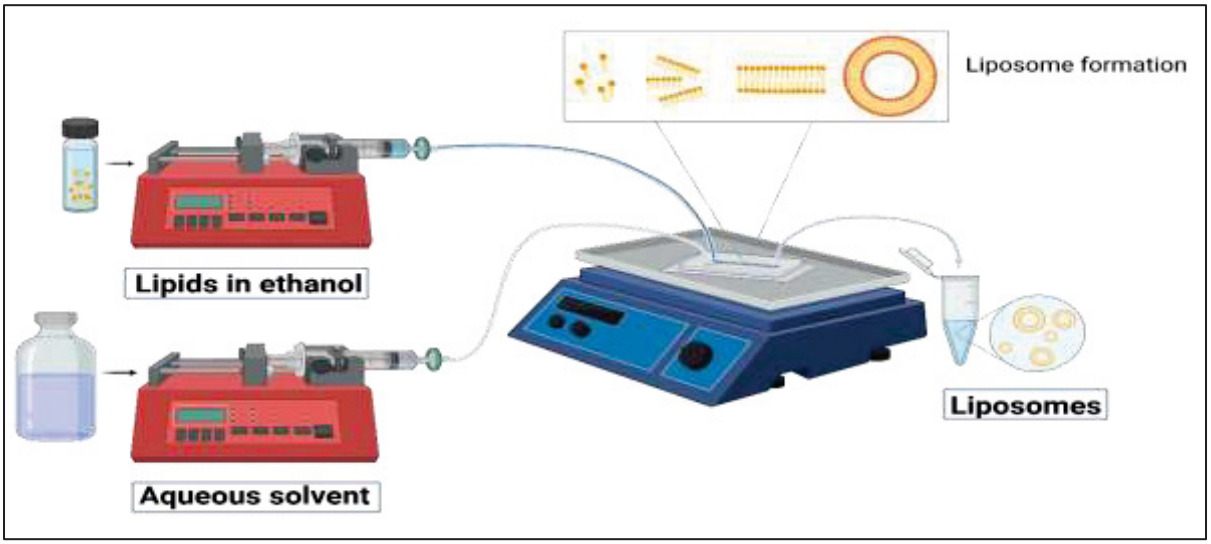

Figure 1.7 Microfluidic synthesis of liposomes
Adapted from Zouggari Ben El Khyat, C. (2022), Master's thesis, ÉTS

A common design in microfluidic mixing is hydrodynamic flow focusing, where a central lipid stream is compressed by aqueous streams from both sides. This enhances rapid mixing and enables precise control over liposome size. Adjusting the flow rate ratio (FRR) typically leads to smaller vesicles, while increasing the total flow rate (TFR) further improves mixing efficiency (Webb et al., 2023; Cheung and Al-Jamal, 2019).

To further improve mixing, the Periodic Disturbance Mixer (PDM) (Figure 1.8) was developed by López et al. (2020). It uses curved microstructures to introduce disturbances that enhance mixing and enable tunable size control between 52 and 200 nm. The PDM also maintains consistent zeta potential across varying conditions, which is important for biological stability.

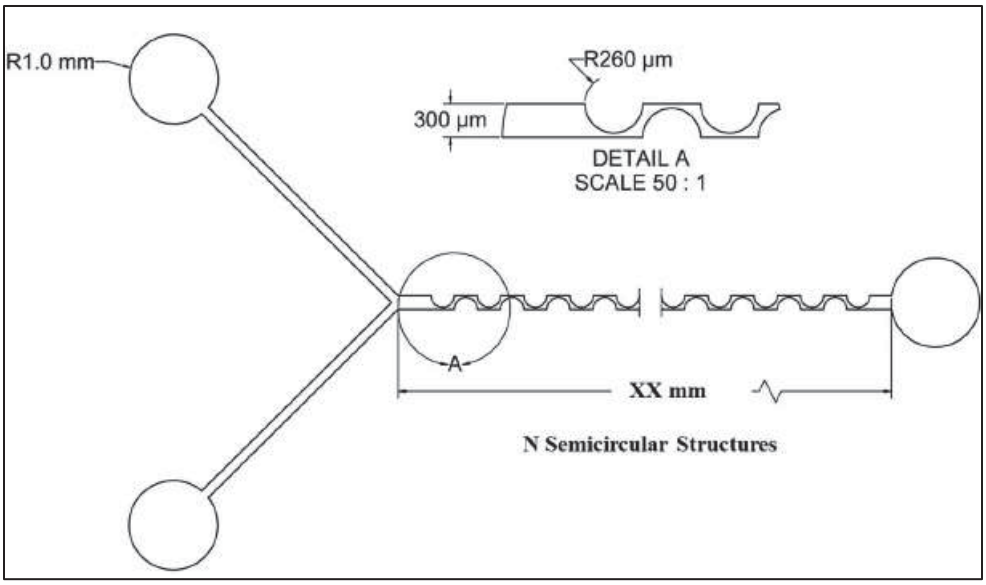

Figure 1.8 Schematic of the 3D-printed polydimethylsiloxane (PDM) micromixer design
Image taken from the thesis of Rubén Rodrigo López Salazar (2023)

In this project, the PDM micromixer developed by Rubén Rodrigo López Salazar was used to establish early protocols for liposome formation and protein encapsulation. During those trials, more protein consumption was observed, which prompted a transition to the Flex S system. Although the exact reason for the loss was not fully explored, the Flex S platform offered improved control over flow conditions and minimized material consumption.

The Flex S system (Precigenome) is a fully automated microfluidic platform offering real-time control over FRR and TFR. It is particularly suited for working with sensitive or expensive cargo such as proteins and RNA. Prior studies have shown that Flex S can achieve over 90% RNA encapsulation efficiency while producing uniform liposomes suitable for scale-up (Hou et al., 2021). Figure 1.9 shows the Flex S NanoGenerator system, which was used in this study for liposome and nanoparticle synthesis.

Figure 1.9 Flex S NanoGenerator system used for liposome and nanoparticle synthesis
Image reproduced from the official website of Precigenome

Statistical modeling approaches, including Design of Experiments (DoE) and Response Surface Methodology (RSM), are also being applied to further optimize microfluidic liposome synthesis. For example, López et al. (2025) used these tools to predict how formulation parameters influence particle size and drug loading, reducing the need for empirical trial-and-error.

While microfluidic systems offer several advantages, challenges remain. Residual ethanol from lipid solvents must be removed through purification steps such as ultracentrifugation, and maintaining consistent performance across parallel channels during scale-up requires careful control (Laouini et al., 2012).

In summary, microfluidic technology enables predictable, tunable, and scalable liposome production. In this study, combining the PDM and Flex S systems allowed us to progress from

initial liposome formation to more advanced protein-loaded formulations designed to mimic extracellular vesicles (EVs).

1.4 Protein Encapsulation in Nanoparticles

Proteins play essential roles in cell signaling, metabolism, and intercellular communication, and their therapeutic use has drawn significant interest. However, delivering functional proteins in vivo is complex due to their sensitivity to degradation and clearance. Liposomes offer a protective environment that can preserve protein structure and extend circulation time. Figure 1.10 presents a comparison of surface protein functionalities on EVs and liposomes, highlighting key molecules involved in immune evasion, targeting, and cellular uptake.

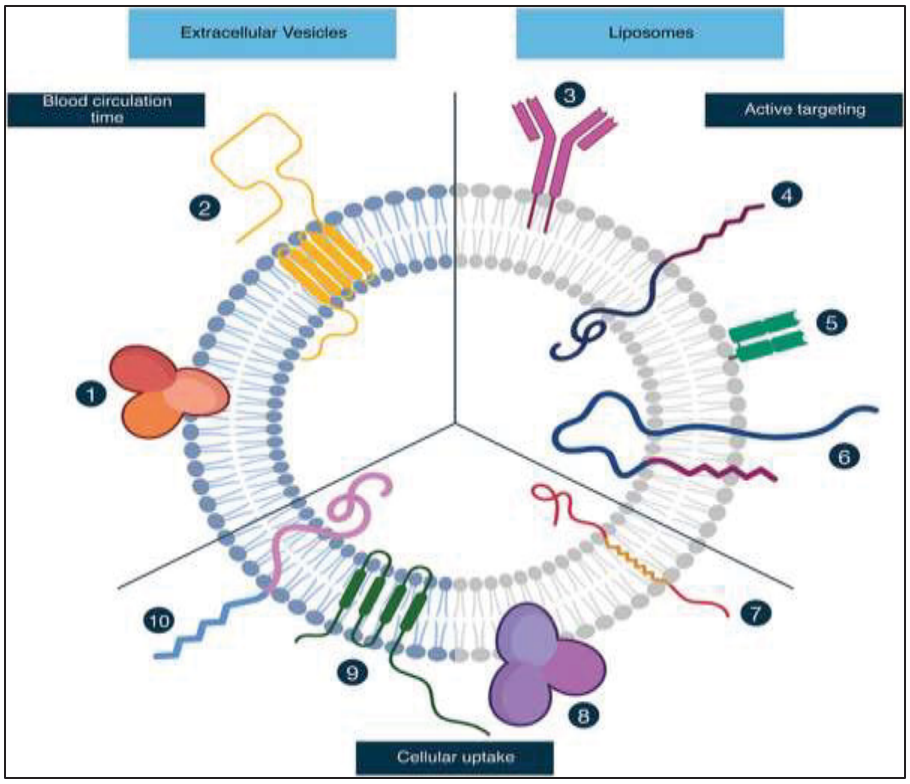

Figure 1.10 Surface proteins enhancing EV and liposome function
From Van der Koog et al., (2021)

Encapsulating proteins in liposomes helps shield them from enzymatic degradation and, with appropriate surface modifications, enables tissue-specific targeting (Sercombe et al., 2015; Bozzuto et al., 2015). However, the process must be optimized to avoid denaturation or loss of activity (Akbarzadeh et al., 2013). Techniques include freeze-thaw cycling (Laouini et al., 2012), electrostatic tuning (Mozafari et al., 2008), and microfluidic-based strategies (Wagner et al., 2002).

In this project, the aim was to mimic cancer-cell-derived EVs using SVs by loading two EV-relevant proteins: HSP70 and CD63. Before doing so, we tested protocol parameters using model proteins like albumin on both the PDM micromixer and Flex S system. Passive loading was selected to minimize complexity and protect protein integrity. HSP70, a cytosolic protein

involved in stress signaling, and CD63, a tetraspanin membrane protein associated with exosome biogenesis, were chosen for their biological relevance in EV function (van Niel et al., 2018; Mathieu et al., 2021). Figure 1.11 outlines the step-by-step microfluidic-based workflow used for protein encapsulation and purification, including synthesis via the PDM micromixer.

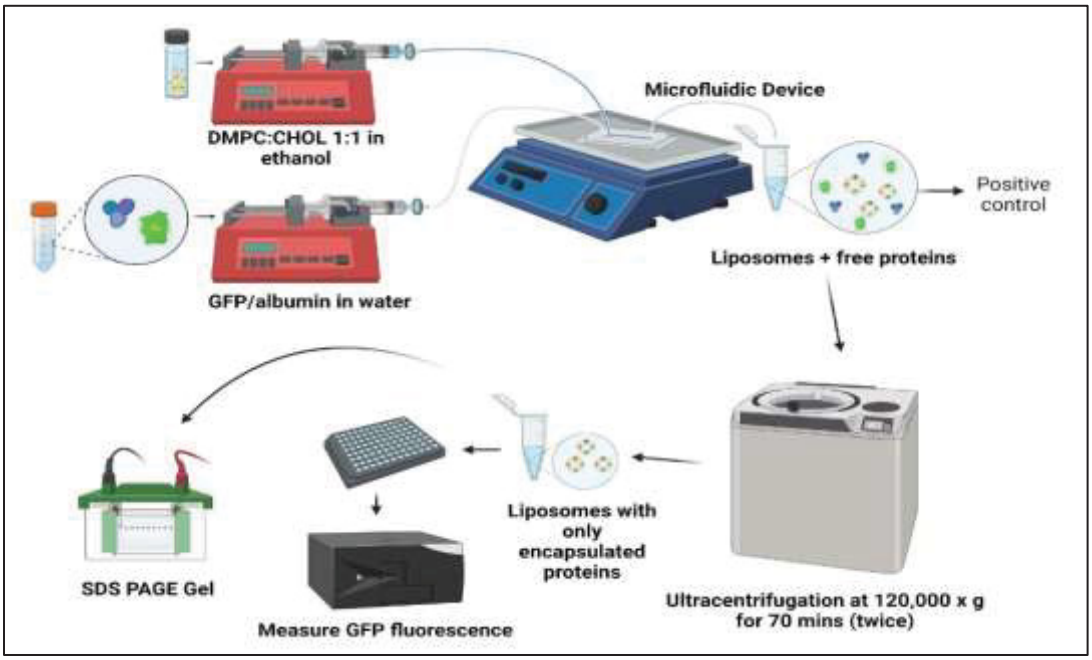

Figure 1.11 Microfluidic-based protein encapsulation and purification workflow using the PDM micromixer
Figure created with Biorender

These proteins were previously identified by our group as enriched in EVs derived from uveal melanoma cell lines and patient samples. Functional assays demonstrated that EVs carrying HSP70 and CD63 promoted fibroblast migration and in vivo tumor growth, supporting their role in pre-metastatic niche formation (Tsering et al., 2020).

1.4.1 Techniques for Protein Loading

Protein encapsulation methods fall into two main categories: passive and active loading. Passive loading involves mixing proteins with the aqueous phase during liposome formation, allowing some to become trapped during self-assembly. This method is gentle but typically results in low and variable efficiency (Sercombe et al., 2015; Akbarzadeh et al., 2013). For instance, passive loading of HSP70 into PS-based liposomes yielded under 20% efficiency (Schilling et al., 2009; Lee et al., 2014).

Active loading, on the other hand, uses transmembrane gradients (e.g., pH or ionic strength) to drive protein incorporation into pre-formed liposomes. Although this can improve loading efficiency, harsh conditions may compromise vesicle stability or protein structure (Kim et al., 2023).

Lipid composition also plays a significant role. Positively charged proteins like Green Fluorescent Protein (GFP) or Superoxide dismutase 1 (SOD1) interact well with anionic lipids such as 1,2-dimyristoyl-sn-glycero-3-phosphoglycerol (DMPG), resulting in higher loading through electrostatic interactions (Wang et al., 2025). Zwitterionic lipids like 1,2-Dimyristoyl-sn-glycero-3-phosphocholine (DMPC), frequently used in microfluidic setups, offer enhanced membrane stability and are compatible with ethanol-based formulations (Rahman et al., 2022). In our work, DMPC was selected for its ability to form stable bilayers suitable for encapsulation.

1.4.2 Challenges

Despite promising results, several challenges remain. Protein stability is a major issue—conditions during encapsulation can alter protein structure and function. Lipids like PS may enhance loading but compromise membrane integrity. Conversely, DMPC offers stability but

lower membrane interaction unless blended with helper lipids such as CHOL (Rahman et al., 2022; Kim et al., 2022).

Scalability is another concern. Microfluidic production is ideal for small-scale research but becomes difficult to standardize when scaled up, especially across multiple chips (Webb et al., 2023). Solvent removal also adds steps to the workflow.

Lastly, functional validation is essential. Proteins must remain active after encapsulation. One study found only 60% of BSA retained activity post-microfluidics (Patel et al., 2024). Overall, while technical hurdles remain, microfluidic encapsulation of EV-relevant proteins into liposomes offers a promising strategy for building biomimetic delivery systems. Our work contributes to this growing field by exploring different lipid formulations and evaluating microfluidic encapsulation approaches for loading EV-relevant proteins.

1.5 Conclusion

This chapter provided an overview of the rationale for using EVs and SVs in cancer research and drug delivery. While EVs play important roles in cell communication and are being explored for therapeutic use, challenges such as low yield and batch variability limit their clinical potential.

As a more controllable alternative, liposomes offer advantages in scalability, tunability, and safety. The use of microfluidic systems like the PDM and Flex S platforms has further improved liposome production, enabling more uniform and reproducible formulations, especially for sensitive cargo like proteins.

Protein loading techniques were also discussed, with a focus on passive encapsulation during microfluidic mixing. While some proteins, like HSP70, were successfully incorporated, others such as CD63 posed challenges due to their structural characteristics, including its multi-pass

transmembrane domains and sensitivity to structural modifications (Curley et al., 2025; Bobbili et al., 2025; Zhao et al., 2020).

Altogether, this background helped guide the experimental design in the following chapters, where SVs were engineered to mimic EV function using selected EV-relevant proteins.

CHAPTER 2

MATERIALS AND METHODS

2.1 Introduction

This chapter outlines the experimental procedures used to model cancer extracellular vesicles (EVs) using synthetic liposomes. It includes detailed protocols for EV isolation from colorectal cancer (CRC) cells, preparation of liposomes using microfluidic systems, and encapsulation of selected proteins to mimic EV content. Characterization techniques were employed to assess the physicochemical properties of both EVs and liposomes, followed by cellular uptake studies to evaluate their functional behavior. Figure 2.1 shows a schematic overview of the experimental workflow and organization of this chapter.

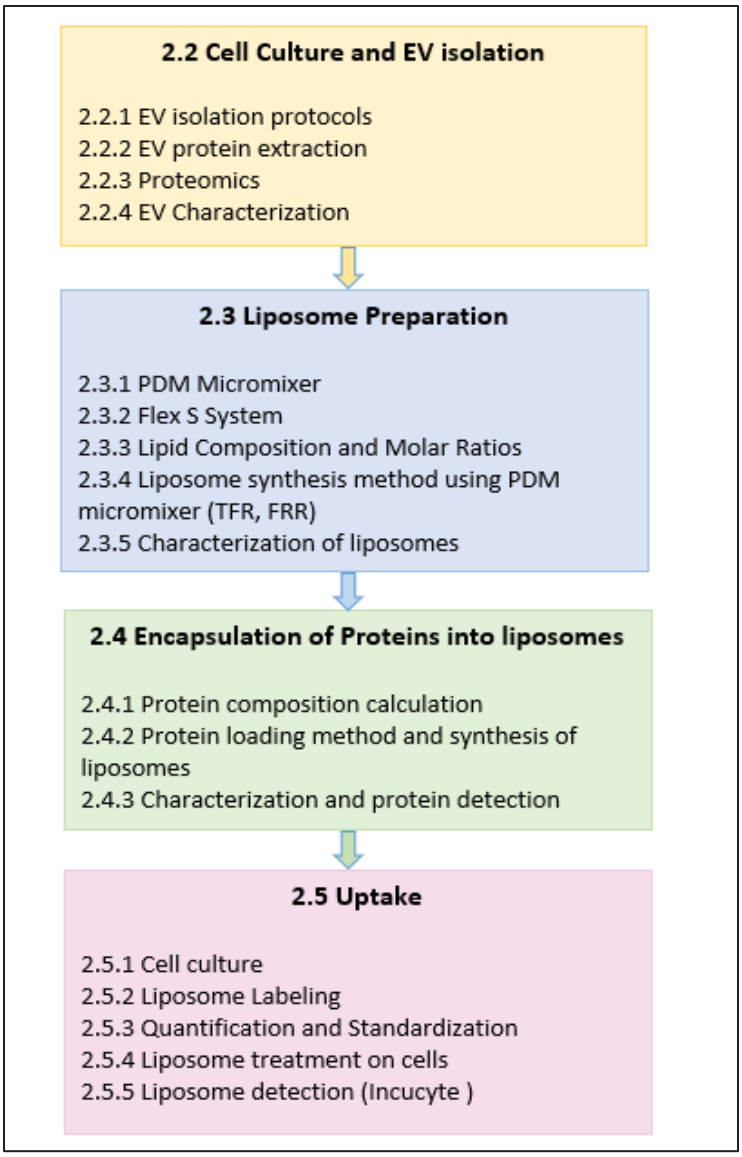

Figure 2.1 Overview of Chapter 2: Materials and Methods

2.2 Cell culture and EV isolation

The human CRC cell line SW620, originally derived from a lymph node metastasis of a primary tumor, was used in this study. Due to its high tumorigenic and metastatic potential, SW620 is commonly employed in CRC research. Stein et al. (2020) reported that these cells express MACC1, a metastasis-associated gene, and demonstrate a high frequency of liver metastasis *in vivo*, supporting their relevance for studying metastatic mechanisms. SW620 cells were kindly provided by Dr. Peter Metrakos lab at the Research Institute of the Mc Gill University Health Centre. Upon receipt, frozen cells were thawed rapidly in a 37°C bead bath for approximately 2 minutes. The cell suspension was then transferred into a T-75 culture flask containing 15 mL of pre-warmed complete Dulbecco's Modified Eagle Medium/Nutrient Mixture F-12 (DMEM/F-12) to dilute residual Dimethyl sulfoxide (DMSO) and support initial recovery. Cells were incubated overnight at 37°C with 5% CO_2 in a humidified atmosphere prior to the first medium change.

Complete culture medium was prepared using DMEM/F-12 (Gibco, USA), supplemented with 10% fetal bovine serum (FBS; Gibco, USA), 5 mL of 100 mM sodium pyruvate (Gibco, USA), 9 mL of 45% glucose solution (Sigma-Aldrich, USA) to reach a final glucose concentration of 4.5 g/L, and 5 mL of penicillin-streptomycin (10,000 U/mL penicillin and 10,000 µg/mL streptomycin; Gibco, USA).

To reduce contamination from bovine-derived EVs, FBS was subjected to ultracentrifugation at 120,000 × g for 18 hours at 4°C, followed by filtration through a 0.22 µm membrane. This exosome-depletion method effectively minimizes residual vesicle content (Beckman Coulter, 2020).

Cells were maintained at 37°C with 5% CO_2 and the culture medium was refreshed every 2–3 days. Subculturing was performed upon reaching 80–90% confluency. Cells were washed twice with Phosphate Buffered Saline (PBS) and detached using 0.25% trypsin-EDTA (Gibco, USA) for 3–5 minutes at 37°C. Trypsin activity was neutralized by adding an equal volume of

complete medium. The cell suspension was centrifuged at 500 × g for 5 minutes, and the resulting pellet was resuspended in fresh medium. Cells were then seeded into new flasks at a 1:3 to 1:5 split ratio, depending on confluency and growth rate.

2.2.1 EV isolation protocols

EVs were isolated from the conditioned medium of SW620 cells using differential ultracentrifugation, a widely accepted method for obtaining high-purity EVs. Prior to collection, cells were cultured in exosome-depleted DMEM/F-12 for 48 hours to allow EV secretion into the medium. This timepoint was selected to balance EV yield with cell viability, as prolonged incubation may increase cellular stress and release of apoptotic bodies. The overall workflow for EV isolation is illustrated in Figure 2.2.

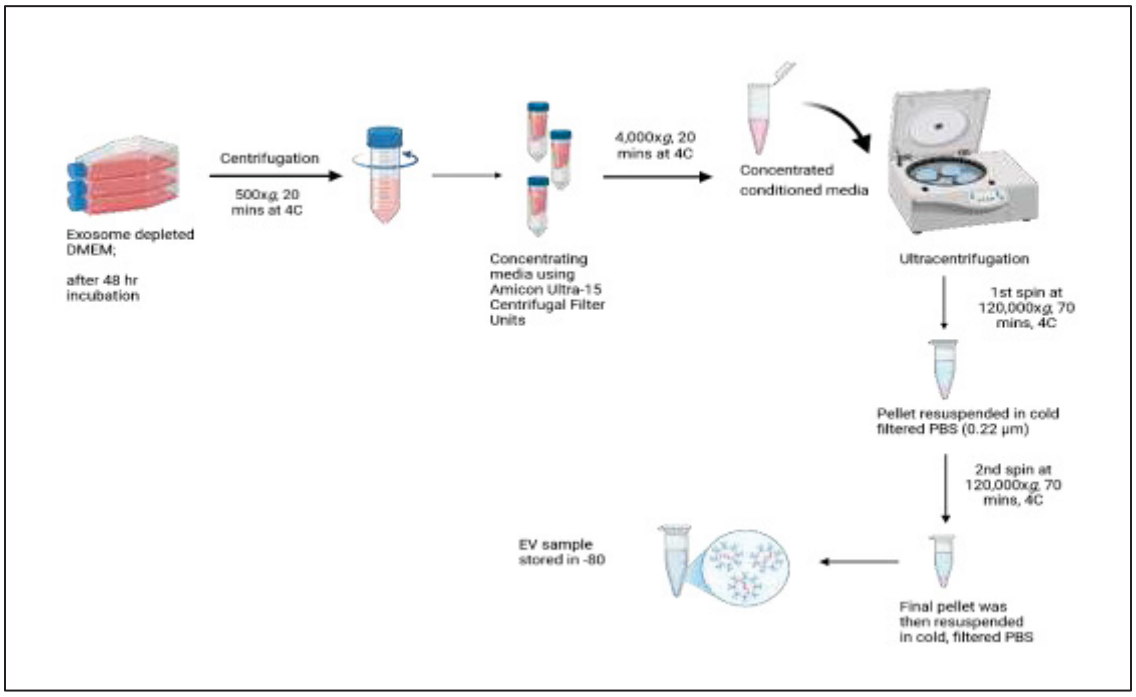

Figure 2.2 Schematic representation of extracellular vesicle (EV) isolation from SW620 conditioned medium
Created using Biorender

After 48 hours, the conditioned medium was carefully collected to avoid disturbing the adherent cell layer. The medium was first centrifuged at 500 × g for 20 minutes at 4°C to remove cells and large debris. It was then concentrated and further clarified using Amicon Ultra-15 Centrifugal Filter Units (100 kDa MWCO, Millipore, USA) by centrifugation at 4,000 × g for 20 minutes at 4°C. The flow-through was discarded, and the process was repeated until the entire volume had been processed. In total, approximately 540 mL of conditioned medium was used per isolation cycle.

Following concentration, the medium was filtered through a 0.22 µm syringe filter (Millipore, USA) to remove any remaining particles larger than the vesicle size range. The filtered medium was then transferred into polycarbonate ultracentrifuge tubes and subjected to ultracentrifugation at 120,000 × g for 70 minutes at 4°C using an Optima MAX-XP ultracentrifuge (Beckman Coulter, USA) equipped with a TLA-110 rotor. After centrifugation, the supernatant was discarded, and the EV pellet was resuspended in 1 mL of cold, filtered PBS (0.22 µm).

A second ultracentrifugation step was performed under the same conditions (120,000 × g for 70 minutes at 4°C) to remove residual non-vesicular contaminants. The final pellet was then resuspended in 100–200 µL of cold, filtered PBS. The pellet was often faint and difficult to visualize, so care was taken during handling to avoid sample loss or vesicle damage. As a practical aid, the outer tube wall was marked prior to centrifugation to indicate where the pellet would form.

The final EV preparation was aliquoted into multiple tubes to avoid repeated freeze-thaw cycles, which can compromise vesicle integrity. Each tube was labeled with the isolation date and stored at −80°C until further use.

During early optimization, low EV yield was a recurring issue, particularly after the low-speed centrifugation steps. Improvements in yield were achieved by refining centrifugation parameters, ensuring optimal cell confluency prior to medium collection, and balancing the rotor carefully. This optimized protocol resulted in consistent and reproducible EV isolations suitable for downstream characterization and functional studies.

2.2.2 EV protein extraction

Proteins were extracted from isolated EVs to prepare samples for downstream applications, including proteomic profiling and functional assays. EVs were lysed using radioimmunoprecipitation assay (RIPA) buffer supplemented with 1% protease inhibitor cocktail (Sigma-Aldrich, USA). This lysis method was selected to efficiently disrupt the vesicle membrane while preserving protein integrity. Protease inhibitors were essential, as EVs inherently contain proteolytic enzymes that could degrade internal cargo. The workflow for EV protein extraction is illustrated in Figure 2.3.

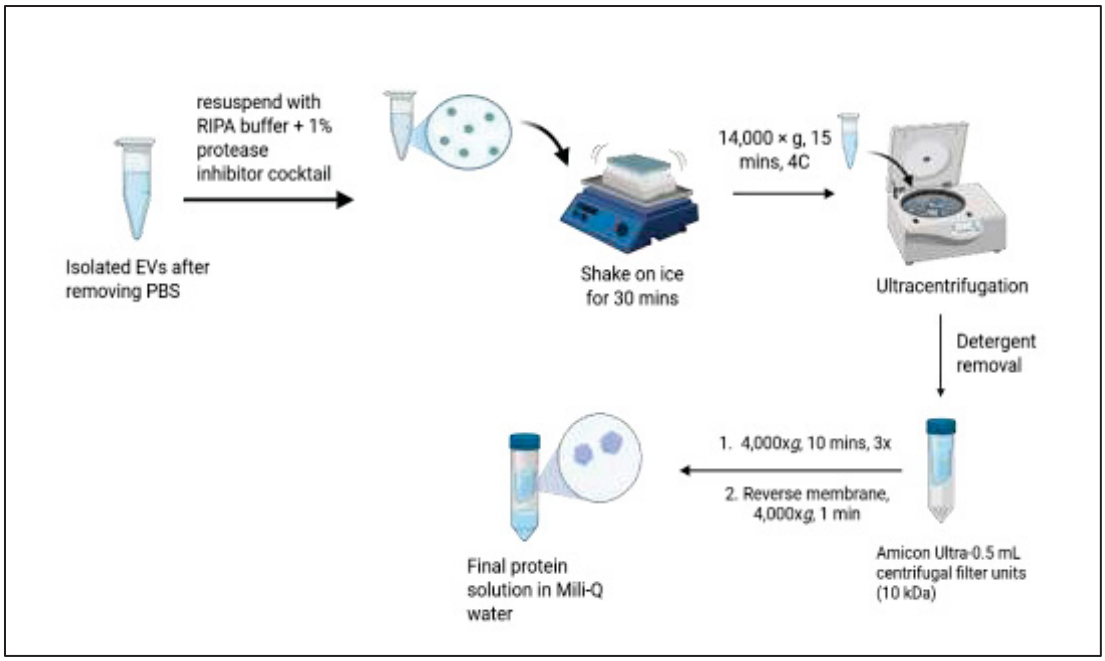

Figure 2.3 Workflow for protein extraction from extracellular vesicles (EVs)
Created using Biorender

The lysate was incubated on ice for 30 minutes, with gentle mixing every few minutes to enhance lysis while preventing thermal degradation. Following incubation, samples were centrifuged at 14,000 × g for 15 minutes at 4°C to pellet insoluble debris. Tubes were carefully balanced using water-filled counterparts to ensure safe and accurate centrifugation.

Since RIPA buffer contains ionic detergents that can interfere with mass spectrometry and enzymatic assays, detergent removal was necessary prior to analysis. This was achieved using Amicon Ultra-0.5 mL centrifugal filter units (10 kDa MWCO, Millipore, USA), which retain proteins while allowing small molecules to pass through. The lysate was added to the filter and centrifuged at 4,000 × g for 10 minutes at 4°C. This process was repeated twice to ensure effective detergent removal. A final reverse spin (4,000 × g for 1 minute) was performed to recover proteins that may have adhered to the filter membrane. In earlier trials, noticeable protein loss occurred at this step; the reverse spin was introduced to improve recovery.

The final protein solution was brought to a total volume of 700 µL using cold Milli-Q water to ensure consistency across replicates. To minimize degradation due to freeze-thaw cycles, proteins were aliquoted into smaller volumes and were stored at −80°C for proteomic analysis. The remaining volume was divided into three equal aliquots designated for liposome production.

2.2.3 Proteomics

Proteomic profiling of EV-derived proteins was performed in collaboration with the RI-MUHC Proteomics Core Facility. As the facility required specific sample preparation protocols, all samples were processed according to their guidelines to ensure compatibility with the LC-MS/MS analysis workflow. Protein concentrations were standardized to approximately 10 µg per sample, as recommended for optimal sensitivity in liquid chromatography–tandem mass spectrometry (LC-MS/MS).

Prior to submission, protein concentrations were quantified using the BCA assay (Thermo Fisher Scientific) to ensure consistency across samples. To meet volume requirements for LC-MS/MS input, each sample was concentrated to ≤50 µL using Amicon Ultra-0.5 mL centrifugal filter units (10 kDa MWCO, Millipore, USA). This step also helped remove excess buffer components that could interfere with mass spectrometry.

Protein identification was carried out via LC-MS/MS. The resulting data were processed using Scaffold DDA (v6.6.0, Proteome Software), which enabled high-confidence filtering, identification, and organization of detected proteins. Proteomic results were later used to compare EV-derived protein cargo with that of SVs, providing insight into how effectively the engineered systems mimicked natural EVs.

2.2.4 EV Characterization

Isolated extracellular vesicles (EVs) were characterized using multiple techniques to evaluate their size, concentration, surface charge, and morphology. These analyses were essential to confirm the successful isolation of EVs and assess their purity and stability for downstream applications. An overview of various analytical techniques used for EV and SV characterization is shown in Figure 2.4.

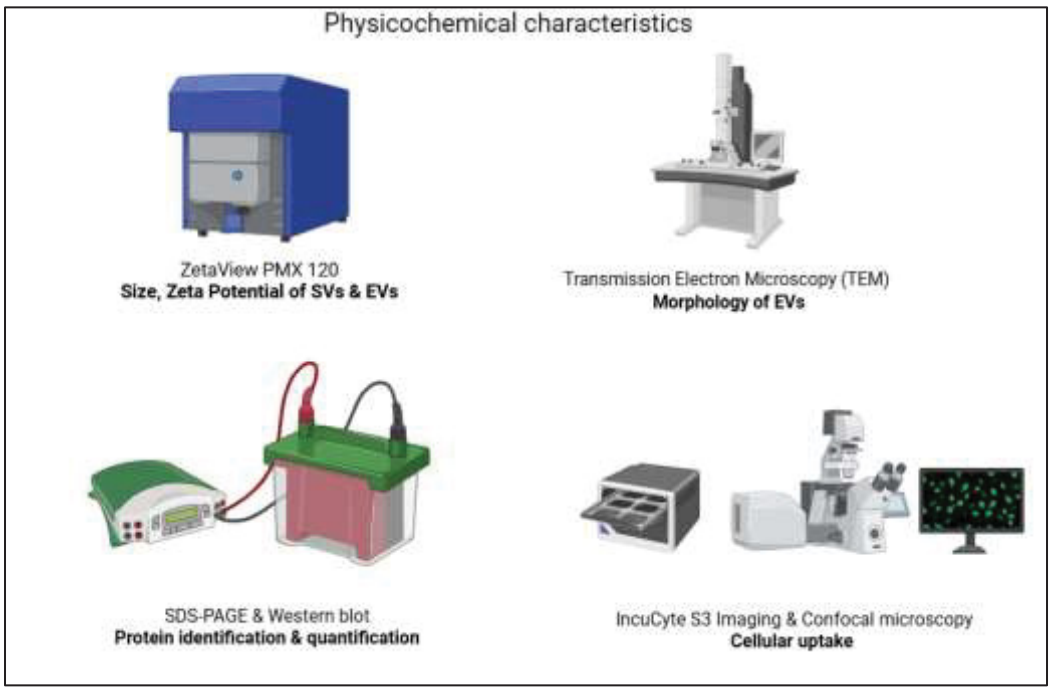

Figure 2.4 Overview of analytical techniques used to characterize the physicochemical properties of extracellular vesicles (EVs) and synthetic vesicles (SVs)
Adapted from Biorender

Measurement of Size, Concentration, and Surface Charge

Nanoparticle tracking analysis (NTA) was performed using the ZetaView PMX-120 (Particle Metrix, Germany) (Figure 2.5) to determine the size distribution and concentration of EVs. This technique tracks the Brownian motion of individual vesicles in suspension and calculates their hydrodynamic diameter based on diffusion speed. Particle concentration was also quantified by measuring the number of vesicles per unit volume.

Figure 2.5 ZetaView PMX 120 nanoparticle tracking analyzer (Particle Metrix) used for measuring size distribution and zeta potential of extracellular vesicles (EVs) and synthetic vesicles (SVs)

EV samples were diluted in Milli-Q water to achieve a concentration within the instrument's optimal detection range. Dilution factors ranged from 1:100 to 1:1,000, adjusted based on initial readings. Each sample was measured at a controlled temperature. Zeta potential, a measure of surface charge, was also assessed using the same instrument. This parameter is critical for evaluating colloidal stability.

Visualization of EV Morphology

Transmission electron microscopy (TEM) shown in Figure 2.6 was used to visualize the morphology of the isolated EVs. A small volume of EV suspension was deposited onto Formvar-carbon coated copper grids and allowed to adsorb. The samples were then negatively stained with 2% uranyl acetate to enhance membrane contrast. TEM imaging revealed nano-sized vesicles with a spherical morphology and a visible lipid bilayer, consistent with previously reported EV structures.

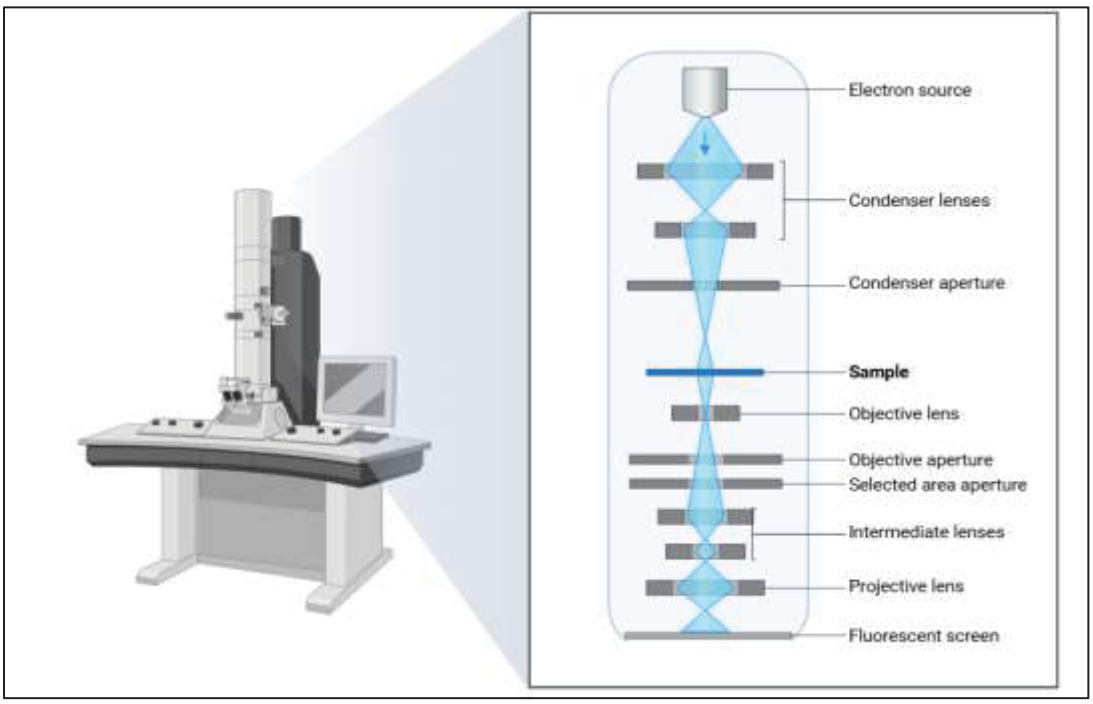

Figure 2.6 Schematic representation of Transmission Electron Microscopy (TEM)
Created using Biorender

By combining all these methods of NTA for size and concentration, TEM for visualization, and stain free SDS page gel for protein characterization, EVs were thoroughly characterized.

This provided confidence that the vesicles were properly isolated and suitable for downstream studies.

2.3 Liposome Preparation

Liposomes were synthesized using microfluidic technology, which enables the production of nano-sized particles with controlled size, uniformity, and reproducibility. Two microfluidic platforms were employed in this study: the Periodic Disturbance Mixer (PDM micromixer) and the Flex S NanoGenerator™ system. Both systems operate on the same principle of rapid mixing of a lipid solution (organic phase) with an aqueous phase inside microchannels, resulting in spontaneous liposome formation at the interface.

2.3.1 PDM Micromixer

Initial experiments were conducted using the PDM micromixer to establish baseline protocols and test various parameters. Liposomes were formed using a lipid mixture of 1,2-dimyristoyl-sn-glycero-3-phosphocholine (DMPC) and cholesterol (CHOL), which was dissolved in ethanol. These early trials focused on empty liposome synthesis to optimize flow rate ratios (FRR), total flow rates (TFR), and rinsing protocols.

To prepare for synthesis, microfluidic chips were preheated to 42°C, and lipid mixtures were sonicated at 45°C for 5 minutes to ensure complete dissolution, following the method described by Zinger et al. (2021). The microfluidic chip used is shown in Figure 2.7.

Figure 2.7 Polydimethylsiloxane (PDMS)-based microfluidic chip used for the synthesis of synthetic liposomes via passive mixing
Originally developed by López et al. (2021)

The organic and aqueous phases were introduced into the system using programmable syringe pumps. After each run, the system was cleaned with filtered 20% ethanol and Milli-Q water (40 mL/h, 4 mL total per wash). Additionally, the organic phase line was rinsed at 20 mL/h for 150 seconds between runs to minimize carryover from residual lipids or proteins.

Although the PDM micromixer was effective for protocol standardization, it required a higher input of protein for encapsulation. Given the limited availability and cost of EV-relevant proteins, the Flex S system was adopted for subsequent protein loading experiments due to its improved efficiency with smaller sample volumes.

2.3.2 Flex S System

The Flex S NanoGenerator™ is an automated microfluidic platform that allows for fine-tuned control of flow rates, mixing, and temperature. This system addressed many limitations

encountered with the PDM setup, particularly during protein encapsulation. Its automated design reduced sample handling errors, minimized material loss, and improved batch-to-batch consistency. An image of the Flex S system used in this study is shown in Figure 2.8.

Figure 2.8 Flex S NanoGenerator system (Precision NanoSystems Inc.) used for the microfluidic synthesis of synthetic vesicles (SVs)

Liposome synthesis using the Flex S system followed the same lipid formulation and general workflow. The key advantages of this platform included:

- Greater precision in adjusting flow parameters and temperature
- Reduced sample and protein wastage
- Enhanced reproducibility due to automation
- Higher production volumes suitable for downstream applications

Overall, using both the PDM and Flex S systems enabled method optimization at different stages of the project. The PDM system allowed for early troubleshooting and condition testing, while the Flex S platform supported reproducible, large-scale liposome production for protein loading and cellular assays.

2.3.3 Lipid Composition and Molar Ratios

Liposomes used in this study were prepared using a 1:1 molar ratio of DMPC (Avanti Polar Lipids, Catalog #850345C-1G) and CHOL (Sigma-Aldrich, Catalog #C8667-1G). This lipid combination is widely used due to its ability to form stable and well-ordered bilayer structures.

A 20 mM lipid stock solution was prepared in chloroform for long-term storage. CHOL was obtained in powder form and dissolved in chloroform to prepare the stock. Lipids were weighed using an analytical balance (Sartorius Cubis II, Model). To prepare 15 mL of a 20 mM lipid solution in a 1:1 molar ratio, the required mass of each lipid was calculated using the following equation:

$$\text{Mass}_{\text{lipid}} = R \times C_f \times V_T \times M_w \tag{2.1}$$

Where:

- R is the molar ratio of the lipid (0.5 for 1:1),
- C_f is the final lipid concentration (20 mM),
- V_f is the total volume (15 mL), and
- M_w is the molecular weight of the lipid (DMPC = 677.93 g/mol, CHOL = 386.65 g/mol).

For CHOL (powder), the required mass was:

$$\text{Mass}_{\text{CHOL}}=0.5\times0.02\times0.015\times386.65=0.0580\,\text{g} \quad (2.2)$$

For DMPC, which was supplied as a commercial lipid stock in liquid form at a concentration of 25 mg/mL, the required mass was first calculated:

$$Mass_{DMPC}= 0.5\times0.02\times0.015\times677.93=0.1017\text{g} \quad (2.3)$$

Then, the corresponding volume of DMPC stock solution needed was determined using:

$$\text{Volume}_{\text{DMPC}} = (0.1017\ \text{g} \times 1000) / (25\ \text{mg/mL}) = 4.068\ \text{mL} \quad (2.4)$$

Thus, 4.068 mL of liquid DMPC (25 mg/mL) was used.

Table 2.1 Molecular weights and calculated masses required to prepare 15 mL of a 20 mM lipid solution of DMPC and cholesterol (CHOL)

Component	Molecular Weight (g/mol)	Mass required for 15ml of 20mM Solution (g)
DMPC	677.93	0.1017
CHOL	386.65	0.058

The two lipids were added to a 20 mL PTFE-lined glass vial, followed by the addition of approximately 12 mL of chloroform. The mixture was vortexed thoroughly to ensure complete dissolution, and the volume was adjusted to 15 mL with additional chloroform.

The lipid solution was transferred to a round-bottom flask, and chloroform was evaporated using a rotary evaporator (Büchi Rotavapor R-215) at ~40°C in a water bath. After complete evaporation, the dried lipid film was placed in a vacuum desiccator for 16–18 hours to remove any residual solvent.

The following day, 30 mL of 100% ethanol was added to re-dissolve the dried lipids. The flask was gently swirled and sealed with parafilm, then placed in a 45°C water bath inside a sonicator for 5 minutes to facilitate complete dissolution. This resulted in a 20 mM lipid stock solution in ethanol.

Prior to use, the lipid stock was filtered through a 0.2 µm Polyvinylidene fluoride (PVDF) syringe filter (Millipore Sigma, Catalog #SLGV033RB) to remove any undissolved particles. The filtered solution was stored in a clean, labeled 20 mL glass vial at room temperature and used within one month to minimize ethanol-induced degradation.

This ethanol-based lipid stock was used for liposome production in both the PDM and Flex S systems. The 1:1 DMPC:CHOL ratio was maintained across all experiments to ensure batch-to-batch consistency.

2.3.4 Liposome synthesis method using PDM micromixer (TFR, FRR)

The microfluidic setup used for liposome synthesis is shown in Figure 2.9.

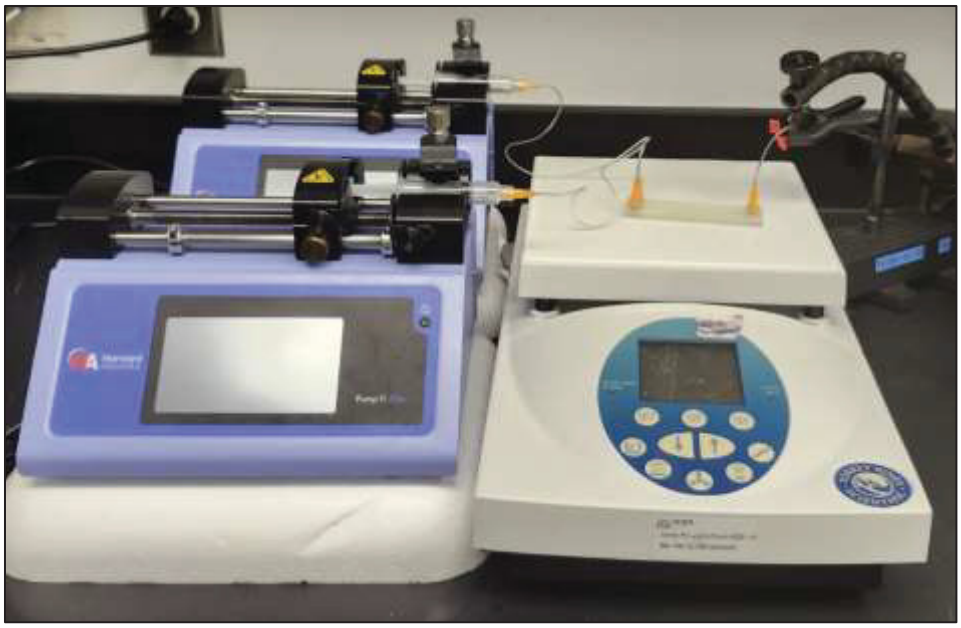

Figure 2.9 Experimental setup for microfluidic synthesis of synthetic vesicles (SVs) using the PDM micromixer

For each run, 10 mL syringes (BD Biosciences, Catalog #309604) were filled with filtered lipid solution and Milli-Q water, respectively. Before collecting any sample, the system was allowed to stabilize for approximately 60 seconds to ensure smooth and consistent flow. This step was essential for maintaining steady-state conditions during liposome formation.

The TFR and FRR combinations listed in Table 2.2 were systematically tested to determine optimal synthesis parameters for producing stable liposomes using the PDM micromixer.

Table 2.2 Total flow rate (TFR) and flow rate ratio (FRR) conditions used for liposome synthesis using the PDM micromixer

Experiment	TFR (mL/min)	FRR (Aqueous:Organic)
1	3	2:1
2	4	2:1
3	3	3:1
4	4	3:1
5	3	4:1

These experiments helped assess how flow speed and mixing ratios influenced liposome size and uniformity. In each run, the organic phase (lipid solution in ethanol) and aqueous phase (Milli-Q water) were injected into the microfluidic chip at predefined flow rates. Liposome suspensions were collected directly into clean, sterile glass vials and immediately stored on ice to minimize aggregation.

To remove ethanol and any unencapsulated material, the liposome suspensions were purified by ultracentrifugation at 120,000 × g for 70 minutes at 4°C using the Optima MAX-XP Ultracentrifuge (Beckman Coulter, USA) as shown in figure 2.10.

Figure 2.10 Beckman Coulter Optima™ MAX-XP ultracentrifuge used for the isolation and purification of extracellular vesicles SVs

This step was repeated twice to improve sample purity. After each centrifugation, the supernatant was carefully discarded, and the liposome pellet was resuspended in an equal volume of Milli-Q water.

The same flow conditions and purification protocol were maintained when transitioning to the Flex S system. However, the Flex S platform provided enhanced precision in flow control, which improved reproducibility and reduced batch-to-batch variability during liposome synthesis.

2.3.5 Characterization of liposomes

After synthesis, liposomes were characterized to assess their size distribution, concentration, and surface charge, key indicators of formulation quality and colloidal stability. All

measurements were performed using the ZetaView PMX-420 nanoparticle tracking analyzer (Particle Metrix, Germany). This system enables real-time tracking of individual particles to determine hydrodynamic diameter and particle count, and measures zeta potential to assess surface charge.

Prior to analysis, liposome samples were diluted in Milli-Q water to achieve the recommended concentration range. A typical dilution of 1:20,000 provided optimal particle counts (50–200 particles/frame). Each sample was analyzed in triplicate. The instrument's sensitivity was set to 75 and the trace length was adjusted to 30 frames for consistent size measurements and 15 frames for consistent zeta potential measurements.

The same measurement settings and conditions were used as in EV characterization to allow direct comparison between the two nanoparticle types. All samples were kept on ice before and after analysis to reduce aggregation.

2.4 Encapsulation of Proteins into liposomes

This part of the project focused on encapsulating proteins into SVs using a microfluidic approach. The goal was to build upon previous work conducted in the lab—specifically, the production of empty liposomes optimized by Zouggari Ben El Khyat (2022) using the PDM micromixer, and the original development and validation of the PDM system by López Salazar (2020). While earlier studies focused primarily on tuning liposome size and structural properties, this project aimed to advance the platform by incorporating biologically relevant proteins to mimic the functional cargo of natural EVs.

Albumin was used initially as a model protein to optimize encapsulation conditions and assess baseline performance. Once these protocols were established, the focus shifted to EV-associated proteins. Protein-loaded liposomes were synthesized using both the PDM

micromixer and the Flex S NanoGenerator™ systems. The following sections describe the materials used, detailed loading procedures, and results obtained from these experiments.

2.4.1 Protein composition calculation

Bovine serum albumin (BSA) was used due to their low cost, ease of handling, and frequent use in encapsulation studies. After the initial trials, the study moved toward encapsulating proteins that are commonly found in extracellular vesicles (EVs), CD63 and HSP70. Although attempts were made to extract these proteins from SW620-derived EVs, the yield was too low and not consistent. To move forward with a reproducible system, the proteins were sourced commercially. CD63 was obtained from Sino Biological (Catalog No. 1127-H08H) and used at a concentration of 250 µg/mL. HSP70 was obtained from R&D Systems (Catalog No. AP-100-100) and reconstituted to 250 µg/mL in Milli-Q water.

Protein volumes used during encapsulation were calculated based on the desired target dose and the known stock concentration using the equation:

$$\text{Protein volume (µL)} = \frac{\text{Target protein amount (µg)}}{\text{Stock concentration (µg/µL)}} \tag{2.5}$$

For example, to encapsulate 2 µg of protein from a 250 µg/mL stock (0.25 µg/µL):

$$\text{Protein volume} = \frac{2\ \text{µg}}{0.25\ \text{µg/µL}} = 8\ \text{µL} \tag{2.6}$$

To encapsulate 10 µg of protein:

$$\text{Protein volume} = \frac{10\ \text{µg}}{0.25\ \text{µg/µL}} = 40\ \text{µL} \tag{2.7}$$

The amount of Milli-Q water was then calculated by subtracting the protein volume from the total aqueous phase. The aqueous phase was determined based on the flow rate ratio (FRR = 2:1 aqueous:organic), which corresponds to two-thirds of the total production volume:

$$\text{Aqueous phase}(\mu L) = \frac{2}{3} \times \text{Total run volume} \quad (2.8)$$

Table 2.3 Aqueous phase composition for protein encapsulation at different volumes

Protein	Target Dose (µg)	Stock Conc. (µg/mL)	Production Volume (µL)	Aqueous Volume (µL)	Protein Volume (µL)	Water Volume (µL)	Notes
CD63	2	250	500	333.3	8	325.3	Initial trial
CD63	10	250	500	333.3	40	293.3	Higher dose
HSP70	2	250	500	333.3	8	325.3	Initial trial
HSP70	10	250	500	333.3	40	293.3	Higher dose
CD63	10	250	200	133.3	40	93.3	Optimized setup
HSP70	10	250	200	133.3	40	93.3	Optimized setup

2.4.2 Protein loading method and synthesis of liposomes

Proteins were encapsulated into liposomes using two microfluidic systems: the PDM micromixer and the Flex S NanoGenerator.

A. Protein Encapsulation Using the PDM Micromixer

Protein-loaded liposomes were synthesized using the PDM micromixer, a curved microchannel system designed to enhance mixing efficiency via Dean flow vortices (López Salazar, 2020). The setup included dual syringe pumps and a heated stage maintained at 42°C, following protocols optimized by Zouggari Ben El Khyat (2023).

Before each run, the chip was cleaned with Milli-Q water and 20% ethanol. A lipid-only rinse was also performed at 20 mL/h to clear residual materials from previous runs, with rinsing times adjusted based on the subsequent flow rates.

Protein encapsulation trials were performed at four total flow rates (TFRs: 60, 300, 600, and 900 mL/h), keeping the flow rate ratio (FRR) fixed at 2:1 (aqueous:organic). BSA was freshly diluted in Milli-Q water before each run. Liposome suspensions were collected in sterile 1.5 mL tubes and immediately stored on ice for downstream analysis. Table 2.4 outlines the specific flow conditions used during liposome synthesis using the PDM micromixer.

Table 2.4 Flow conditions for liposome synthesis using the PDM micromixer

Sample Type	Total Flow Rate (TFR) (mL/h)	Flow Rate Ratio (FRR) (Aqueous:Organic)	Aqueous Phase Flow (mL/h)	Lipid (Organic) Phase Flow (mL/h)	Rinsing Time (sec)
Empty or BSA sample 1	60	2:1	40	20	150
Empty or BSA sample 2	300	2:1	200	100	10
Empty or BSA sample 3	600	2:1	400	200	6
Empty or BSA sample 4	900	2:1	600	300	4

After synthesis, liposome suspensions were purified by ultracentrifugation at 120,000 × g for 70 minutes at 4°C using a Beckman Coulter Optima MAX-XP ultracentrifuge with a TLA-100 rotor. This step was performed twice to ensure removal of residual solvent and unencapsulated material. Following each spin, the supernatant was carefully discarded, and the pellet was resuspended in Milli-Q water. The final pellet was suspended in 200 µL of Milli-Q water and stored at 4°C for downstream analysis.

While the PDM micromixer was effective for testing different flow conditions, protein input requirements were relatively high, especially at faster flow rates. To address this, the Flex S NanoGenerator system was adopted for subsequent encapsulation experiments, allowing for reduced input volumes and improved sample retention.

B. Protein Encapsulation Using the Flex S NanoGenerator

The Flex S NanoGenerator™ (Precigenome, USA) is an automated microfluidic system designed for precise synthesis of lipid nanoparticles. Compared to manual micromixer setups, it offers enhanced control over flow rate, temperature, and production volume. For each run,

the device was preheated and primed with 5 µL of ethanol to stabilize internal channels. A new single-use chip was inserted, and 25 µL of PBS was applied along chamber walls to minimize sample loss due to surface adsorption.

The aqueous phase (protein + Milli-Q water) was loaded into the left chamber, and the lipid phase (DMPC:CHOL in ethanol) into the right chamber. The system was operated at a 2:1 aqueous-to-organic flow rate ratio (FRR). Initial production volumes of 500 µL were reduced to 200 µL in later runs to maximize material retention in the outlet channel and ensure full sample recovery.

Protein solutions of CD63 and HSP70 were freshly prepared at 250 µg/mL for each run. Required protein and water volumes were calculated based on target input amounts (see Section 3.3.1). In some experiments, the lipid ratio was adjusted to 2:1 or 3:1 (DMPC:CHOL) to assess its effect on HSP70 encapsulation efficiency.

Liposome suspensions were collected in sterile Eppendorf tubes, stored on ice, and purified by ultracentrifugation twice at 120,000 × g for 70 minutes at 4°C. After the first spin, the pellet was diluted in Milli-Q water and re-centrifuged. Final pellets were resuspended in 200 µL Milli-Q water and stored at 4°C.

Control conditions included:

- Empty liposomes (aqueous phase = Milli-Q water only)
- Free protein controls (protein + water, with ethanol replacing lipids)

These controls were used to confirm that observed protein signals were due to actual encapsulation rather than surface adsorption or contamination.

2.4.3 Characterization and protein detection

Following synthesis, all liposome formulations—both empty and protein-loaded—were characterized using NTA and zeta potential measurements to assess particle size distribution, surface charge, and overall stability. Measurements were performed using the ZetaView® PMX-420 instrument (Particle Metrix, Germany).

Prior to sample analysis, the instrument was calibrated with 100 nm polystyrene beads (1:500 dilution in Milli-Q water) to confirm accurate particle tracking and laser alignment.

For size analysis, liposome samples were diluted in filtered Milli-Q water to achieve a concentration of 50–200 particles per frame, as recommended by the manufacturer. A 1 mL aliquot of the diluted sample was loaded into the sample cell, and measurements were collected across 11 positions with triplicate readings per position. The system settings were sensitivity = 75, shutter speed = 100, frame rate = 30 frames per second, and trace length = 30. The instrument software calculated the mean size, standard deviation, and particle concentration automatically.

Zeta potential was measured using the instrument's zeta cell module. Samples were diluted in low-conductivity Milli-Q water (<50 µS/cm) to minimize ionic interference. Measurements were performed in triplicate with a trace length of 15, and zeta potential was calculated based on electrophoretic mobility.

All liposome samples were washed by ultracentrifugation prior to measurement to eliminate residual ethanol and unincorporated components. Controls included free protein solutions and empty liposomes, which were analyzed under identical conditions. The system was rinsed thoroughly between samples with 2 mL of Milli-Q water to prevent cross-contamination, and care was taken to avoid air bubble formation during sample loading.

2.4.3.1 Protein Quantification by Micro BCA Assay

To confirm successful protein encapsulation, total protein content in liposome samples was quantified using the Micro BCA Protein Assay Kit (Thermo Scientific). After synthesis and purification, liposomes were lysed using RIPA buffer to release encapsulated proteins. Lysates were combined with the BCA working reagent in a 96-well plate and incubated at 37°C for 30 minutes. Absorbance was measured at 562 nm using a microplate reader.

Protein concentrations were determined by comparison to a BSA standard curve and normalized to lipid input volume for cross-sample comparison. Each measurement was performed in technical duplicates or triplicates to ensure reproducibility.

To minimize variability, only freshly prepared or properly stored samples were used, and potential protein loss during ultracentrifugation was considered when interpreting results.

2.4.3.2 Protein detection by Stain-Free Gel

Protein detection was also confirmed using stain-free gel electrophoresis. A 4–20% Mini-PROTEAN® TGX Stain-Free™ gel (Bio-Rad) was used. Samples were mixed with reducing buffer prepared by combining 120 µL of 4× Laemmli buffer and 12 µL of β-mercaptoethanol (BME), enough for approximately 10 samples. For each run, 30 µL of sample was combined with 11.4 µL of reducing buffer, then heated at 95°C for 5 minutes.

Electrophoresis was carried out at 150 V for 30 minutes using 800 mL of running buffer. Gels were imaged immediately after the run under UV illumination using the ChemiDoc™ MP

imaging system (Bio-Rad). Control lanes included purified CD63 and HSP70 proteins to verify expected band positions.

2.5 Uptake

2.5.1 Cell culture

Two CRC cell lines, SW620 and HCT 116, were selected for uptake studies due to their relevance in liver metastasis models. Cells were thawed and cultured in T-25 or T-75 flasks using DMEM/F12 supplemented with 10% fetal bovine serum (FBS), 4.5 g/L glucose, 5 ml 100mM sodium pyruvate, and 1% penicillin-streptomycin. Once 80% confluency was reached, cells were passaged using 1 mL of 0.25% trypsin-EDTA and incubated at 37°C for 2 minutes. Detached cells were centrifuged at 500 × g for 5 minutes, resuspended in fresh medium, and counted using trypan blue exclusion and the Countess™ automated cell counter.

For IncuCyte-based uptake assays, SW620 and HCT116 cells were seeded in 96-well plates (Corning 3595) at a density of 2500 cells per well in 100 µL of media. Plates were incubated overnight to allow cell adherence before treatment (Figure 2.11)

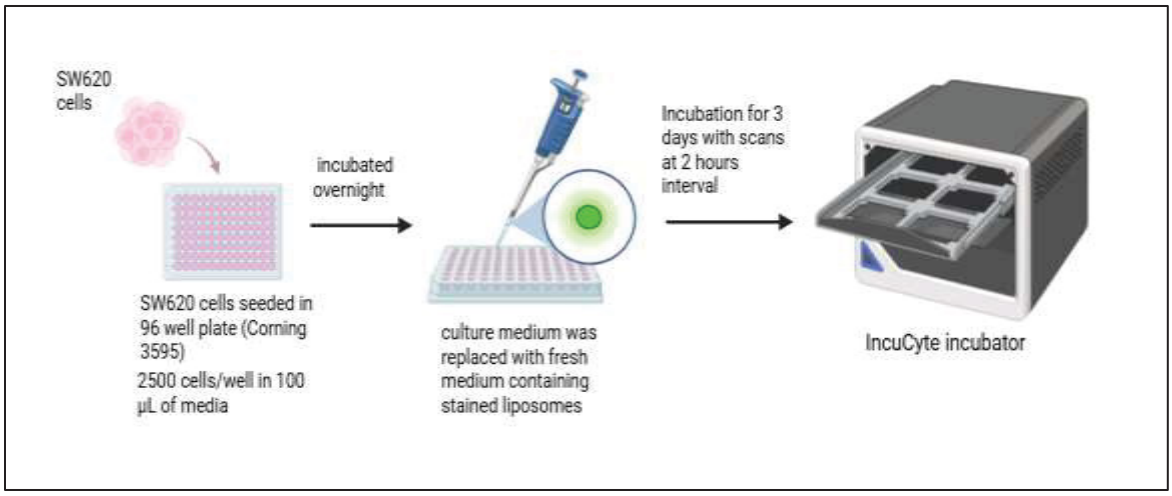

Figure 2.11 Workflow for IncuCyte-based cellular uptake assay
Created using Biorender

2.5.2 Liposome Labeling

To enable visualization of liposome internalization, samples were fluorescently labeled using the lipophilic dye sp-DiIC18 (3) (Thermo Fisher Scientific). For each sample, 100 µL of liposome suspension was incubated with 11.1 µL of 100 µ M dye solution, yielding a final dye concentration of 10 µ M. Incubation was carried out at room temperature for 30 minutes in the dark.

Following staining, unbound dye was removed by ultracentrifugation at 120,000 × g for 70 minutes at 4°C. Pellets were resuspended in 200 µL of Milli-Q water and stored at 4°C until use. These labeled liposomes were then used for cellular uptake assays via IncuCyte imaging, as detailed in the following section.

Control conditions included dye-only samples and unstained liposomes to confirm signal specificity and rule out non-specific background fluorescence.

2.5.3 Quantification and Standardization

To standardize the number of liposomes used in each treatment, particle concentration was determined using the ZetaView PMX-420 nanoparticle tracking analyzer. The average particle concentration obtained from ZetaView measurements was used to calculate the volume of liposomes required to deliver approximately 1×10^9 particles per well in uptake experiments.

2.5.4 Liposome treatment on cells

After 24 hours of incubation to allow cell attachment, the culture medium was replaced with fresh medium containing stained liposomes. The number of particles added per well was standardized based on ZetaView measurements to ensure consistency across experiments.

Cells were treated with varying concentrations of liposomes to optimize dosing conditions for subsequent protein encapsulation studies. In select experiments, uptake was compared between empty and protein-loaded liposomes to evaluate the potential impact of protein cargo on internalization efficiency.

2.5.5 Liposome detection (Incucyte)

Live-cell imaging was performed using the IncuCyte® system to monitor liposome uptake in real time. Following treatment with DiIC18-labeled liposomes, the 96-well plate was placed in the IncuCyte incubator, and scans were scheduled at regular 2-hour intervals. Images were acquired using the red fluorescence channel to track internalized liposomes.

Fluorescence signal intensity was measured over time and used as an indicator of liposome uptake efficiency. This approach enabled non-invasive, time-resolved monitoring of

internalization under physiological conditions, supporting dose optimization for future protein-loaded formulations.

2.6 Conclusion

This chapter described the methods used to create and test synthetic vesicles designed to mimic extracellular vesicles (EVs) from colorectal cancer cells. It began with the isolation and analysis of natural EVs to understand their size, protein content, and structure. These findings helped to compare the characteristics of EVs with the synthetic vesicles.

Liposomes were produced using two microfluidic systems: the PDM micromixer and the Flex S NanoGenerator. Both allowed precise control over particle size and mixing conditions. After testing different flow rates and lipid compositions, stable liposomes were successfully made. Proteins,both model (like albumin) and EV-related (like HSP70 and CD63), were loaded into these liposomes to simulate the cargo of natural EVs.

After protein loading, the liposomes were analyzed for size, charge, and protein content. They were then tested in CRC cells to study how well they were taken up. The uptake experiments helped understand whether the synthetic vesicles could behave like natural EVs. Together, these methods created a step-by-step approach to design, test, and evaluate EV-like liposomes. This setup forms the foundation for the experimental results shared in the next chapter.

CHAPTER 3

RESULTS

3.1 Introduction

This chapter summarizes the main findings from the development and evaluation of EV-inspired liposomes. It begins with the characterization of native EVs from CRC cells and compares them with SVs produced using two microfluidic systems.

Protein encapsulation was tested using albumin, CD63, and HSP70 to assess loading efficiency across different formulations and flow conditions. Additional experiments focused on encapsulating total EV proteins into liposomes and comparing their content and uptake to native EVs.

The block diagram below provides a quick overview of the main sections included (Figure 3.1).

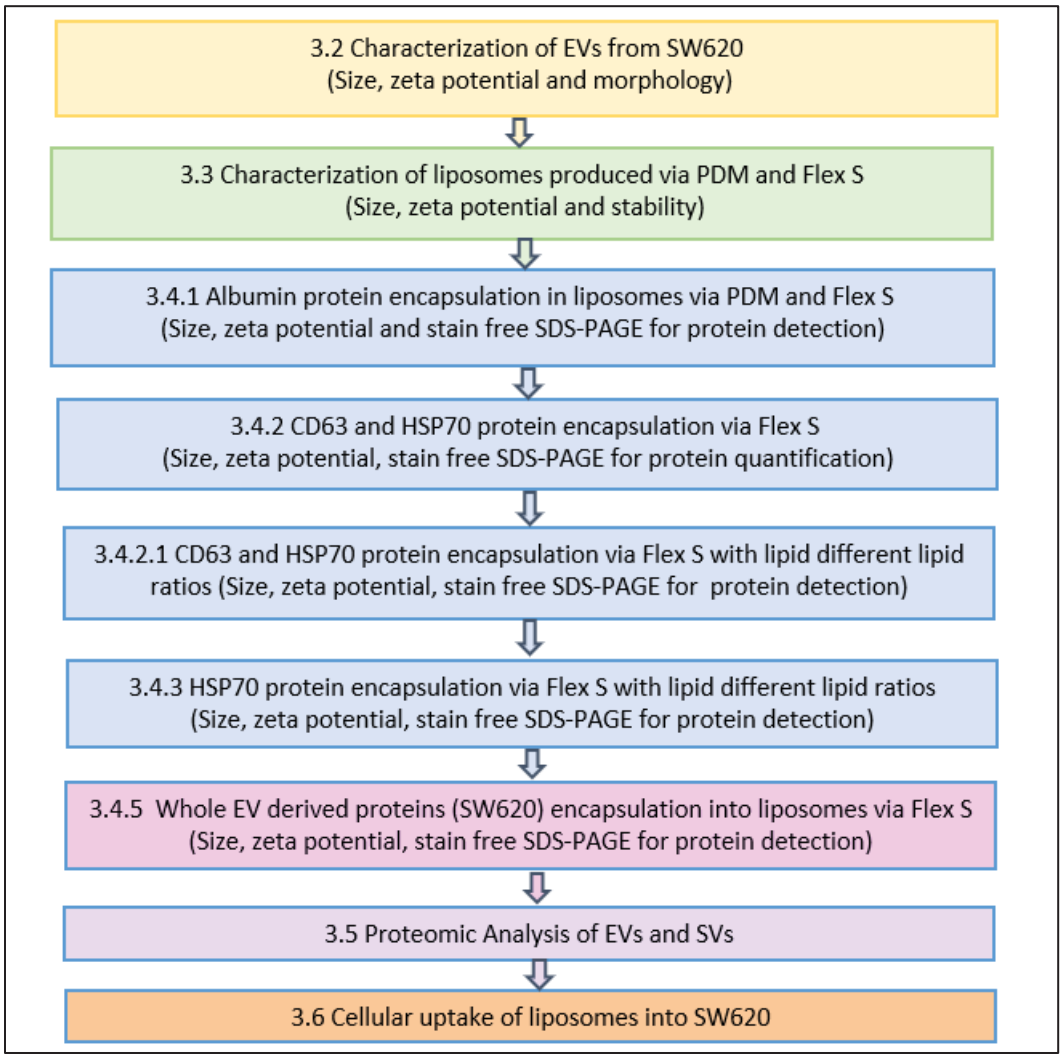

Figure 3.1 Summary of Results Chapter Structure

3.2 Characterization of Extracellular Vesicles (EVs) from SW620

After isolating EVs from SW620 CRC cells using ultracentrifugation, a series of characterization experiments were performed to check their size, charge, structure, and

protein content. This step was important before comparing them to synthetic liposomes later on in the project. The characterization was done using Zeta View for both size and zeta potential, TEM for visual confirmation of morphology. These experiments helped confirm whether the EVs were properly isolated and suitable for further use.

3.2.1 Size and zeta potential (ZetaView)

The size of the EVs was measured using the ZetaView® instrument, which works based on NTA. Three EV samples (EV1, EV2, and EV3) were tested to check for consistency. The size results were very close across all three replicates: 163.8 nm for EV1, 164.3 nm for EV2, and 168.4 nm for EV3, with an average of 165.5 ± 2.06 nm (Figure 3.2). These values are within the expected range for small EVs, especially those released from CRC cells (Théry et al., 2018).

The small difference in size between the samples and the low standard deviation show that the EVs were quite uniform. This means the isolation protocol worked well and gave a consistent batch of particles. Uniform size is important for experiments that compare EVs with SVs or when looking at how cells take up these particles. In earlier experiments, it was noticed that size sometimes increased when EVs were stored for too long or when the washing steps were not done carefully. These issues were later corrected by improving handling and timing during isolation. The final results showed a stable and reliable size distribution, and these EV samples were used as the standard for later comparisons with liposomes.

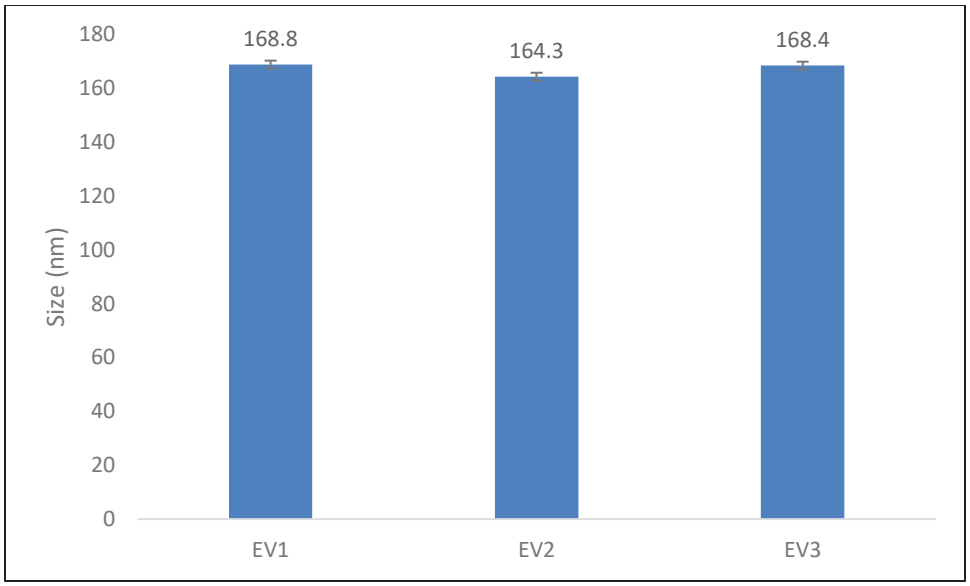

Figure 3.2 Size distribution of EVs measured by ZetaView

Zeta potential was measured using the same ZetaView instrument to understand the surface charge of the isolated EVs. This parameter is important because it gives an idea about the stability of the particles in suspension. When particles have a higher zeta potential (either strongly negative or positive), they tend to repel each other, which helps prevent aggregation over time. The surface charge of extracellular vesicles (EVs) derived from SW620 cells was evaluated (Figure 3.3). Three technical replicates were recorded, with zeta potential values of –36.29 ± 1.14 mV, –34.13 ± 0.95 mV, and –34.15 ± 0.73 mV. The average zeta potential was calculated as –34.85 ± 1.16 mV.

These values indicate that the EVs carried a strong negative surface charge, which is consistent with previously reported values for CRC derived EVs (Midekessa et al., 2020) A negative zeta potential suggests good colloidal stability and low aggregation in suspension. Minimal variation across the replicates also confirms consistency in the isolation and measurement process.

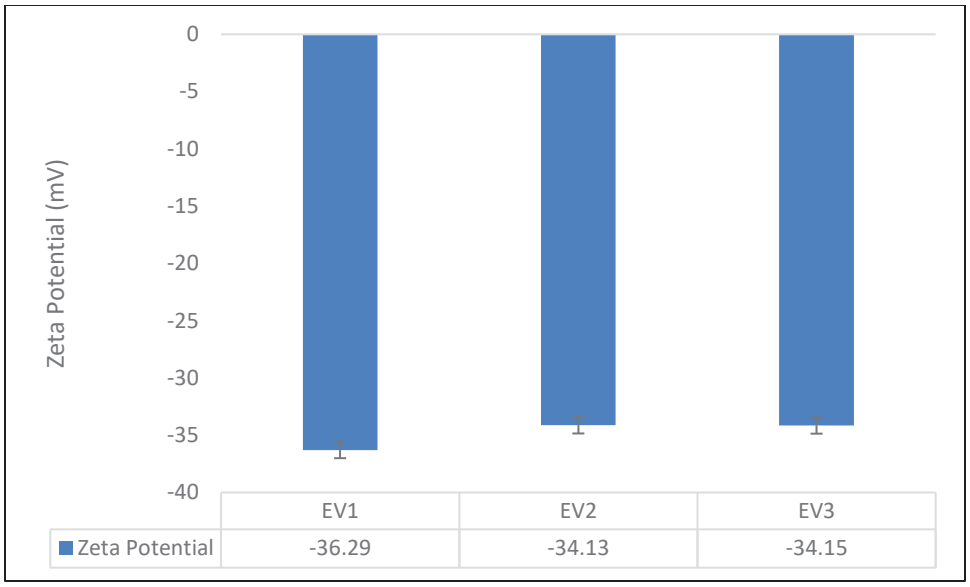

Figure 3.3 Zeta Potential of Isolated EVs from SW620 cells

3.2.2 Morphological Assessment by Transmission Electron Microscopy (TEM)

Transmission electron microscopy (TEM) was employed to evaluate the morphology of EVs isolated from SW620 CRC cells. Representative images from three technical replicates are shown in Figure 3.4. At 11,000× magnification (Figures 3.4A and 3.4B), the vesicles exhibited spherical morphology and appeared as membrane-enclosed structures with homogeneous electron density. These images confirm the structural integrity of the isolated vesicles and the effectiveness of the ultracentrifugation protocol.

A higher magnification image acquired at 30,000× (Figure 3.4C) provided enhanced resolution, clearly revealing the lipid bilayer surrounding each vesicle. The vesicle size and morphology are consistent with previously described small EVs, including exosomes derived from cancer cells (Théry et al., 2018). Collectively, these TEM observations validate the successful isolation of intact nano-sized EVs for downstream comparative analyses.

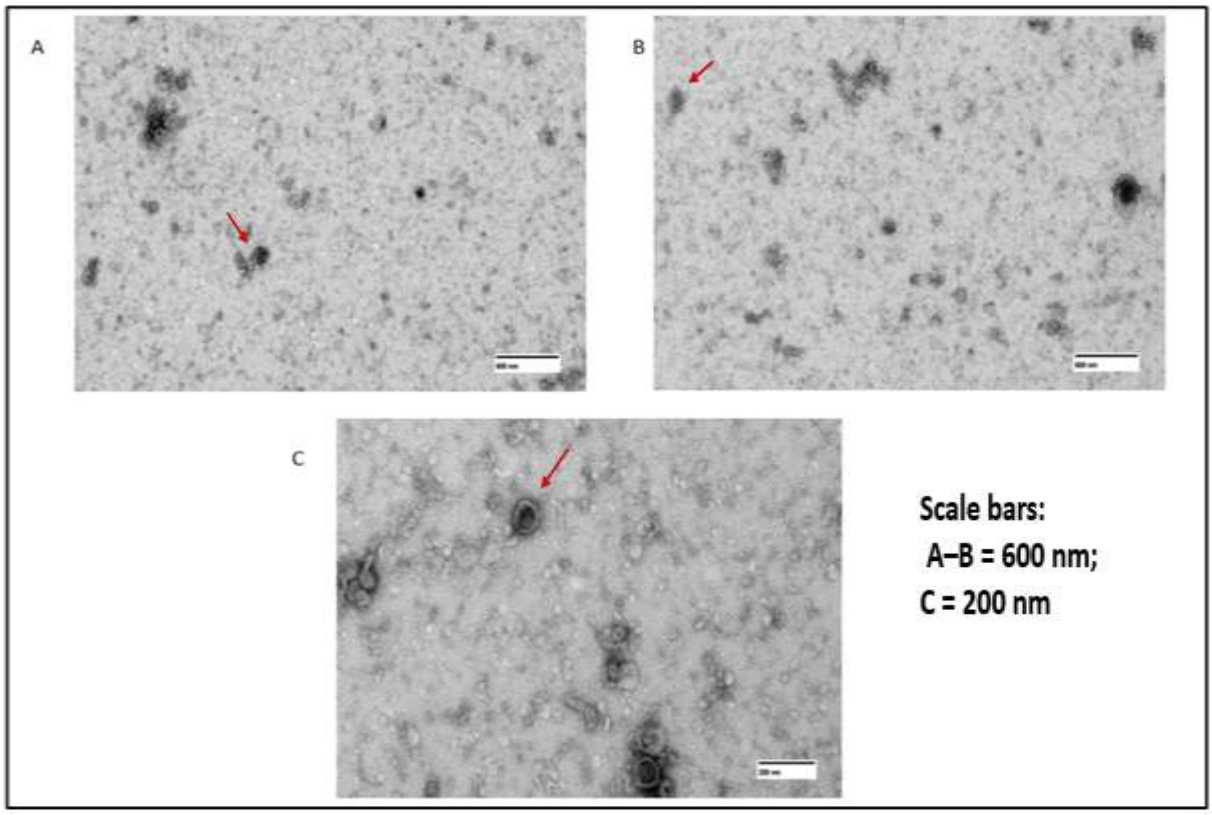

Figure 3.4 Morphological analysis of EVs from SW620 cells. (A–B) TEM at 11,000× shows spherical, membrane-bound vesicles. (C) At 30,000×, lipid bilayers are clearly visible. Scale bars: A–B = 600 nm; C = 200 nm

3.3 Liposome Synthesis Using the PDM System

3.3.1 Size Distribution and Stability of Empty Liposomes

Empty liposomes were synthesized using the PDM micromixer at different total flow rates (TFR), while maintaining a constant flow rate ratio (FRR) of 2:1 (aqueous:organic). This was chosen based on previous reports demonstrating that this ratio supports efficient ethanol dilution and controlled lipid self-assembly in PDM micromixer systems (López Salazar et al., 2020). Both experimental and modeling studies have shown that 2:1 balances solvent diffusion with bilayer formation, resulting in vesicles ranging from 27–200 nm and improved

polydispersity and stability compared to other ratios (López Salazar et al., 2021; Darooei Zadeh et al., 2021).

The goal was to understand how changing TFR affects liposome size and surface charge. Measurements were performed using ZetaView for both NTA and zeta potential (Figure 3.5 and Figure 3.6 respectively).

At 60 mL/h, the average liposome size was 178.7 nm, and the zeta potential was –25.09 ± 0.61 mV, indicating stable, negatively charged particles. Increasing the TFR to 300 mL/h resulted in a slightly larger size of 183.8 nm, with the zeta potential becoming less negative (–13.06 ± 0.62 mV). At 600 mL/h, the size increased further to 234.4 nm, and the zeta potential was estimated at –10.50 ± 0.70 mV, suggesting lower colloidal stability. Interestingly, at 900 mL/h, the size decreased to 205.4 nm, while the zeta potential returned to –13.87 ± 0.69 mV.

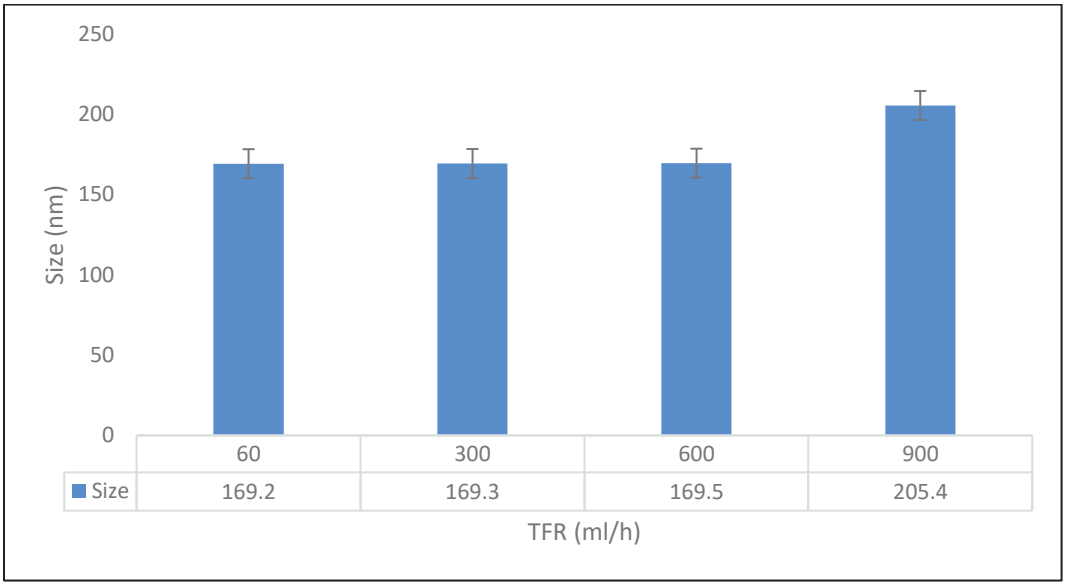

Figure 3.5 Size distribution of empty liposomes synthesized via PDM at varying TFRs (FRR 2:1). ZetaView analysis shows larger vesicles at higher TFRs, peaking at 600 mL/h

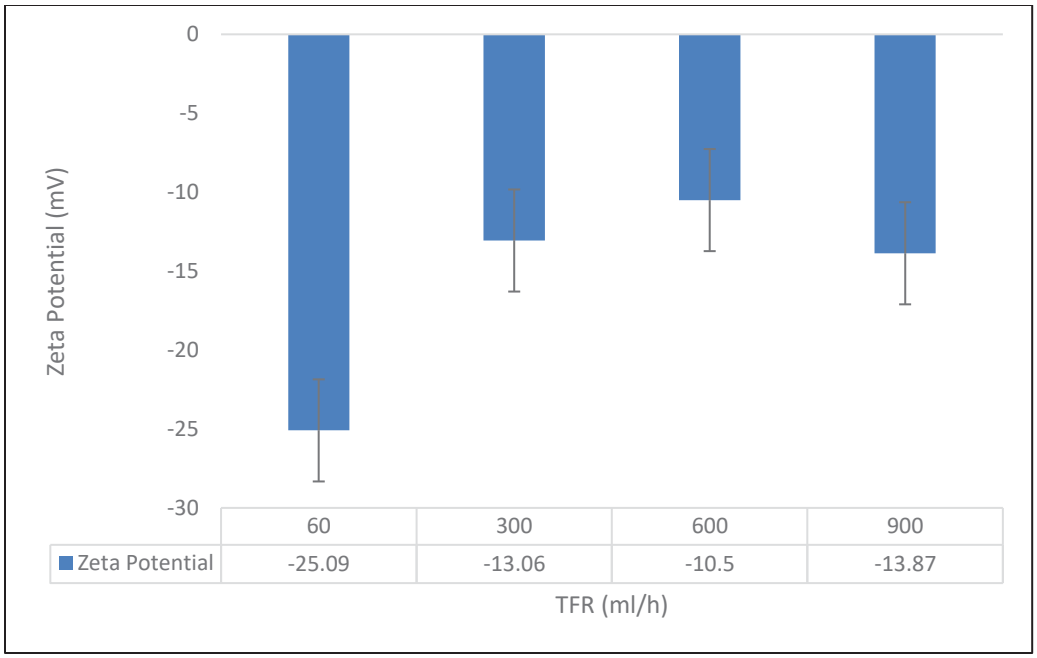

Figure 3.6 Zeta potential of empty liposomes synthesized using the PDM micromixer at varying total flow rates (TFR)

These results show that TFR plays a significant role in modulating both liposome size and surface charge. Higher flow rates likely reduce the precision of mixing inside the micromixer, leading to broader size distributions and weaker electrostatic stability. The shift in zeta potential between 300 and 900 mL/h, despite similar magnitudes, may reflect changes in lipid packing or interfacial interactions under different mixing conditions. Similar observations have been reported in other hydrodynamic flow-focusing systems (reviewed in Jahn et al., 2007; van Swaay and deMello, 2016).

3.3.2 Protein Loading Trials with Albumin

Albumin was selected as a model protein to evaluate the feasibility of passive protein loading using the PDM micromixer. Liposomes were synthesized using the PDM micromixer at four different total flow rates (TFRs): 60, 300, 600, and 900 mL/h, with the flow rate ratio (FRR) fixed at 2:1 for all conditions. The albumin-containing aqueous phase was introduced through

the designated inlet, and passive encapsulation was performed during vesicle formation. Following synthesis and purification, the size and surface charge of albumin-loaded liposomes were assessed using ZetaView. Size remained consistent across all conditions, ranging from 169.2 to 170.1 nm (Figure 3.7), suggesting that the presence of albumin did not significantly affect liposome formation. Zeta potential measurements (Figure 3.8) showed minor variation for 60–600 mL/h (–21.64 to –18.26 mV), but a notable increase in negative surface charge was observed at 900 mL/h (–54.54 mV), potentially reflecting differences in lipid packing or protein interaction at higher flow rates.

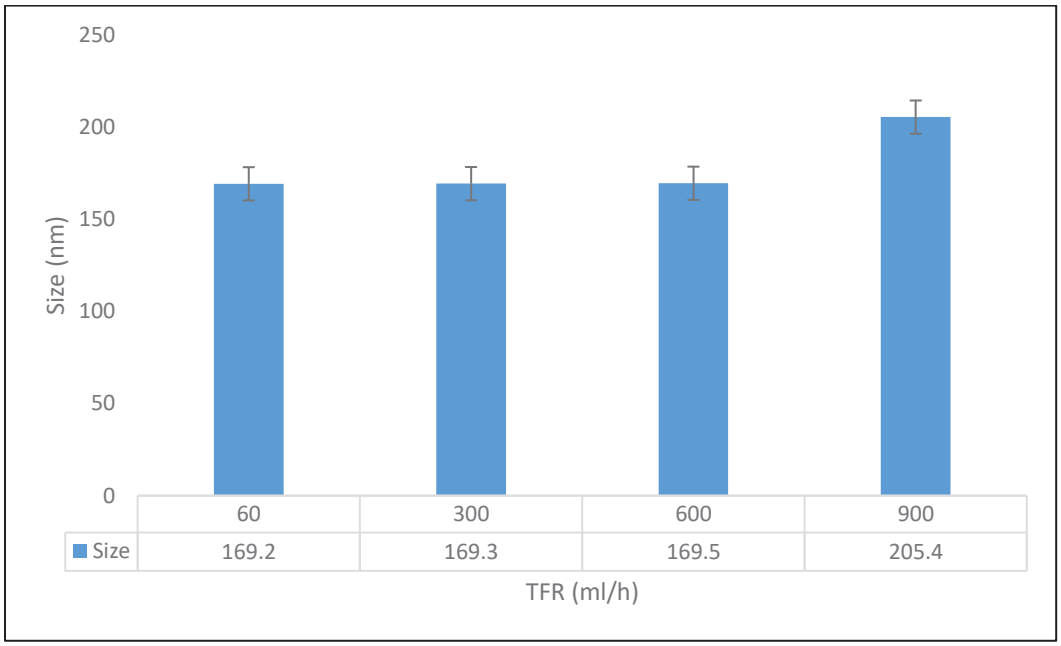

Figure 3.7 Size distribution of albumin-loaded liposomes synthesized using the PDM micromixer at different total flow rates (TFR). All formulations were prepared at an FRR of 2:1. Sizes were measured using ZetaView

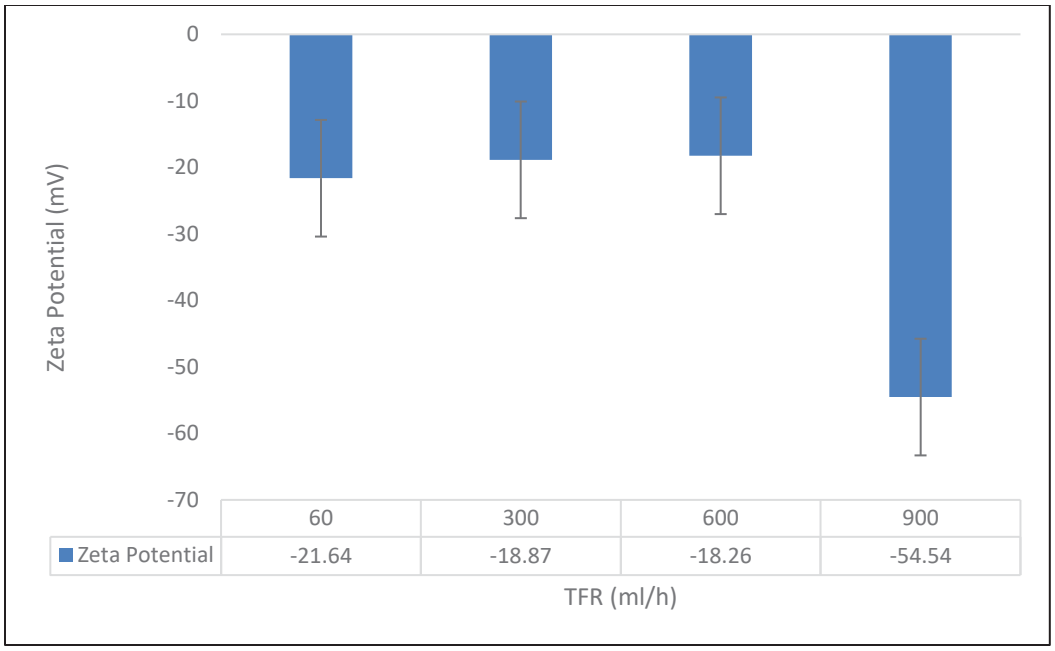

Figure 3.8 Zeta potential of albumin-loaded liposomes synthesized using the PDM micromixer at different total flow rates (TFR). Zeta potential was measured using ZetaView

Stain-free SDS-PAGE analysis was performed to detect protein retention post-encapsulation. Among all tested conditions, a faint band at approximately 66 kDa was observed only in the 600 mL/h sample (Figure 3.9), corresponding to the molecular weight of BSA. No visible bands were detected for other samples, indicating that either protein retention was minimal or below the gel's detection limit.

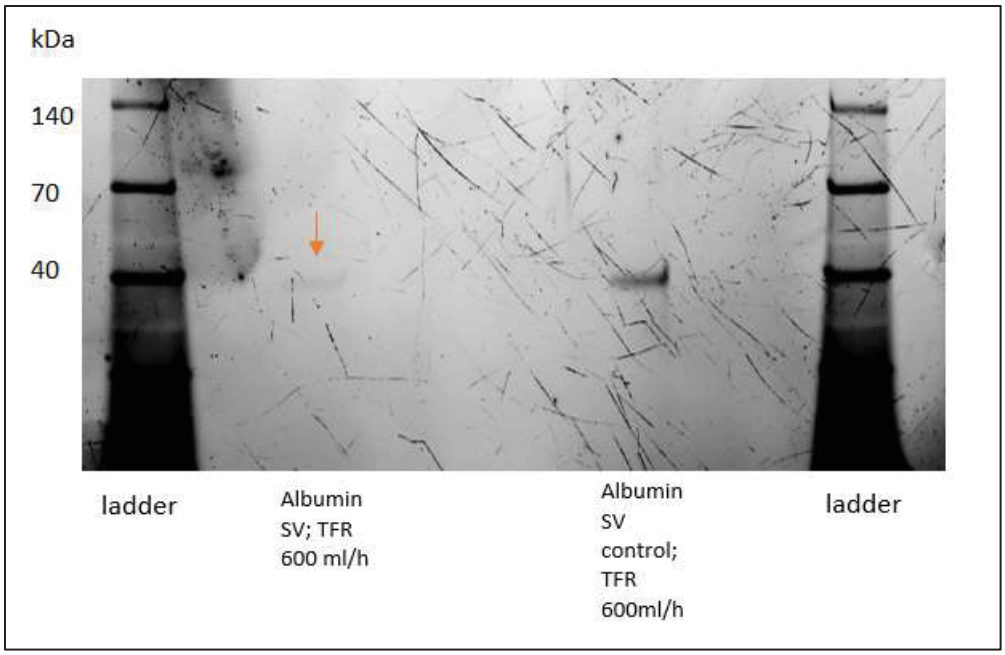

Figure 3.9 Stain-free SDS-PAGE analysis of albumin-loaded liposomes synthesized using the PDM micromixer. A faint band is observed near ~66 kDa in the SV lane, consistent with the molecular weight of BSA (orange arrow)

Although a band was detected at 600 mL/h, overall protein retention across conditions was low, and encapsulation was not reproducible at other flow rates. The process also required large working volumes, leading to high protein input with minimal recovery. These limitations became more important when planning to encapsulate extracellular vesicle (EV)-associated proteins such as HSP70 and CD63, which are significantly more expensive and available in limited amounts.

3.4 Liposome Synthesis Using the Flex S System

3.4.1 Albumin Encapsulation and Comparison with PDM

To evaluate passive protein loading across different microfluidic platforms, liposomes loaded with albumin were synthesized using both the PDM micromixer and the Flex S NanoGenerator system. These experiments were performed using a 33.3 μg/mL input concentration of BSA, selected based on previous trials, and the same lipid formulation (DMPC:CHOL, 1:1 molar ratio). Aqueous-to-organic flow rate ratios (FRRs) of 2:1, 3:1, and 4:1 were tested at total flow rates (TFRs) of 3 or 4 mL/min. The goal was to compare how both systems performed under matched conditions in terms of particle size, surface charge, and protein retention.

Particle size measurements using ZetaView showed that both systems produced liposomes in the expected range, typically between 140–175 nm (Figure 3.10). Flex S formulations tended to be slightly larger across most flow conditions, with the highest average size observed at TFR 4 mL/min and FRR 3:1 (177.5 nm). The PDM system produced smaller particles at higher FRRs, with the smallest size observed at TFR 3 mL/min and FRR 4:1 (138.9 nm).

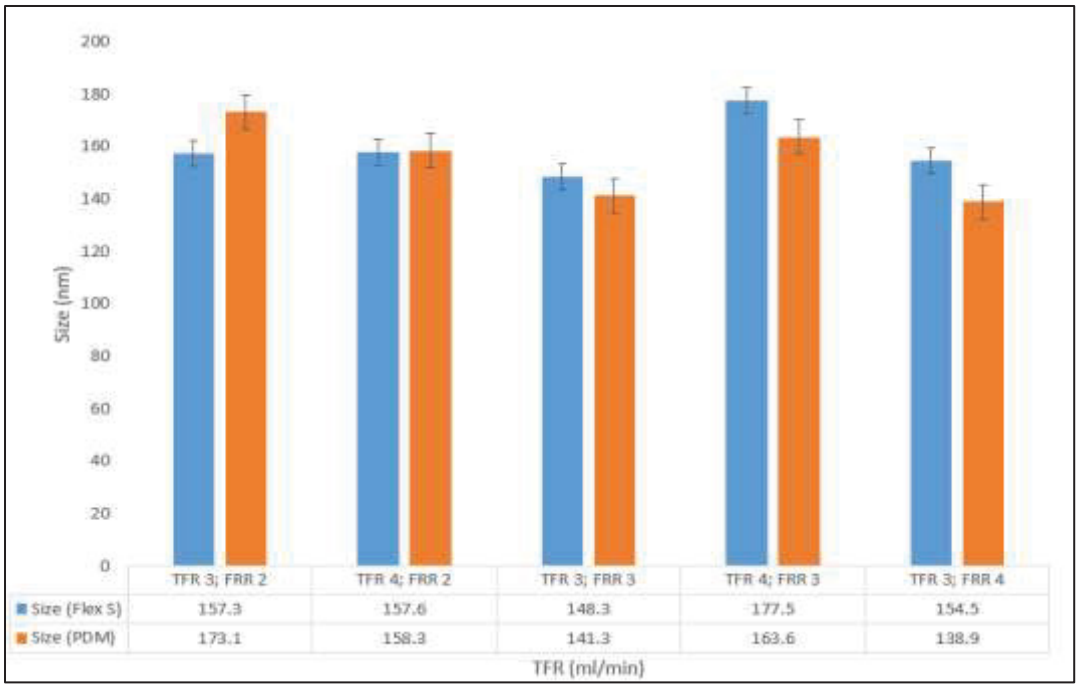

Figure 3.10 Size comparison of albumin-loaded liposomes synthesized using Flex S and PDM micromixers

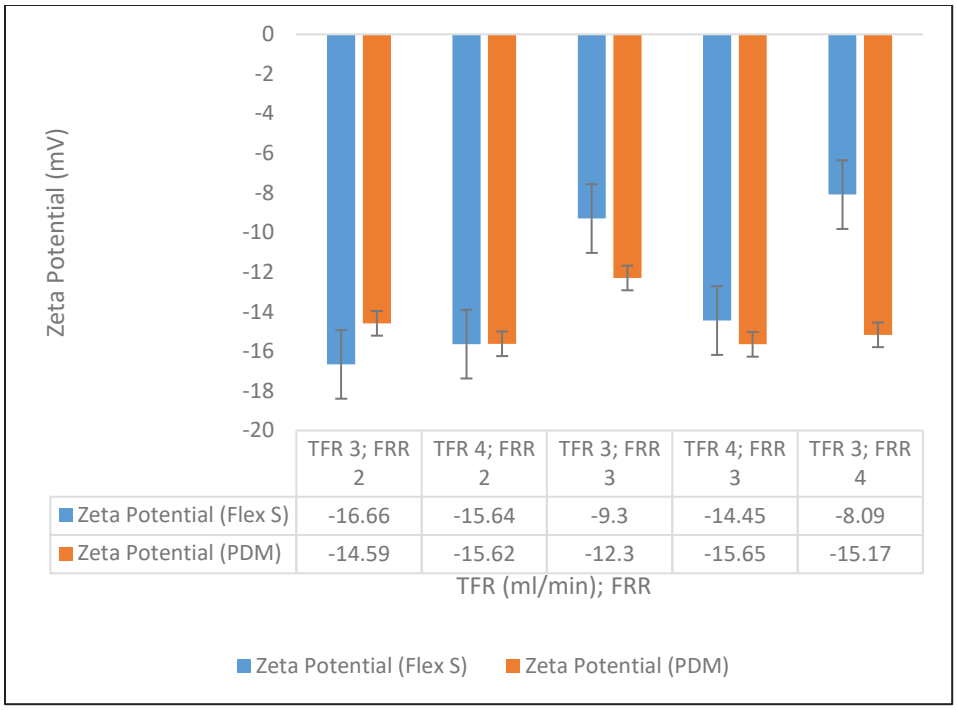

Figure 3.11 Zeta potential of albumin-loaded liposomes produced using Flex S and PDM systems

Zeta potential values (Figure 3.11) confirmed that all samples carried a negative surface charge, ranging from –8.09 mV to –16.66 mV. Overall, PDM samples showed slightly more negative surface charge compared to Flex S at the same TFR and FRR.

Although both systems produced albumin-loaded liposomes with comparable size and zeta potential, neither platform demonstrated strong retention of protein under the passive loading conditions used. Stain-free SDS-PAGE analysis (Figure 3.12 and Figure 3.13) showed no visible bands in the vesicle lanes across either system. Faint bands were occasionally seen in the supernatant lanes, suggesting that most of the input protein remained unencapsulated and was removed during purification. While the PDM gel appeared slightly cleaner and better contrasted, the outcomes were effectively the same.

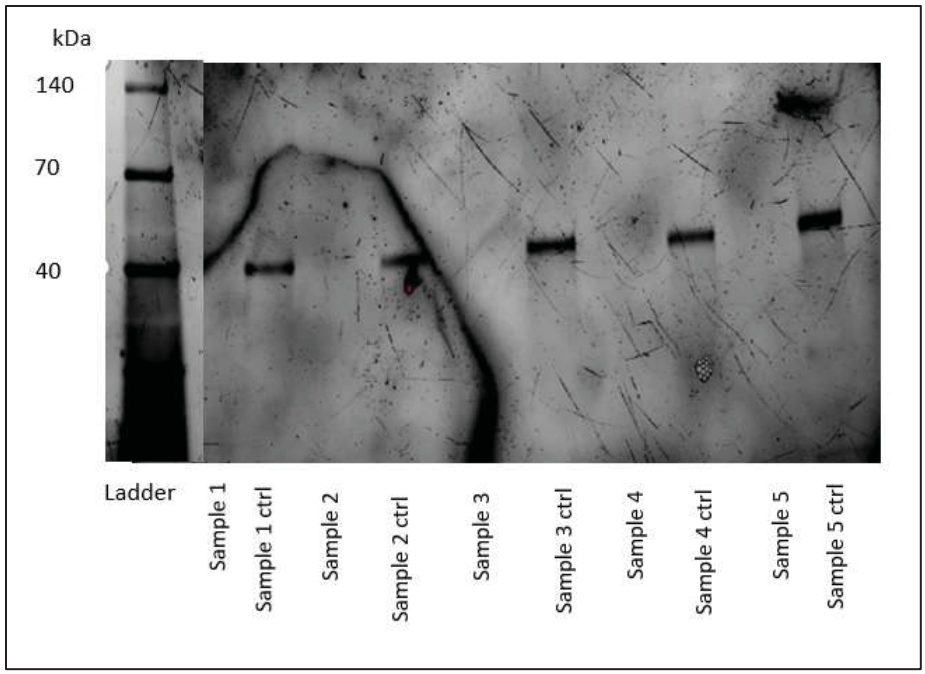

Figure 3.12 Stain-free SDS-PAGE analysis of albumin-loaded liposomes synthesized using the Flex S NanoGenerator system. Lanes represent alternating liposome samples and their respective supernatant controls after ultracentrifugation

.

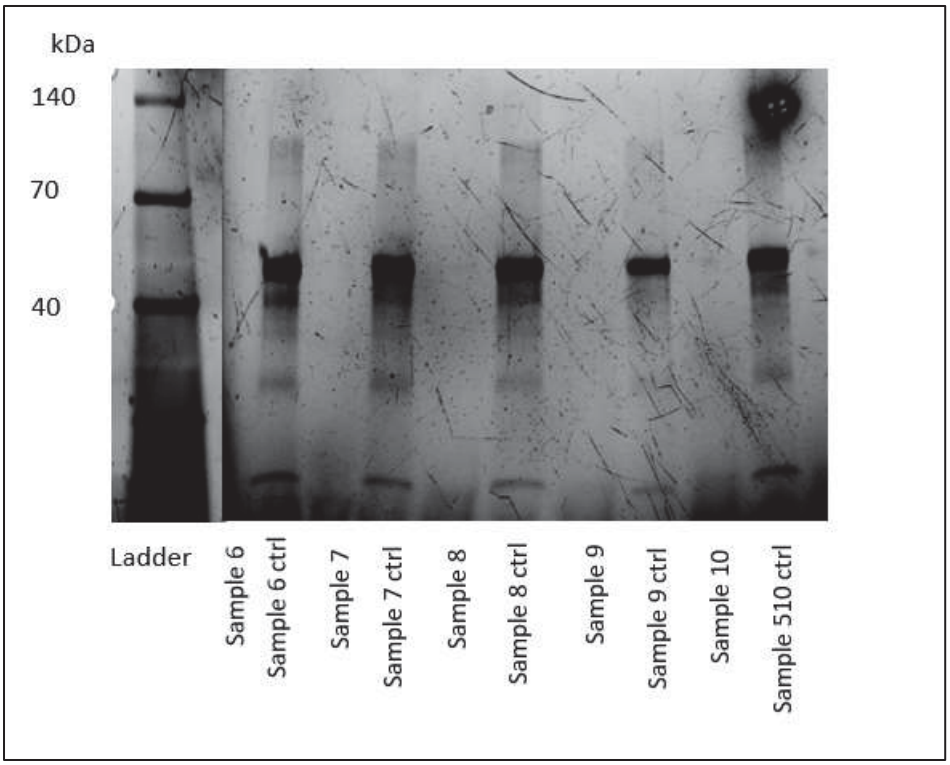

Figure 3.13 Stain-free SDS-PAGE analysis of albumin-loaded liposomes synthesized using the PDM micromixer. Lanes represent alternating liposome samples and their respective supernatant controls after ultracentrifugation

These observations further supported the need for a system with lower protein input requirements, especially as the study progressed toward encapsulating costly EV-relevant proteins like CD63 and HSP70. While neither platform showed success in this early phase, the Flex S system was chosen moving forward due to its smaller working volume, and better compatibility with limited protein amounts.

3.4.2 Targeted Protein Encapsulation: CD63 and HSP70

The first set of encapsulation experiments aimed to test whether EV associated proteins CD63 and HSP70 could be loaded into liposomes using the Flex S NanoGenerator. To minimize degradation, nuclease-free water was pre-cooled at –20 °C for five minutes prior to

reconstituting the proteins. Each vial containing 100 µg of protein was dissolved in 400 µL of water, resulting in a final concentration of 250 µg/mL. Aliquots of 20 µL (containing 5 µg protein) were prepared and stored at –80 °C for single-use encapsulation.

Liposomes were synthesized using a total flow rate (TFR) of 4 mL/min and a flow rate ratio (FRR) of 2:1, corresponding to 333 µL of aqueous phase and 167 µL of organic lipid solution per 500 µL run. The lipid formulation used was DMPC:CHOL in a 1:1 molar ratio. Four samples were prepared: empty liposomes (control), CD63-loaded liposomes (10 µg input), HSP70-loaded liposomes (10 µg input), and a co-loaded formulation containing both CD63 and HSP70 (10 µg each). In all protein-loaded samples, the aqueous phase was adjusted to accommodate the protein input while maintaining the total volume at 333 µL.

ZetaView measurements revealed size increases upon protein loading, with empty liposomes averaging 135.6 nm in diameter. Protein-loaded samples showed larger sizes, increasing to 147.6 nm for CD63, 145.5 nm for HSP70, and 158 nm for the co-loaded formulation (Figure 3.14). This trend suggests partial surface adsorption or internal incorporation of proteins, particularly in the co-loaded sample.

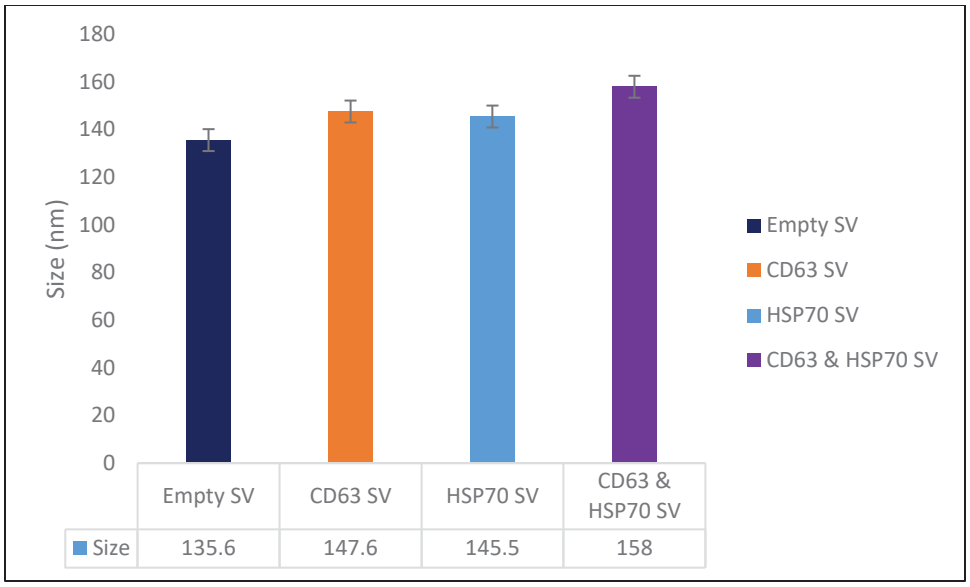

Figure 3.14 Size distribution of empty and protein-loaded liposomes measured by ZetaView

Zeta potential values also varied with protein encapsulation (Figure 3.15). Empty liposomes exhibited a moderately negative charge (–17.57 mV), while HSP70-loaded liposomes showed a more negative potential (–21.83 mV), potentially indicating improved stability. In contrast, CD63-loaded liposomes had a significantly less negative surface charge (–8.08 mV), possibly reflecting minimal incorporation or altered surface interactions. The co-loaded sample showed an intermediate potential of –18.23 mV.

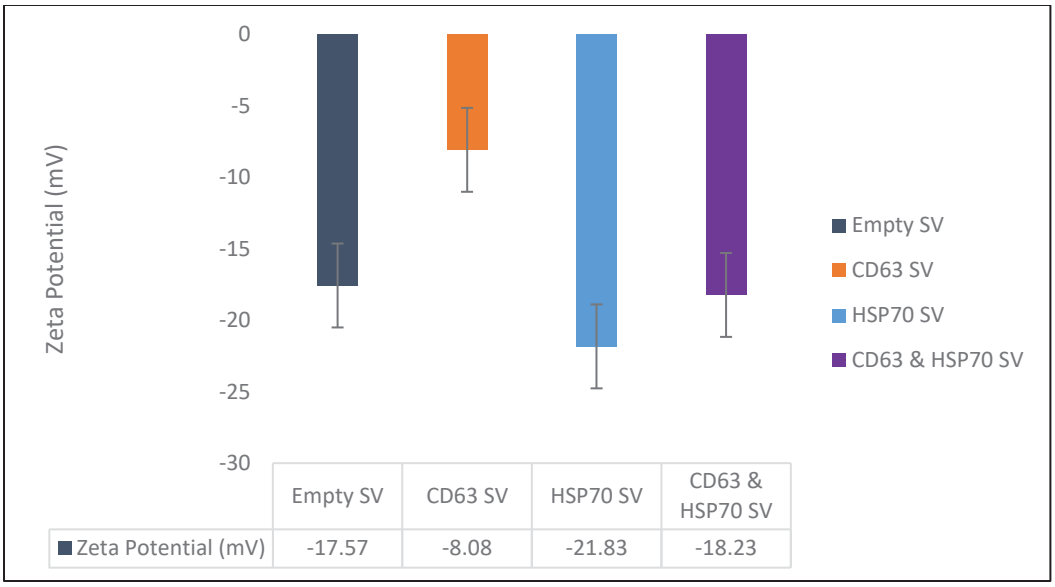

Figure 3.15 Zeta potential of empty and protein-loaded liposomes measured by ZetaView

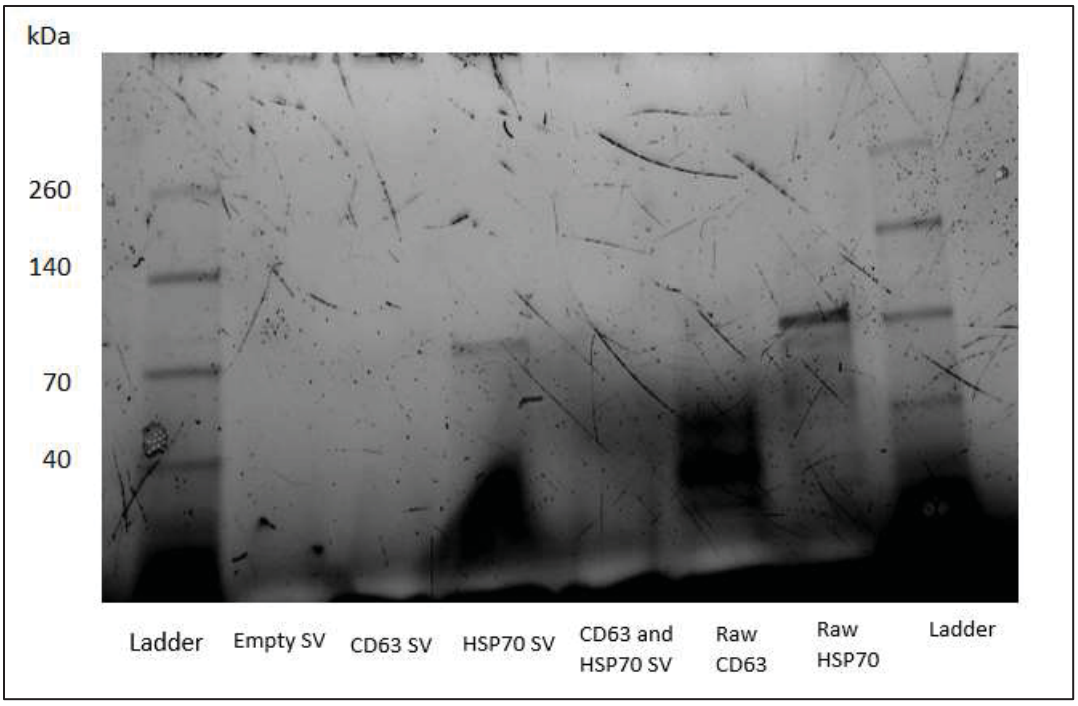

Figure 3.16 Stain-free SDS-PAGE analysis of protein-loaded liposomes and raw proteins

Encapsulation was assessed by stain-free SDS-PAGE, with raw CD63 and HSP70 proteins loaded as references (Figure 3.16). As expected, both raw proteins produced visible bands at their corresponding molecular weights. Among the liposome samples, only the HSP70-loaded condition showed a detectable band, suggesting successful protein loading. No visible band was seen for CD63, either alone or in the co-loaded formulation, indicating minimal or undetectable encapsulation of CD63. Table 3.1 summarizes the Micro BCA quantification results, showing measured protein concentrations and encapsulation efficiencies across different formulations.

Table 3.1 Micro BCA quantification of protein-loaded liposomes. No band was observed in the corresponding gel for CD63, indicating possible overestimation by BCA or non-encapsulated protein remaining after purification

Sample	Measured protein (ul)	Encapsulation efficiency (%)
Empty SV	-	-
CD63 SV	25.19	67
HSP70 SV	25.7	74
CD63 & HSP70 SV	21.68	88

Together, these initial experiments suggested that HSP70 could be successfully encapsulated using the Flex S system at a 1:1 DMPC:CHOL ratio. However, CD63 did not appear to load effectively, prompting further optimization of lipid composition and encapsulation parameters in further experiments.

3.4.2.1 Optimization of lipid ratio and protein input

Following the successful encapsulation of HSP70 using a DMPC:CHOL 1:1 lipid ratio, further experiments aimed to determine whether adjusting the lipid composition could influence encapsulation efficiency. Both HSP70 and CD63 were tested again, this time using lipid ratios of 1:1 and 2:1 (increasing the DMPC proportion), while all other parameters, including flow rate and protein input, remained constant. Each sample was synthesized using the Flex S NanoGenerator at a total flow rate of 4 mL/min and FRR of 2:1, with a protein input of 40 µL per formulation. Protein loading was evaluated using stain-free SDS-PAGE and size and surface charge were characterized by ZetaView.

As observed previously, HSP70 encapsulation was successful, and an increase in band intensity was detected in the 2:1 condition (18% encapsulation detected by Image Lab) compared to 1:1, suggesting improved loading efficiency with higher DMPC content (Figure

3.17). In contrast, CD63 again failed to show a detectable band in either condition, reinforcing its poor encapsulation under the tested formulations.

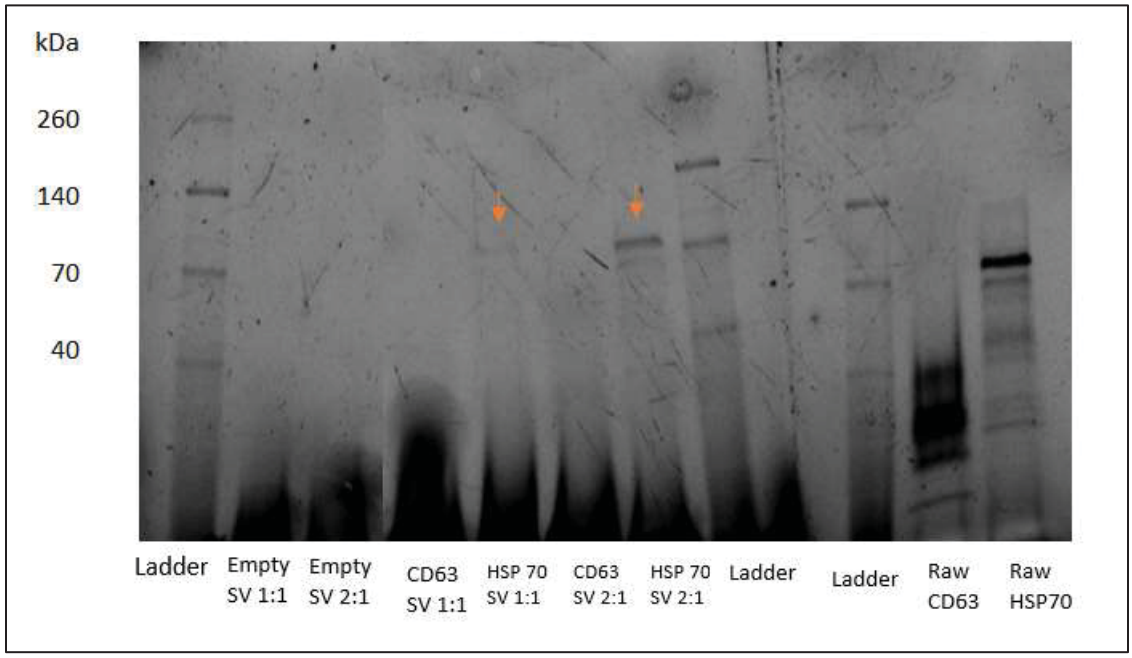

Figure 3.17 Stain-free SDS-PAGE analysis of protein-loaded liposomes prepared at different DMPC:CHOL ratios. HSP70-loaded liposomes showed increased band intensity at 2:1 lipid ratio, indicating enhanced encapsulation. Raw proteins were included as references to confirm expected molecular weights

This observation aligns with prior results and suggests that CD63 either remains unencapsulated or is present at levels below the gel detection threshold.

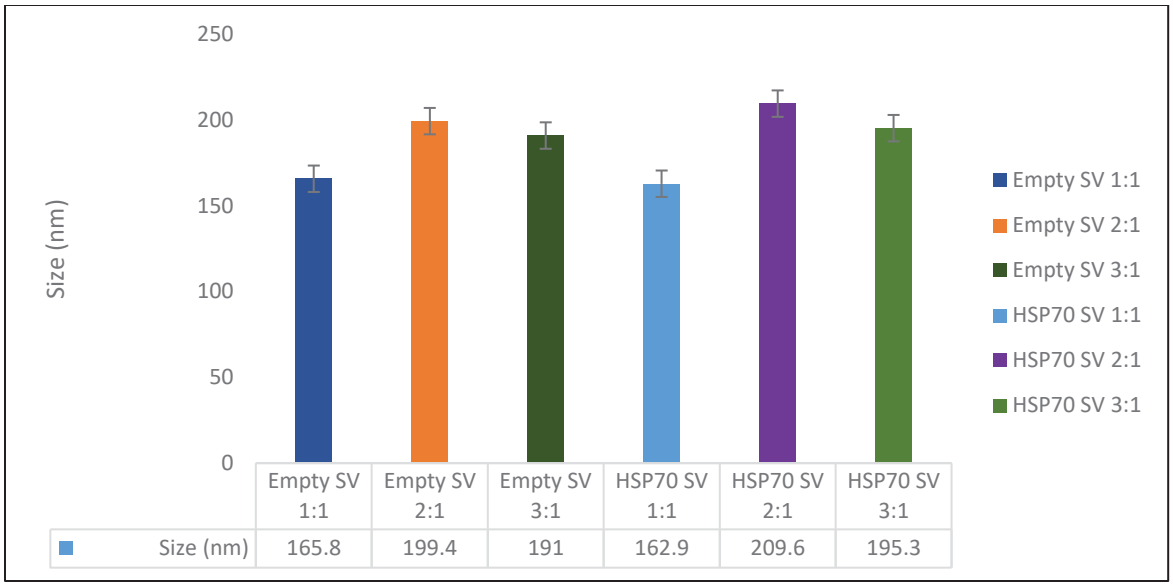

Figure 3.18 Effect of lipid ratio on size distribution of protein-loaded liposomes measured by ZetaView. Liposome size increased with higher DMPC content, particularly in HSP70-loaded samples (124.6 nm at 1:1 vs. 151.8 nm at 2:1)

Interestingly, the liposome size distribution also reflected formulation-dependent trends. HSP70-loaded liposomes increased in size from 124.6 nm (1:1) to 151.8 nm (2:1), consistent with increased protein incorporation (Figure 3.18). CD63-loaded samples showed markedly larger particle sizes in both ratios (210.8 nm and 203.4 nm), but without corresponding protein bands, these increases may reflect surface aggregation or instability rather than successful encapsulation.

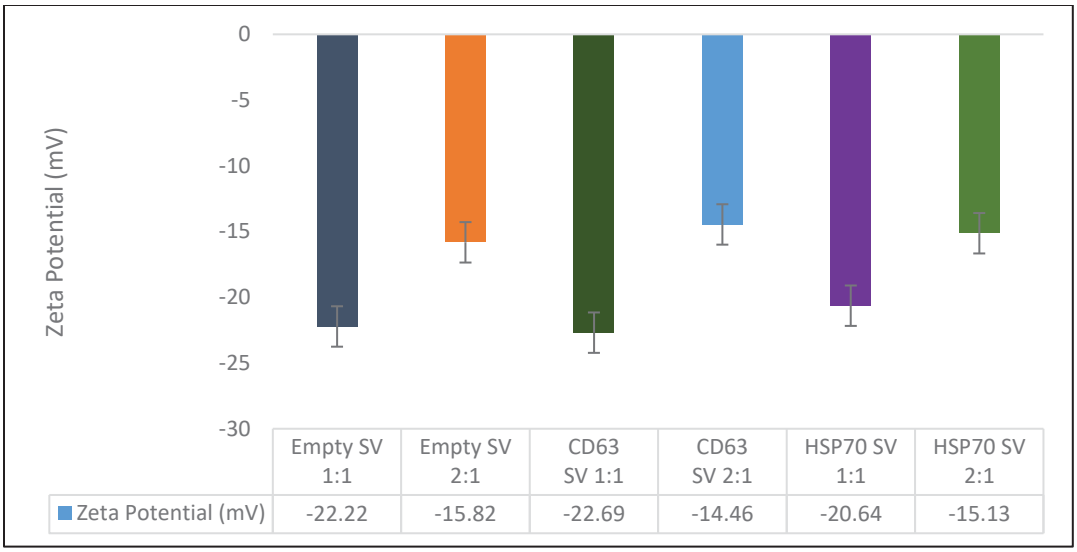

Figure 3.19 Zeta potential of protein-loaded liposomes at different DMPC:CHOL ratios measured by ZetaView

Zeta potential analysis showed more negative values for 1:1 formulations across all samples (Figure 3.19). In HSP70-loaded liposomes, the zeta potential shifted from –20.6 mV to –15.1 mV with increasing DMPC, indicating reduced surface charge and potential changes in stability. For CD63-loaded liposomes, the zeta potential became significantly less negative at 2:1 (–14.5 mV), further suggesting altered surface interactions or reduced vesicle uniformity. Empty liposomes followed similar trends, with a decrease in surface charge at higher DMPC ratios.

Taken together, these results show that lipid composition significantly influences HSP70 encapsulation and affects the physicochemical properties of the resulting liposomes. Increasing the DMPC proportion appears to enhance HSP70 loading, possibly by improving membrane flexibility or interaction with the protein. However, CD63 remained undetectable under both conditions, highlighting that lipid ratio adjustments alone may not be sufficient to achieve its encapsulation and that further formulation or method optimization is needed.

3.4.3 Enhanced Encapsulation of HSP70 Across Varying Lipid Ratios

Following the trend observed in earlier experiments, where HSP70 encapsulation increased with a higher DMPC:CHOL ratio, a final optimization study was conducted to test three lipid compositions: 1:1, 2:1, and 3:1. All formulations were prepared using the Flex S NanoGenerator with a total flow rate of 4 mL/min and an FRR of 2:1. The lipids were dissolved in ethanol, and HSP70 (10 µg) was loaded using a fixed input of 40 µL per run. Post-synthesis, samples were analyzed using stain-free SDS-PAGE, ZetaView (for size and zeta potential), and a control experiment using free protein in ethanol was included to assess any false-positive band detection.

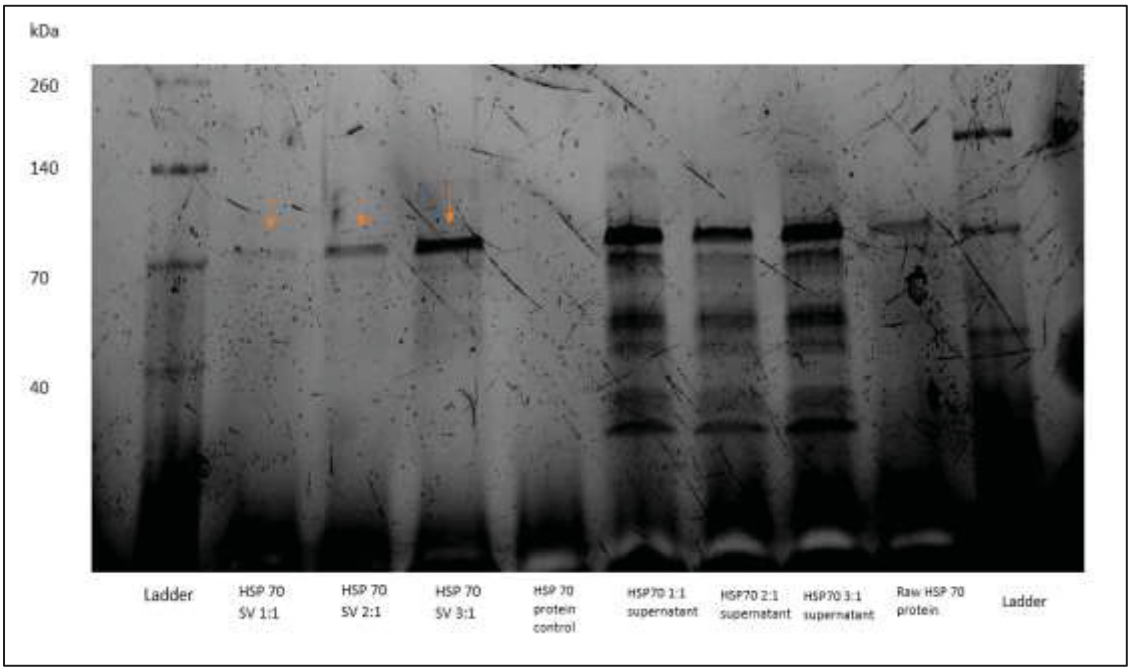

Figure 3.20 Stain-free SDS-PAGE analysis of HSP70-loaded liposomes at 1:1, 2:1, and 3:1 lipid ratios. HSP70 bands intensified with increasing DMPC content, with the strongest signal observed at 3:1

All three HSP70-loaded liposome samples produced visible bands near the expected molecular weight (~70 kDa) on the SDS-PAGE gel, with the band intensity increasing progressively from the 1:1 to the 3:1 formulation (Figure 3.20). The clearest band was seen in the 3:1 condition, suggesting enhanced protein encapsulation at higher DMPC content. No band was observed in the protein control (HSP70 mixed with ethanol), confirming that the detected bands were due to successful encapsulation rather than residual unbound protein. Supernatants from all three conditions showed minimal signal, further supporting efficient incorporation of the protein into the liposome core.

Sample	EE (%) run 1	EE (%) run 2	Average EE %
HSP70 SV 1:1	10.5	13	11.8
HSP70 SV 2:1	36	41	38.5
HSP70 SV 3:1	51	54	52.5

Table 3.2 Encapsulation efficiency (EE%) of HSP70-loaded SVs prepared with varying DMPC:CHOL molar ratios

The above table 3.2 presents the encapsulation efficiency (EE%) of HSP70 in liposomes synthesized using three different DMPC:CHOL molar ratios: 1:1, 2:1, and 3:1. Encapsulation efficiency was calculated from two independent experimental runs based on band intensity quantification using Image Lab software and stain-free SDS-PAGE. Results show a progressive increase in average EE% from 11.8% at 1:1 to 52.5% at 3:1, indicating that higher DMPC:CHOL enhances protein loading efficiency.

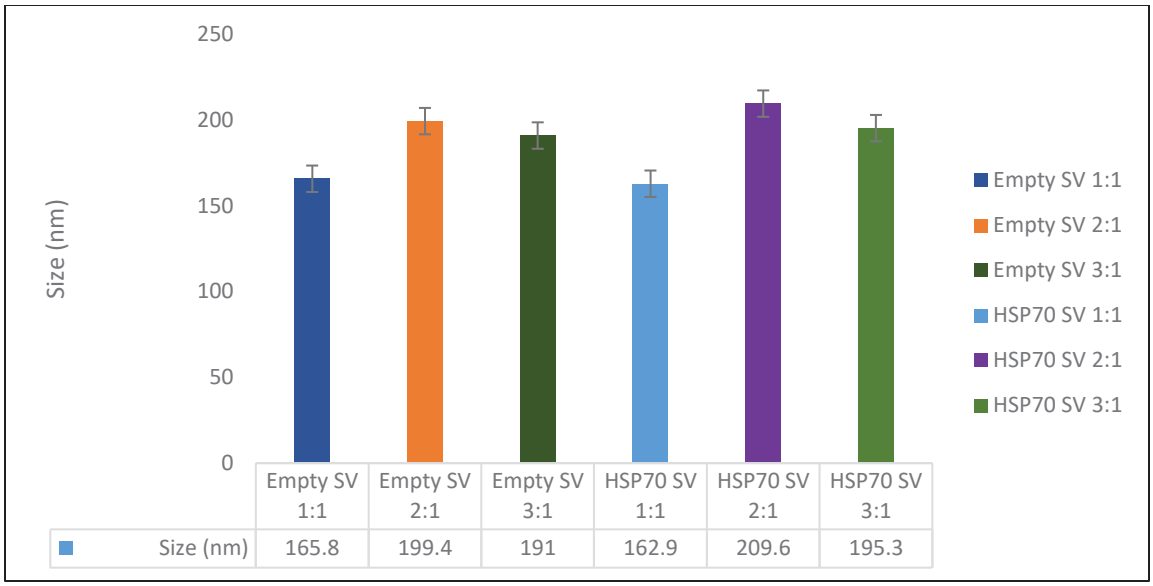

Figure 3.21 Size distribution of HSP70-loaded liposomes at different lipid ratios measured by ZetaView

ZetaView analysis revealed size increases corresponding to higher lipid ratios. HSP70-loaded liposomes measured 162.9 nm, 209.6 nm, and 195.3 nm for 1:1, 2:1, and 3:1 ratios, respectively, with the 2:1 sample exhibiting the largest average diameter (Figure 3.21). This may reflect an optimal balance between membrane fluidity and vesicle structure.

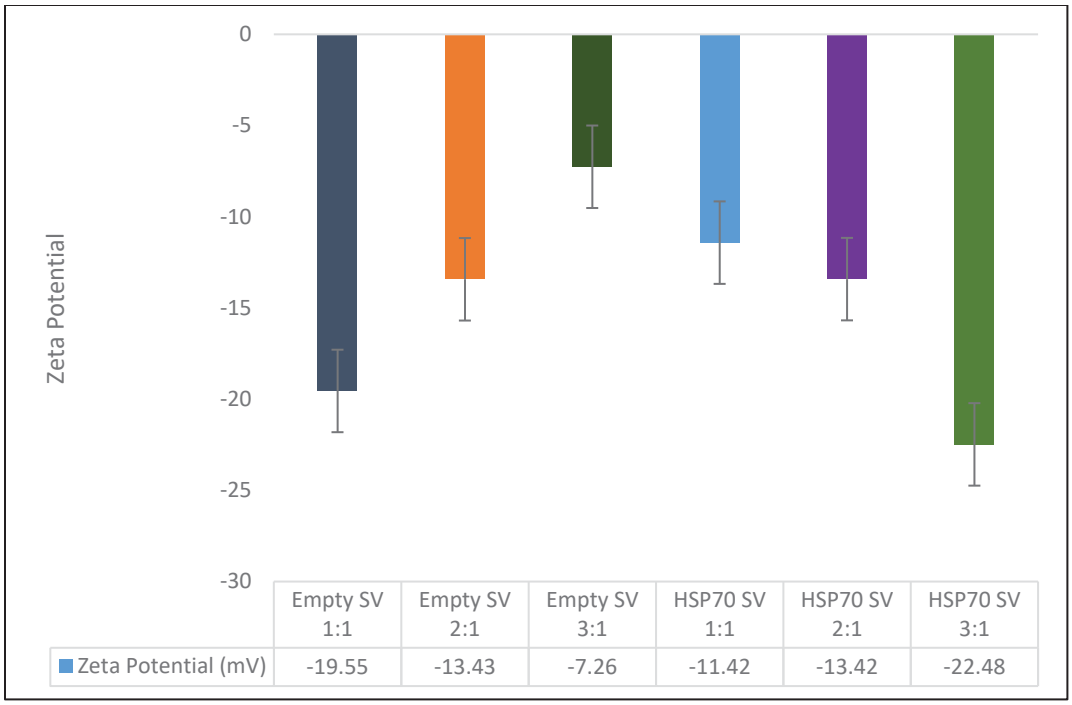

Figure 3.22 Zeta potential of HSP70-loaded liposomes at varying DMPC:CHOL ratios

In terms of surface charge, zeta potential became more negative in the 3:1 condition (–22.48 mV), compared to –13.42 mV and –11.42 mV for the 2:1 and 1:1 conditions, respectively (Figure 3.22). Interestingly, this suggests that the 3:1 formulation offered both improved loading and electrostatic stabilization.

Overall, this demonstrated that lipid composition plays a significant role in determining protein encapsulation efficiency and vesicle characteristics. The 3:1 DMPC:CHOL formulation emerged as the most effective condition for HSP70 loading, highlighting the value of fine-tuning lipid ratios when designing SVs for protein delivery.

3.4.4 Summary of Protein Encapsulation Outcomes (CD63 and HSP70)

Encapsulation experiments using the Flex S system showed that HSP70 could be efficiently loaded into DMPC:CHOL liposomes, with increasing encapsulation observed as the lipid ratio shifted from 1:1 to 3:1. This trend was supported by stronger gel band intensity, increasing vesicle size, and more negative zeta potential. CD63 failed to produce detectable bands under any condition, despite measurable protein concentrations by BCA, suggesting poor encapsulation or loss during purification. Overall, lipid composition had a clear impact on HSP70 loading, while CD63 may require alternative encapsulation strategies, such as protein modification, alternative carriers, or affinity-based loading techniques.

3.4.5 Encapsulation of EV-Derived Proteins into SVs

To evaluate whether SVs can accommodate complex protein cargo from natural EVs, total EV proteins were extracted from SW620-derived EVs and encapsulated into DMPC:CHOL (1:1) liposomes using the Flex S NanoGenerator. All experiments were conducted with three biological replicates, and empty liposomes served as controls.

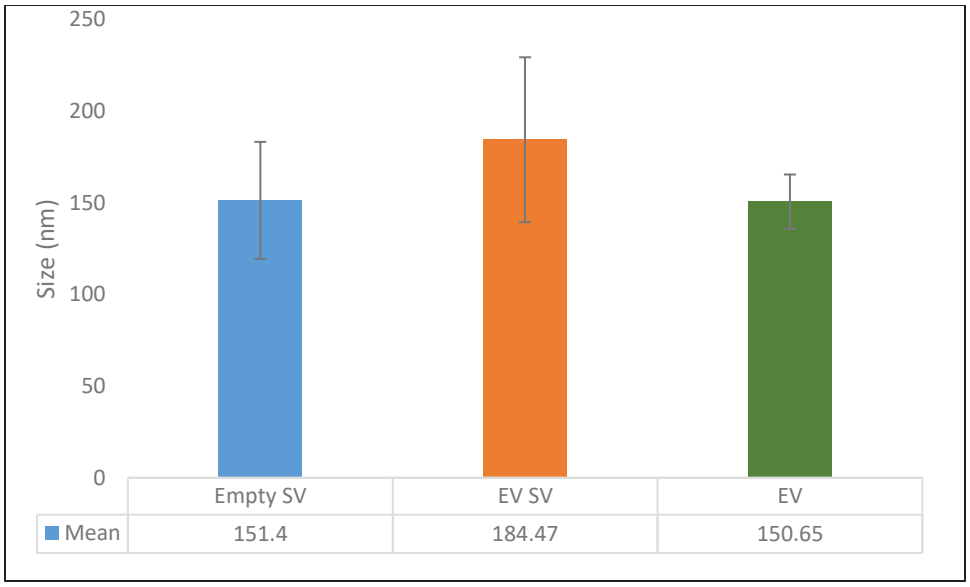

Figure 3.23 Size distribution of EV SVs measured using ZetaView, showing a uniform nano sized population

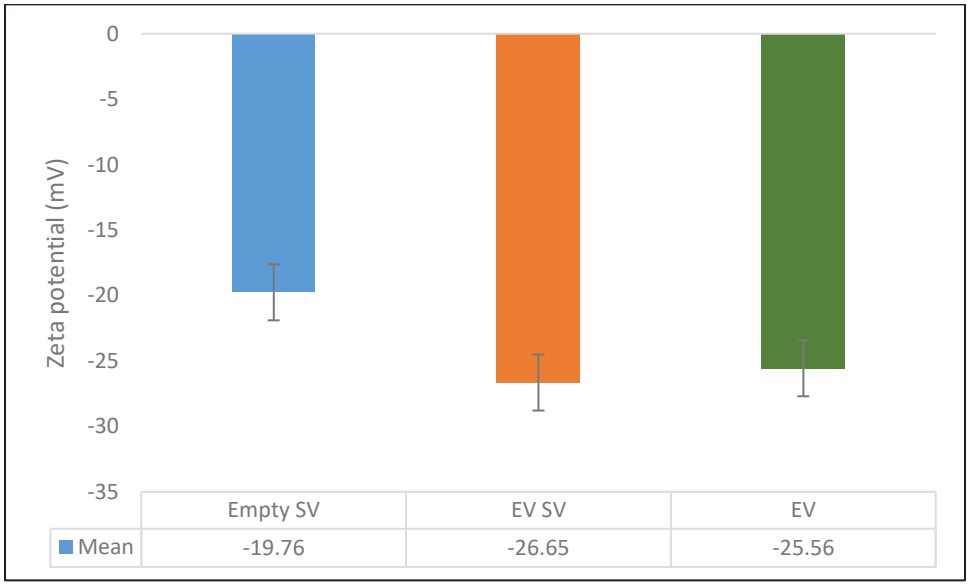

Figure 3.24 Zeta potential analysis of EV SVs indicating stable surface charge

ZetaView analysis showed that the EV protein-loaded liposomes (EV SVs) had a similar size distribution to native EVs, with mean diameters ranging between 150–180 nm (Figure 3.23). Compared to empty SVs, both EV SVs and native EVs displayed increased size and greater variability, consistent with the incorporation of heterogeneous protein cargo. Zeta potential measurements revealed that EV SVs, like EVs, carried a strongly negative surface charge (~–25 mV) (Figure 3.24), suggesting comparable colloidal stability and membrane composition.

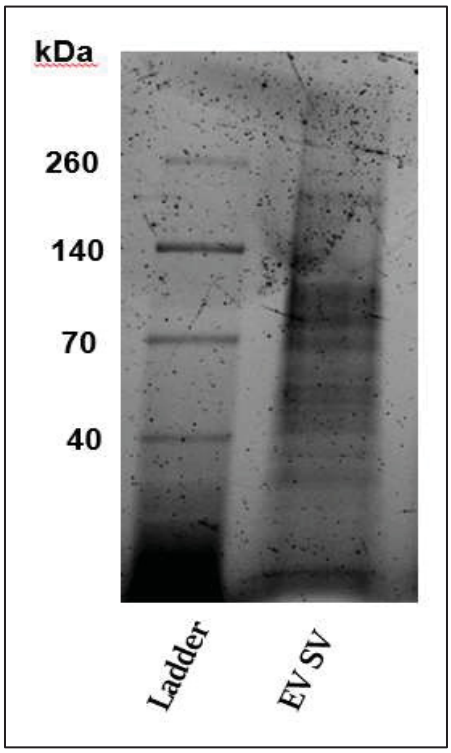

Figure 3.25 Protein profile of EV protein-loaded synthetic vesicles (EV SVs) visualized by stain-free SDS-PAGE**.** Distinct bands spanning a broad molecular weight range confirm successful encapsulation of diverse EV-derived proteins

Stain-free SDS-PAGE confirmed the successful incorporation of a complex protein mixture into the liposomes (Figure 3.25). EV SVs exhibited a distinct and broad banding pattern

reflecting the diversity of loaded EV proteins. Encapsulation efficiency was calculated to be 45.74% using micro BCA.

Together, these findings demonstrate that whole EV protein extracts can be encapsulated into SVs using a microfluidic-based system, producing vesicles with physicochemical properties that closely resemble those of natural EVs.

3.5 Proteomic Analysis of EVs and SVs

To compare the protein content of natural EVs and SVs loaded with EV proteins (EV SV), we performed high-resolution mass spectrometry. This analysis showed that many proteins were shared between the two, but some differences were also seen in how much of each protein was present. The Venn diagram (Figure 3.26) illustrates the overlap of proteins identified in synthetic vesicles loaded with whole EV-derived proteins (EVSV) and natural EVs isolated from SW620 cells.

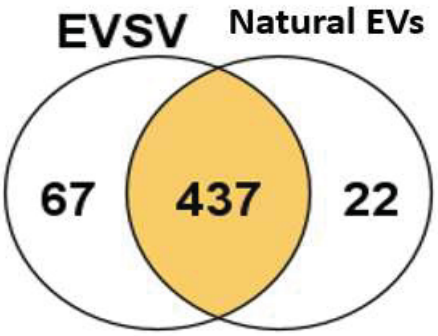

Figure 3.26 Venn diagram comparing protein identities between EVSV and natural EVs.

A total of 437 proteins were common between the two groups, while 67 proteins were unique to EVSV and 22 proteins were exclusive to natural EVs. These shared proteins indicate that EVSVs successfully encapsulated a substantial portion of the natural EV proteome, supporting their potential as biomimetic models. The 67 unique proteins are likely due to the high abundance of albumin present in the EV protein extracts, which can dominate the mass

spectrometry signal and mask the detection of lower-abundance proteins in natural EVs. Figure 3.27 presents the total spectral counts of four EV marker proteins—HSP70, CD63, TSG101, and PDCD6IP (ALIX)—identified through mass spectrometry in two replicates each of EVSVs (synthetic vesicles loaded with whole EV-derived proteins) and natural EVs.

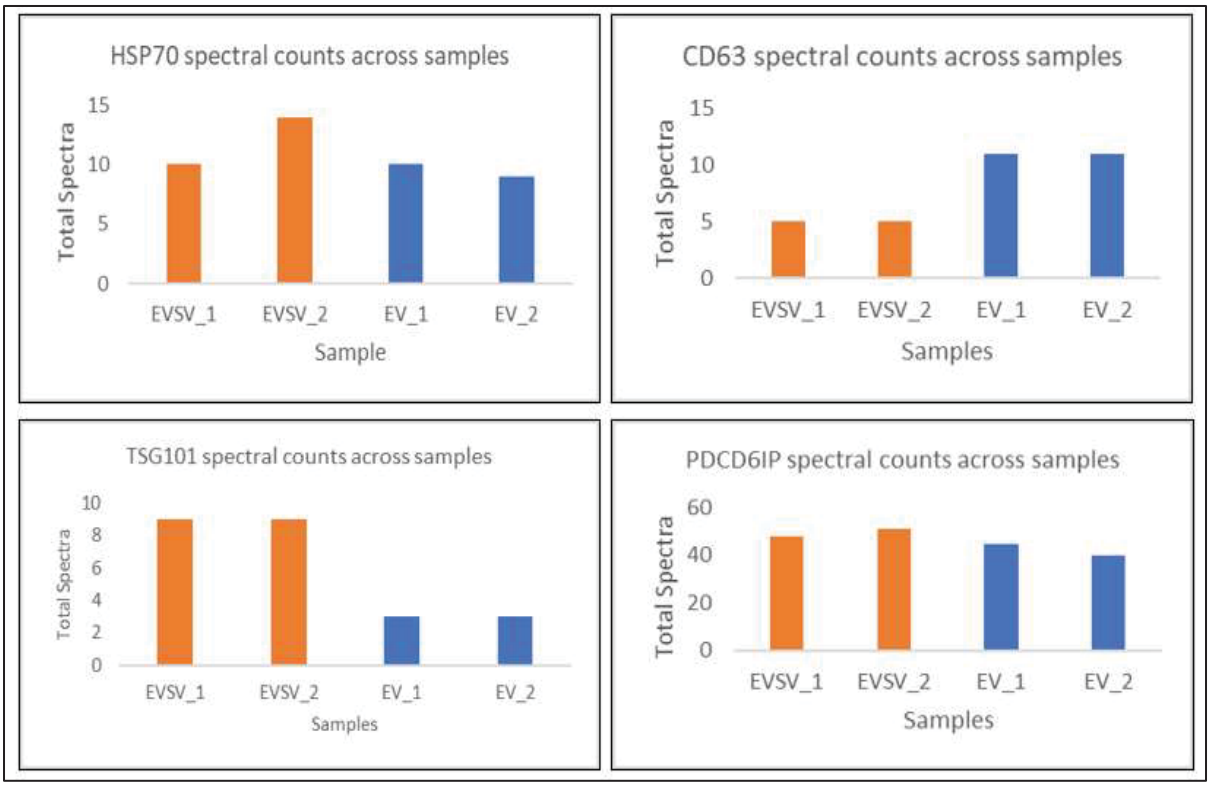

Figure 3.27 Comparative spectral counts of EV marker proteins in EVSV and natural EV samples.

EVSV samples (EVSV_1 and EVSV_2) are shown in orange, while natural EV samples (EV_1 and EV_2) are shown in blue. HSP70 and TSG101 exhibited higher spectral counts in EVSVs, suggesting efficient incorporation or retention of these proteins during vesicle synthesis. In contrast, CD63 was more abundant in natural EVs, indicating lower encapsulation efficiency

for this tetraspanin in the SVs. PDCD6IP levels were high and relatively consistent across both EVSV and EV samples, reflecting successful transfer of core EV-associated proteins. These findings support the ability of EVSVs to recapitulate key elements of the natural EV proteome.

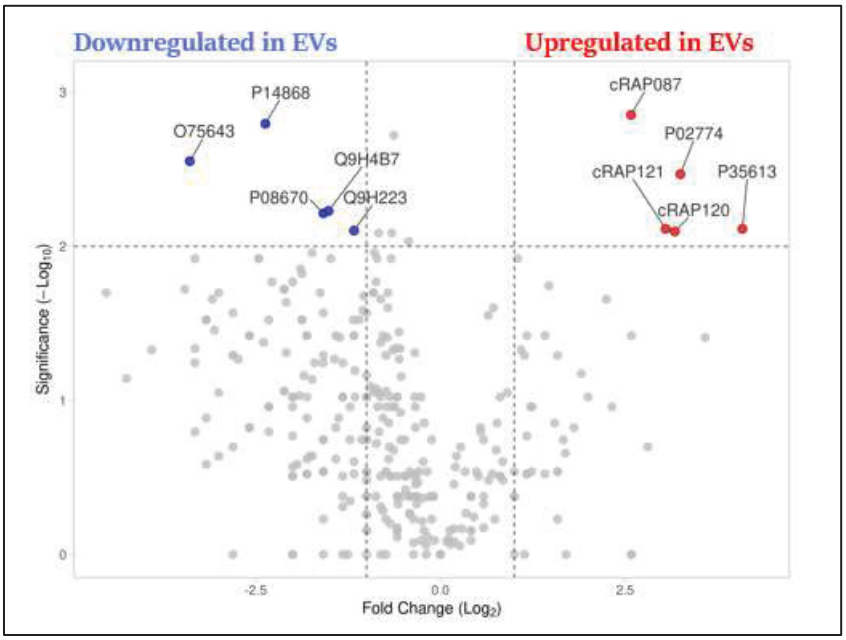

Figure 3.28 Volcano plot of differentially expressed proteins between EVs and EV SVs. Red and blue points represent proteins significantly enriched or depleted in EV SVs compared to native EVs ($p < 0.01$, $|\log_2 FC| > 2$)

The volcano plot (Figure 3.28) showed a few proteins that were significantly more or less abundant in EV SVs compared to EVs. For example, structural and nucleic acid-binding proteins like vimentin (P08670) and (P14868) were found at lower levels in EV SVs, suggesting they were not efficiently encapsulated. On the other hand, proteins like albumin (cRAP087), alpha-2-HS-glycoprotein (cRAP120), and basigin (P35613) were more enriched

in the SVs. These proteins are commonly found in plasma and may have been easier to load due to their abundance or interaction with the liposome surface.

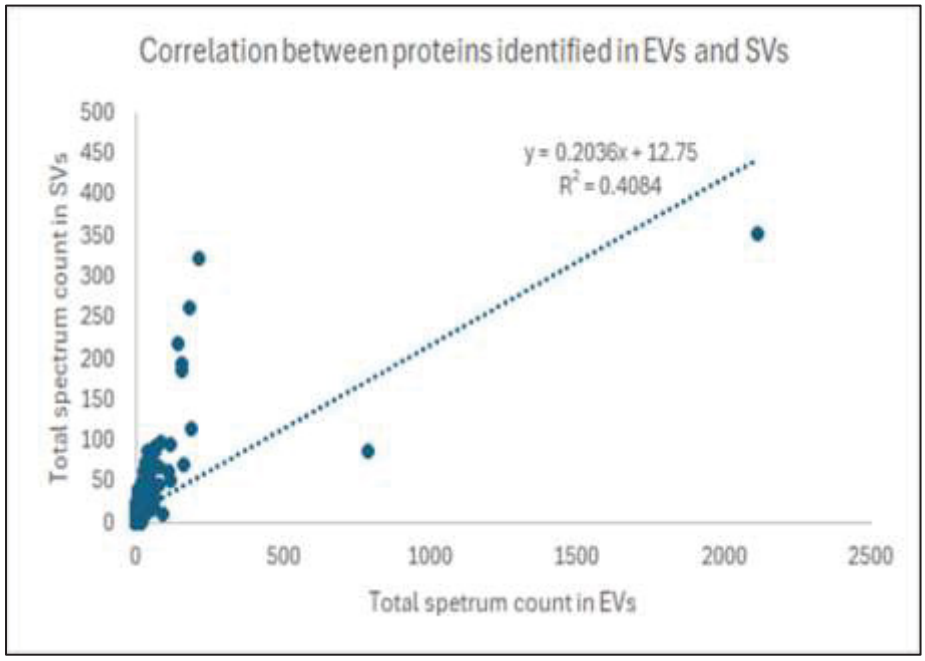

Figure 3.29 Correlation of total spectral counts between EVs and EV SVs

A correlation analysis (Figure 3.29) between EV and EV SV protein levels showed a moderate positive trend ($R^2 = 0.41$), meaning the synthetic system was able to capture part of the EV proteome, but not all. On average, protein amounts in EV SVs were about 20% of those in EVs. This difference likely reflects the simpler, passive loading process used in synthetic systems compared to the complex sorting that happens in cells.

Despite these differences, several functional proteins, such as clathrin and tenascin, were successfully incorporated into the SVs. This suggests that the approach works and can be optimized further to better mimic the content of natural EVs.

3.6 Cellular Uptake Studies

To evaluate whether protein-loaded synthetic vesicles (EVSVs) could be internalized by colorectal cancer (CRC) cells, live-cell imaging was performed using the IncuCyte system. SW620 and HCT116 cells were seeded in 96-well plates (2,500 cells/well) and treated with SP-DiIC18(3)-labeled liposomes encapsulating either EV-derived proteins or HSP70. Imaging was conducted at 10× magnification over two and three days post-treatment to monitor uptake dynamics. Imaging performed at 10× magnification over two and three days post-treatment to assess uptake dynamics.

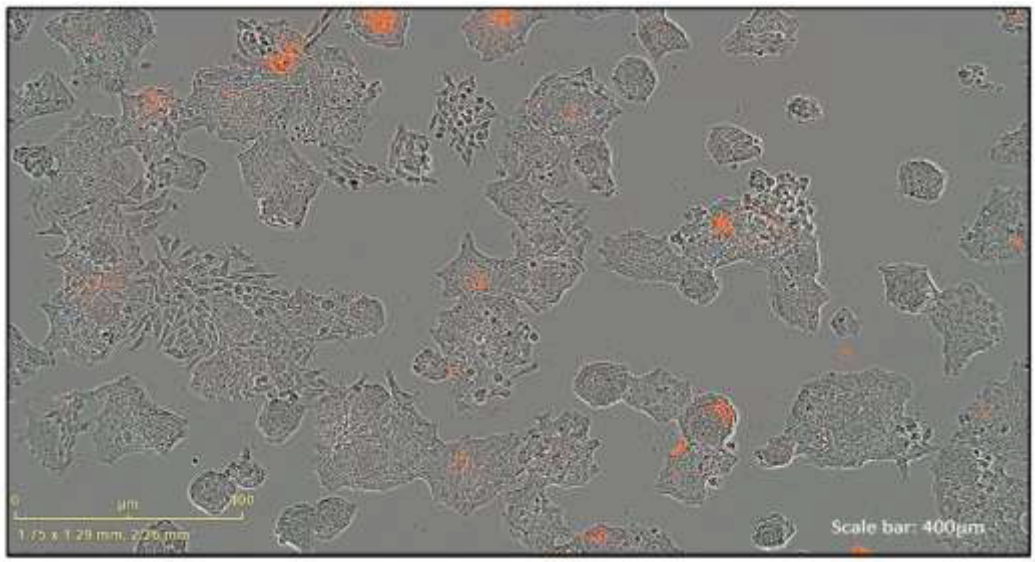

Figure 3.30 A. Uptake of EV protein-loaded liposomes by SW620 cells visualized by IncuCyte at 48 h post-treatment

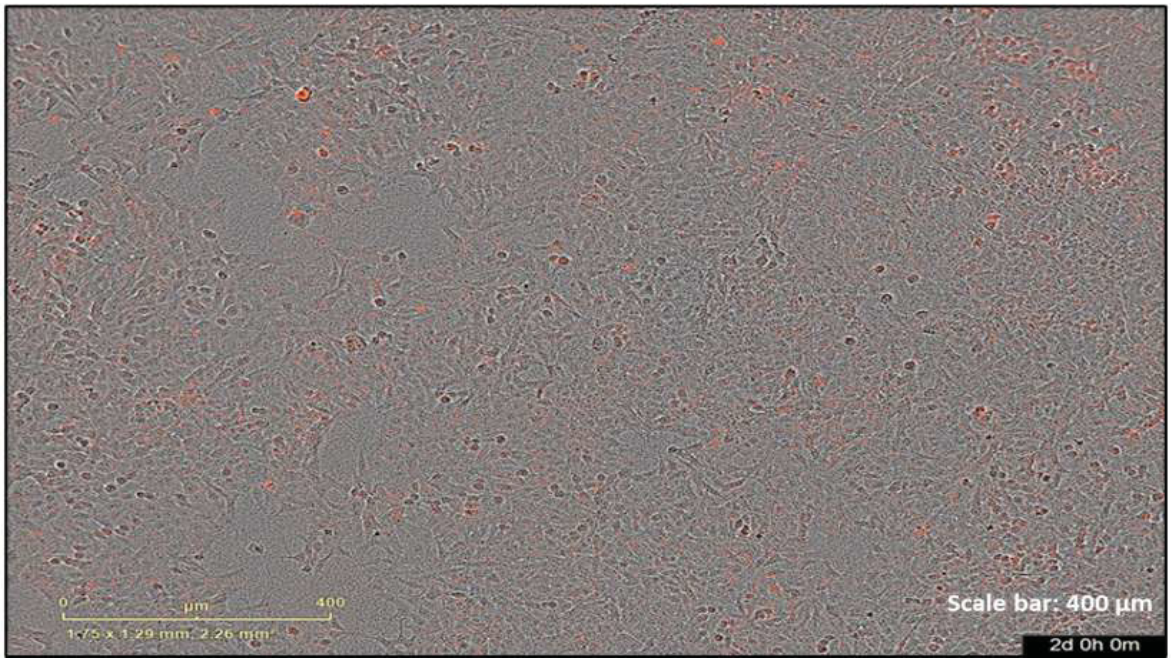

Figure 3.30 B. Uptake of HSP 70 protein-loaded liposomes by HCT 116 cells visualized by IncuCyte at 48 h post-treatment

In cells treated with EV SVs, distinct orange fluorescent was observed within the cytoplasm after 48 hours, and this signal persisted through later timepoints (Figure 3.30 A). These suggest that the labeled vesicles were internalized and localized within intracellular compartments, potentially endosomal or lysosomal structures. The fluorescence appeared dispersed but consistent across multiple cells, indicating successful uptake across the population.

Similarly, cells treated with HSP70-loaded liposomes also showed fluorescent signal (Figure 3.30 B). Although the intensity and distribution of signal varied slightly compared to EV SVs, the presence of intracellular fluorescence confirmed that HSP70-loaded vesicles were also internalized. These observations suggest that the presence of protein cargo may enhance interaction with the cell membrane and facilitate vesicle uptake.

3.7 Conclusion

This chapter focused on making and testing protein-loaded SVs designed to mimic EVs from CRC cells. Changing the ratio of DMPC to CHOL in the liposome formulation had a clear impact on how well proteins could be encapsulated. Liposomes with higher DMPC:CHOL content showed better loading of HSP70 with encapsulation efficiencies increasing from 11.8% at 1:1, to 38.5% at 2:1, and reaching 52.5% at 3:1 DMPC:CHOL ratio. However, not all proteins were successfully loaded. CD63, a well-known EV marker, could not be efficiently encapsulated under the tested conditions. This suggests that protein characteristics such as size, structure, or charge can influence passive encapsulation into liposomes.

A key part of this project was the successful encapsulation of whole EV protein extracts, which achieved an average encapsulation efficiency of 45.7%. These liposomes maintained similar size and surface charge to natural EVs and carried a broad range of proteins. Although proteomic analysis showed only partial overlap between the proteins in EVs and the synthetic vesicles, many important structural and functional markers were retained. Live-cell imaging confirmed that protein-loaded liposomes were taken up by CRC cells. This was observed for both single-protein formulations and those loaded with full EV protein mixtures. These findings support the potential of SVs as biomimetic tools for studying EV functions and as platforms for delivering biological cargo to cancer cells.

DISCUSSION AND CONCLUSION

This study demonstrated that SVs can be designed to closely mimic key features of EVs derived from CRC cells. By systematically optimizing the lipid formulation and encapsulation conditions, the platform successfully achieved the loading of selected EV-associated proteins, particularly HSP70. A consistent finding across experiments was that lipid composition played an important role in protein encapsulation efficiency, vesicle stability, and how well the particles were taken up by cells.

Among the proteins tested, HSP70 showed the most promising encapsulation results. A clear trend was observed: increasing the DMPC:CHOL ratio from 1:1 to 3:1 led to stronger protein loading, as shown by more intense bands on SDS-PAGE and larger vesicle sizes. This suggests that higher DMPC content may improve interactions between the protein and the liposome membrane, possibly by increasing membrane flexibility or surface area. Interestingly, the 3:1 lipid ratio not only improved loading but also resulted in better colloidal stability, as shown by a more negative zeta potential (–22.48 mV). These results underline the importance of tuning lipid ratios to support efficient protein loading and vesicle performance.

In contrast, CD63 - a membrane-bound protein, could not be successfully encapsulated under any tested conditions, even when the lipid composition was changed. This highlights a key limitation of passive loading, which may not be suitable for complex proteins like CD63 due to their structure or surface properties. More targeted strategies such as chemical modification or affinity-based loading may be needed in such cases.

Encapsulating total EV proteins from CRC-derived EVs further confirmed that the system can carry complex protein mixtures. These EV-mimicking synthetic vesicles (EV SVs) closely matched natural EVs in size, surface charge, and protein content, suggesting they could serve as functional EV models. Cellular uptake experiments showed that both HSP70-loaded and

EV SV liposomes were effectively internalized by CRC cells, supporting their biological relevance.

Together, these findings provide a strong basis for designing EV-like liposomes by adjusting lipid composition and production methods. HSP70 proved to be a helpful model for testing and optimizing encapsulation, while successful loading of whole EV proteomes shows the broader potential of the platform.

RECOMMENDATIONS

This study established a reproducible platform for synthesizing EV-like liposomes and evaluating their potential to mimic CRC derived EVs. While key features such as size, surface charge, and cellular uptake were successfully replicated, several challenges emerged that point to areas for improvement.

Encapsulation of soluble proteins like HSP70 was efficient and consistent, particularly at higher DMPC:CHOL ratios. However, attempts to load membrane-associated proteins such as CD63 were unsuccessful. This likely reflects limitations of passive loading methods, which are not suitable for complex or hydrophobic proteins. Future work should explore active strategies, such as lipid conjugation, or affinity-based techniques, to improve loading of transmembrane proteins.

Encapsulation of whole EV protein extracts produced liposomes (EV SVs) with EV-like physical properties, but proteomic analysis revealed selective loading. Structural proteins were often underrepresented, while plasma proteins dominated. This suggests the need for optimized lipid formulations or other protective additives to enhance the retention of diverse protein cargo.

Although uptake was confirmed in CRC cells, functional validation of EV SVs will require in vivo testing. Future studies should use mouse models of CRC metastasis to assess biodistribution, stability, and biological activity in a more physiologically relevant setting.

Lastly, while both the PDM and Flex S systems enabled liposome synthesis, the Flex S system offered smaller volume requirements, and better protein retention. Continued optimization of flow conditions, lipid composition, and protein compatibility will be key to advancing this synthetic platform for research and therapeutic applications.

APPENDIX 1

Raw Proteomics Data

The complete list of 526 proteins identified through high-resolution mass spectrometry from extracellular vesicles (EVs) and EV-derived synthetic vesicles (EV SVs) is provided in Appendix_EV_vs_EVSV_Proteomics.xlsx

Data was processed using Scaffold Viewer.

Probability Legend: over 95% | 80% to 94% | 50% to 79% | 20% to 49% | 0% to 19%

#	Visible?	Starred?	Bio View: Identified Proteins (526)	Accession Number	Alternate ID	Molecular Weight	Protein Grouping Ambiguity	control		EVSV	
								control_1	control_2	EVSV_1	EVSV_2
204	☑	☐	Glyceraldehyde-3-phosphate dehydrogenase OS=Homo sapiens OX=9606 GN=GAPDH PE=1 SV=3	P04406	GAPDH	36 kDa		20	18	30	30
205	☑	☐	Glycogen phosphorylase, liver form OS=Homo sapiens OX=9606 GN=PYGL PE=1 SV=4	P06737	PYGL	97 kDa	*	3	1	1	1
206	☑	☐	Golgi apparatus protein 1 OS=Homo sapiens OX=9606 GN=GLG1 PE=1 SV=2	Q92896	GLG1	135 kDa		0	0	2	3
207	☑	☐	GTP-binding nuclear protein Ran OS=Homo sapiens OX=9606 GN=RAN PE=1 SV=3	P62826	RAN	24 kDa		4	3	5	5
208	☑	☐	GTPase KRas OS=Homo sapiens OX=9606 GN=KRAS PE=1 SV=1	P01116	KRAS	22 kDa	*	0	0	0	3
209	☑	☐	Guanine nucleotide-binding protein G(i) subunit alpha-2 OS=Homo sapiens OX=9606 GN=GNAI2 PE=1 SV=3	P04899	GNAI2	40 kDa	*	4	4	15	19
210	☑	☐	Guanine nucleotide-binding protein G(i) subunit alpha-3 OS=Homo sapiens OX=9606 GN=GNAI3 PE=1 SV=3	P08754	GNAI3	41 kDa	*	3	3	8	13
211	☑	☐	Guanine nucleotide-binding protein G(I)/G(S)/G(T) subunit beta-1 OS=Homo sapiens OX=9606 GN=GNB1 PE=	P62873	GNB1	37 kDa	*	6	5	5	9
212	☑	☐	Guanine nucleotide-binding protein G(s) subunit alpha isoforms short OS=Homo sapiens OX=9606 GN=GNAS	P63092 (+1)	GNAS	46 kDa	*	1	2	6	7
213	☑	☐	Guanine nucleotide-binding protein subunit alpha-13 OS=Homo sapiens OX=9606 GN=GNA13 PE=1 SV=2	Q14344	GNA13	44 kDa		1	0	9	6
214	☑	☐	Heat shock 70 kDa protein 1A OS=Homo sapiens OX=9606 GN=HSPA1A PE=1 SV=1	P0DMV8 (+1)	HSPA1A	70 kDa	*	10	9	10	14
215	☑	☐	Heat shock cognate 71 kDa protein OS=Homo sapiens OX=9606 GN=HSPA8 PE=1 SV=1	P11142	HSPA8	71 kDa	*	27	29	43	46
216	☑	☐	Heat shock protein beta-1 OS=Homo sapiens OX=9606 GN=HSPB1 PE=1 SV=2	P04792	HSPB1	23 kDa			1	2	3
217	☑	☐	Heat shock protein HSP 90-alpha OS=Homo sapiens OX=9606 GN=HSP90AA1 PE=1 SV=5	P07900	HSP90AA1	85 kDa	*	14	15	25	28
218	☑	☐	Heat shock protein HSP 90-beta OS=Homo sapiens OX=9606 GN=HSP90AB1 PE=1 SV=4	P08238	HSP90AB1	83 kDa	*	18	17	31	34
219	☑	☐	Hemoglobin subunit alpha OS=Homo sapiens OX=9606 GN=HBA1 PE=1 SV=2	cRAP035	HBA1	15 kDa		7	6	7	7
220	☑	☐	Hemoglobin subunit delta OS=Homo sapiens OX=9606 GN=HBD PE=1 SV=2	P02042	HBD	16 kDa		3	1	3	5
221	☑	☐	Hepatocyte growth factor activator OS=Homo sapiens OX=9606 GN=HGFAC PE=1 SV=1	Q04756	HGFAC	71 kDa		4	1	2	1
222	☑	☐	Hepatocyte growth factor-like protein OS=Homo sapiens OX=9606 GN=MST1 PE=1 SV=2	P26927	MST1	80 kDa		2	1	2	2
223	☑	☐	Heterogeneous nuclear ribonucleoprotein D0 OS=Homo sapiens OX=9606 GN=HNRNPD PE=1 SV=1	Q14103	HNRNPD	38 kDa				1	2
224	☑	☐	Heterogeneous nuclear ribonucleoprotein F OS=Homo sapiens OX=9606 GN=HNRNPF PE=1 SV=3	P52597	HNRNPF	46 kDa	*		1	2	3
225	☑	☐	Heterogeneous nuclear ribonucleoprotein H OS=Homo sapiens OX=9606 GN=HNRNPH1 PE=1 SV=4	P31943	HNRNPH1	49 kDa	*		0	2	3
226	☑	☐	Heterogeneous nuclear ribonucleoprotein K OS=Homo sapiens OX=9606 GN=HNRNPK PE=1 SV=1	P61978	HNRNPK	51 kDa				2	4
227	☑	☐	Heterogeneous nuclear ribonucleoprotein M OS=Homo sapiens OX=9606 GN=HNRNPM PE=1 SV=3	P52272	HNRNPM	78 kDa		1	1	6	6

Figure A.1.1 Screenshot of raw proteomics data for EV and EV SV samples analyzed using Scaffold Viewer. Spectral counts across replicates (Control_1, Control_2, EVSV_1, EVSV_2) are shown

LIST OF BIBLIOGRAPHICAL REFERENCES

Ahmadi, Mahdi, Zahra Javadinia, Seyed Vahid Hosseini et Mohammad Reza Zali. 2024. « Colorectal Cancer: A Global Concern and Its Liver Metastatic Propensity ». *Journal of Gastrointestinal Oncology*, vol. 15, no 1, p. 45–58.

Akers, J. C., D. Gonda, R. Kim, B. Carter et C. E. Chen. 2013. « Biogenesis of extracellular vesicles (EV): exosomes, microvesicles, retrovirus-like vesicles, and apoptotic bodies ». *Journal of Neuro-Oncology*, vol. 113, no 1, p. 1–11.

Allen, Theresa M., et Pieter R. Cullis. 2013. « Liposomal drug delivery systems: from concept to clinical applications ». *Advanced Drug Delivery Reviews*, vol. 65, no 1, p. 36–48.

American Cancer Society. 2025. « Survival Rates for Colorectal Cancer ». *American Cancer Society*.

Balaj, L., R. Lessard, M. Dai, et X. Skog. 2011. « Tumour microvesicles contain retrotransposon elements and amplified oncogene sequences ». *Nature Communications*, vol. 2, p. 180.

Bangham, A. D., M. M. Standish et G. Weissmann. 1965. « The action of steroids and streptolysin S on the permeability of phospholipid structures to cations ». *Journal of Molecular Biology*, vol. 13, no 1, p. 253–IN28.

Barenholz, Yechezkel. 2012. « Doxil®—the first FDA-approved nano-drug: lessons learned ». *Journal of Controlled Release*, vol. 160, no 2, p. 117–134.

Beh, Cyrus W., et Yvonne Y. Y. Yeo. 2022. « Recent developments in hybrid extracellular vesicle–liposome drug delivery systems ». *Bioconjugate Chemistry*, vol. 33, no 5, p. 868–879.

Bobbili, Dheeraj R., Shweta Mehta, Andrew Baker et Anisha Gupta. 2025. « Engineering liposomes for enhanced protein delivery: Lessons from CD63 encapsulation ». *Molecular Pharmaceutics*, vol. 22, no 1, p. 56–67.

Bozzuto, Giuseppina, et Anna Molinari. 2015. « Liposomes as nanomedical devices ». *International Journal of Nanomedicine*, vol. 10, p. 975–999.

Bruno, Stefania, Maria Deregibus, et Giovanni Camussi. 2013. « Therapeutic application of mesenchymal stem cell-derived extracellular vesicles for kidney injury ». *Frontiers in Immunology*, vol. 4, p. 29.

Bunggulawa, Ezekiel J., Shanshan Wang, Weichen Yin, Huan Liu, Guohua Ye, Zhen Zhang, Xiaojie Li, Yujie Luo, Yujie Wang et Xiaojun Zhang. 2018. « Recent advancements in the use of exosomes as drug delivery systems ». *Journal of Nanobiotechnology*, vol. 16, no 1, p. 81.

Chen, Guoku, Dongdong Huang, Yunmei Liu, Weiming Zhang, Gang Zhang, Meng Wu, Wei Xu, Zhenyu Yu, Jie Yang, Bo Wang, Huan Sun, Hongxia Xia, Qian Man, Wei Zhong, Luis F. Antelo, Bin Wu, Xiaoyun Xiong, Xiaojun Liu, Lili Guan, Ting Li, Shuang Liu, Rui Yang, Yiling Lu, Lei Dong, Sean McGettigan, Radhakrishnan Radhakrishnan, Gregory Mills, Yiling Lu, Joon Kim, Yuhua Chen, Haidong Dong, Yajun Zhao, Giorgos C. Karakousis, Tara C. Mitchell, Lynn M. Schuchter, Meenhard Herlyn, E. John Wherry, Xiaowei Xu et Wei Guo. 2018. « Exosomal PD-L1 contributes to immunosuppression and is associated with anti-PD-1 response ». *Nature*, vol. 560, no 7718, p. 382–386.

Cheung, A. S. T., et Khuloud T. Al-Jamal. 2019. « The application of microfluidics in the synthesis of nanoscale biomaterials ». *Advanced Drug Delivery Reviews*, vol. 132, p. 73–89.

Clayton, Aled, Giampietro Turzanski, Dawn Dewitt, Andrew Steadman, Amy Mason, David Mason, Stephen Tabi et Dennis J. Chaplin. 2005. « A subset of human tumour-derived exosomes induces apoptosis in antigen-specific CD8+ T cells ». *Blood*, vol. 105, no 4, p. 1746–1753.

Costa-Silva, Bruno, Niels Kosaka, Irene Reymond, Fabio G. Valerio, Hoshikage Kikuchi, Harshani Upadhya, Hiroshi Ochiya et Raghu Kalluri. 2015. « Pancreatic cancer exosomes initiate pre-metastatic niche formation in the liver ». *Nature Cell Biology*, vol. 17, no 6, p. 816–826.

Curley, Olivia, Mohammad Shahid, Naureen Fatima et Javed Iqbal. 2025. « Structural considerations in the encapsulation of tetraspanins into synthetic vesicles ». *Nanomedicine*, vol. 44, p. 112003.

Darooei Zadeh, Ramin, Zahra Zarei, Mohammad Mahdi Dehshahri et Majid Motiei. 2021. « Effects of mixing parameters on size and structure of liposomes prepared by microfluidic method ». *Scientific Reports*, vol. 11, no 1, p. 15042.

Elsharkasy, Omar M., Joel Z. Nordin, Daniel W. Hagey, Olivier G. de Jong, Raymond M. Schiffelers, Samir El Andaloussi et Pieter Vader. 2020. « Extracellular vesicles as drug delivery systems: why and how? ». *Advanced Drug Delivery Reviews*, vol. 159, p. 332–343.

Gao, Min, Ling Zeng, et Ke Zhang. 2023. « Functional roles of small extracellular vesicles in colorectal cancer progression and metastasis ». *Signal Transduction and Targeted Therapy*, vol. 8, p. 114.

Gastpar, Roswitha, Annette Gehrmann, Marion Bausero, Tom H. Schröder, Michael Otto, Roland M. Schöniger, Bernd Kampgen, Georg B. Issels et Gunther Multhoff. 2005. « Heat shock protein 70 surface-positive tumor exosomes stimulate migratory and cytolytic activity of natural killer cells ». *Cancer Research*, vol. 65, no 12, p. 5238–5247.

International Society for Extracellular Vesicles. 2018. « Minimal information for studies of extracellular vesicles 2018 (MISEV2018): a position statement and update of the MISEV2014 guidelines ». *Journal of Extracellular Vesicles*, vol. 7, no 1, p. 1535750.

López, Rubén Rodrigo. 2020. *Développement d'un système microfluidique pour la production de vésicules extracellulaires biomimétiques*. Thèse de maîtrise, École de technologie supérieure (ÉTS), Montréal.

López, Rubén Rodrigo, Hélène Delanoë-Ayari, Alexandre Ramos, Stéfanie Boudaoud, Vincent Picard et Julie Burnier. 2021. « Periodic disturbance micromixer enables enhanced liposome production via passive mixing ». *Lab on a Chip*, vol. 21, no 6, p. 1124–1134.

Midekessa, Gudeta, Johanna Godakumara, Kai Ord, Tambet Teesalu, Keijo Lehto, Toomas Neuman et Tambet Põldma. 2020. « Zeta potential of extracellular vesicles: toward understanding the attributes that determine colloidal stability ». *Biochimica et Biophysica Acta (BBA) - Biomembranes*, vol. 1862, no 9, p. 183298.

Raposo, Graça, et Willem Stoorvogel. 2013. « Extracellular vesicles: Exosomes, microvesicles, and friends ». *Journal of Cell Biology*, vol. 200, no 4, p. 373–383.

Sjöblom, Tobias, Anna-Lisa Müller, Erik Holmström et Håkan Melin. 2024. « Metastatic Mechanisms in Colorectal Cancer: A Review of Emerging Targets ». *Cancer Metastasis Reviews*, vol. 43, no 1, p. 1–17.

Stein, Ulrike, Gabriele Arlt, Heike Walther et Carsten M. Smith. 2020. « MACC1 promotes colorectal cancer cell motility, invasion, and metastasis through enhanced MET signaling ». *Clinical Cancer Research*, vol. 26, no 14, p. 3928–3939.

Sung, Hyuna, Jacques Ferlay, Rebecca L. Siegel, Mathieu Laversanne, Isabelle Soerjomataram, Ahmedin Jemal et Freddie Bray. 2021. « Global cancer statistics 2020: GLOBOCAN estimates of incidence and mortality worldwide for 36 cancers in 185 countries ». *CA: A Cancer Journal for Clinicians*, vol. 71, no 3, p. 209–249.

Tsering, Thupten, Alexander Laskaris, Mohamed Abdouh, Prisca Bustamante, Sabrina Parent, Eva Jin, Sarah Tadhg Ferrier, Goffredo Arena et Julia V. Burnier. 2020. « Uveal Melanoma-Derived Extracellular Vesicles Display Transforming Potential and Carry Protein Cargo Involved in Metastatic Niche Preparation ». *Cancers*, vol. 12, no 10, p. 2923.

Torchilin, Vladimir P. 2005. « Recent advances with liposomes as pharmaceutical carriers ». *Nature Reviews Drug Discovery*, vol. 4, no 2, p. 145–160.

Wu, Jiyang, Xiaoxing Wang, Zhengzhe Li, Xiaomei Yi, Die Hu, Qi Wang et Tianyu Zhong. 2024. « Small extracellular vesicles promote the formation of the pre-metastatic niche through multiple mechanisms in colorectal cancer ». *Cell Cycle*, vol. 23, no 2, p. 131–149.

Zinger, Alice, Valentina Barone, Sarah Butler, Amrita Sharma, Thomas Baigude et Dan Peer. 2021. « Lipid-based nanoparticles for cancer therapy: state of the art and future directions ». *Pharmacological Research*, vol. 169, p. 105643.

Zouggari Ben El Khyat, Chaymaa. 2022. *Development of a microfluidic system for biomimetic extracellular vesicle production*. Master's thesis, École de technologie supérieure (ÉTS), Montréal.